Beyond the Classical Performance Limitations Controlling Uncertain MIMO Systems: UAV Applications

2nd Session

Mario Garcia-Sanz

Automatic Control & Computer Science Department

Public University of Navarra
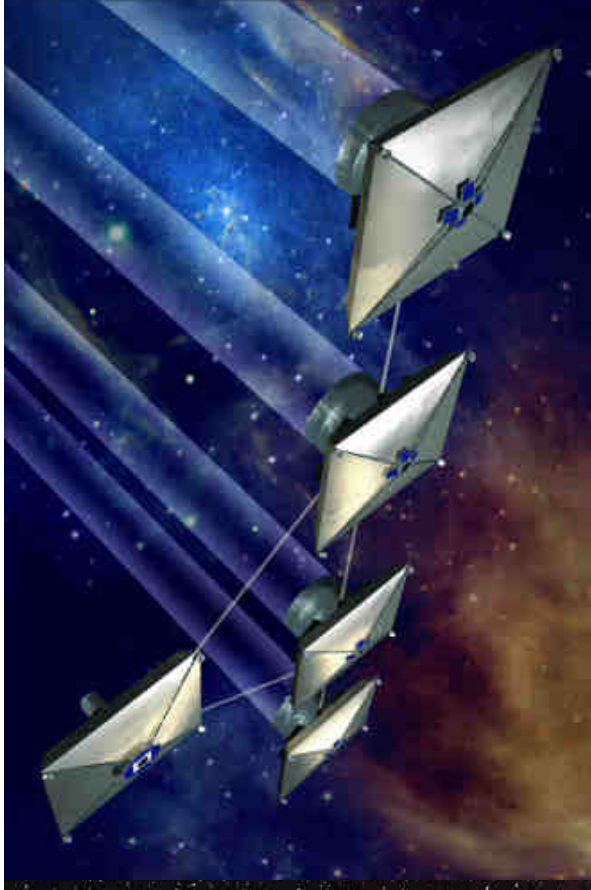
31006 Pamplona, Spain

(Email: mgsanz@unavarra.es)

NATO. RTO-LS-SCI-195, May-June 2008

2.1

Report Documentation Page		Form Approved OMB No. 0704-0188

Public reporting burden for the collection of information is estimated to average 1 hour per response, including the time for reviewing instructions, searching existing data sources, gathering and maintaining the data needed, and completing and reviewing the collection of information. Send comments regarding this burden estimate or any other aspect of this collection of information, including suggestions for reducing this burden, to Washington Headquarters Services, Directorate for Information Operations and Reports, 1215 Jefferson Davis Highway, Suite 1204, Arlington VA 22202-4302. Respondents should be aware that notwithstanding any other provision of law, no person shall be subject to a penalty for failing to comply with a collection of information if it does not display a currently valid OMB control number.

1. REPORT DATE **MAY 2008**	2. REPORT TYPE	3. DATES COVERED **00-00-2008 to 00-00-2008**
4. TITLE AND SUBTITLE **Beyond the Classical Performance Limitations Controlling Uncertain MIMO Systems: UAV Applications**		5a. CONTRACT NUMBER
		5b. GRANT NUMBER
		5c. PROGRAM ELEMENT NUMBER
6. AUTHOR(S)		5d. PROJECT NUMBER
		5e. TASK NUMBER
		5f. WORK UNIT NUMBER
7. PERFORMING ORGANIZATION NAME(S) AND ADDRESS(ES) **Public University of Navarra,Automatic Control & Computer Science Department,31006 Pamplona Spain,**		8. PERFORMING ORGANIZATION REPORT NUMBER
9. SPONSORING/MONITORING AGENCY NAME(S) AND ADDRESS(ES)		10. SPONSOR/MONITOR'S ACRONYM(S)
		11. SPONSOR/MONITOR'S REPORT NUMBER(S)

12. DISTRIBUTION/AVAILABILITY STATEMENT
Approved for public release; distribution unlimited

13. SUPPLEMENTARY NOTES
See also ADM002223. Presented at the NATO/RTO Systems Concepts and Integration Panel Lecture Series SCI-195 on Advanced Autonomous Formation Control and Trajectory Management Techniques for Multiple Micro UAV Applications held in Glasgow, United Kingdom on 19-21 May 2008.

14. ABSTRACT

15. SUBJECT TERMS

16. SECURITY CLASSIFICATION OF:			17. LIMITATION OF ABSTRACT	18. NUMBER OF PAGES	19a. NAME OF RESPONSIBLE PERSON
a. REPORT **unclassified**	b. ABSTRACT **unclassified**	c. THIS PAGE **unclassified**	**Same as Report (SAR)**	**86**	

Standard Form 298 (Rev. 8-98)
Prescribed by ANSI Std Z39-18

Outline

1.- QFT Controller Design Technique Fundamentals

2.- Real-world QFT control applications and examples

3.- Non-diagonal MIMO QFT controller design methodologies

4.- Application: Robust QFT control for a MIMO Spacecraft with flexible sunshield

5.- Switching robust control: Beyond the linear limitations.

6.- Example: Switching control for Unmanned Vehicles

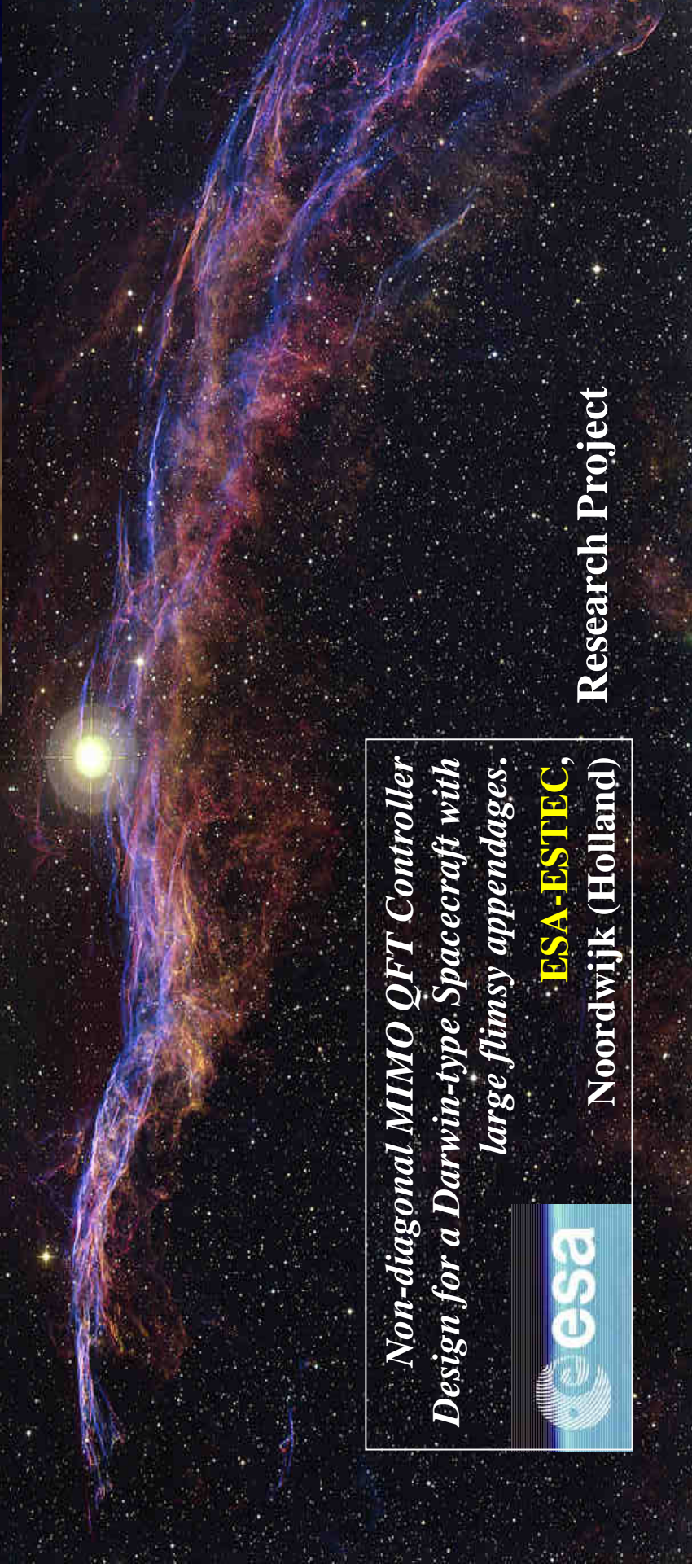**4.- Application:** *Robust QFT control for a MIMO Spacecraft with flexible sunshield*

Non-diagonal MIMO QFT Controller Design for a Darwin-type Spacecraft with large flimsy appendages.

ESA-ESTEC, Noordwijk (Holland)

Research Project

4.1.- Introduction

Telescopes:

From Greek's Gnomon,

Tycho's Quadrants,

Kepler's and Galileo's
Refractor,

or Newton's Reflector.

To Modern telescopes / Radio-telescopes on Earth:
Mauna Kea, Monte Palomar, Cerro Paranal,
Arecibo, etc).

Hubble: a telescope in space (1990)
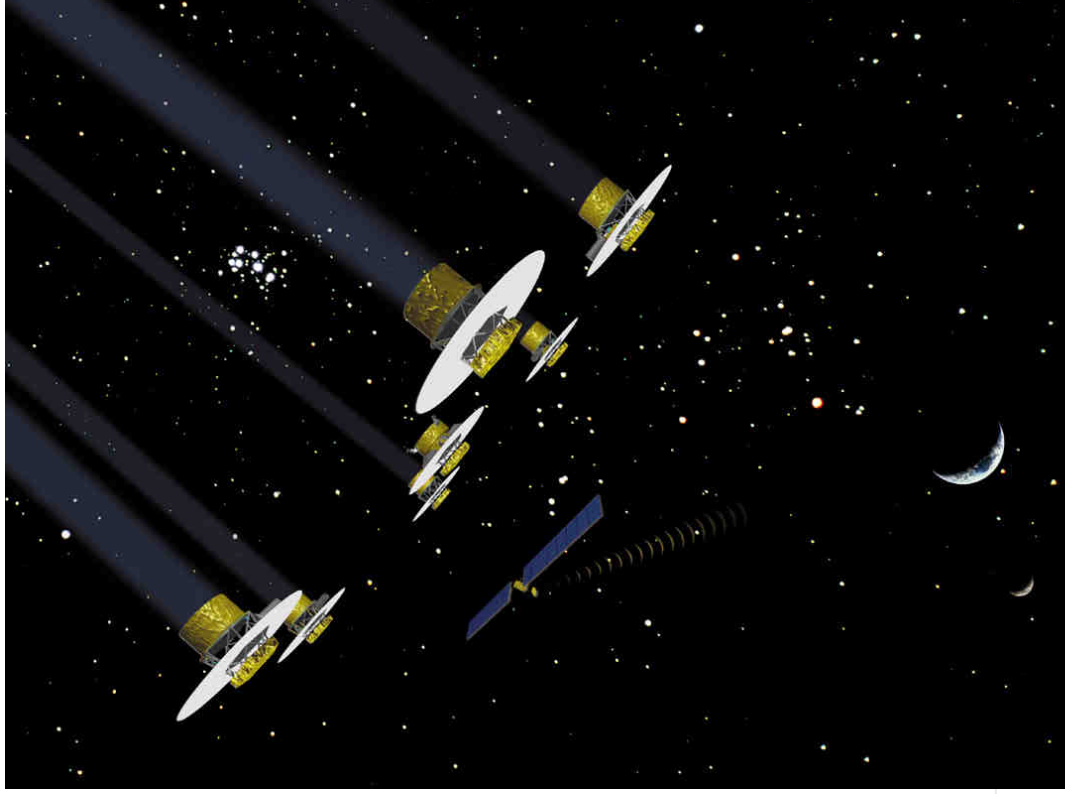
(*Hubble Space Telescope*, **HST**):

- Refractor telescope. Aperture of 2.4 m.
- Magnification power much higher than
the one allowed on Earth.
- Orbit: 600 km above Earth's surface.

Discoveries of First Magnitude

4.2.- Control of Darwin-type Spacecraft with Large Flexible Appendages.

Non-diagonal MIMO QFT Controller Design for a Darwin-type Spacecraft with large flimsy appendages.

ESA-ESTEC, Noordwijk (Holland)

Ref: M. Garcia-Sanz, I. Eguinoa, M. Barreras, S. Bennani

"Non-diagonal MIMO QFT Controller Design for Darwin-type Spacecraft with large flimsy appendages".

Journal of Dynamic Systems, Measurement and Control, **ASME**, USA. Vol. 130, January 2008.
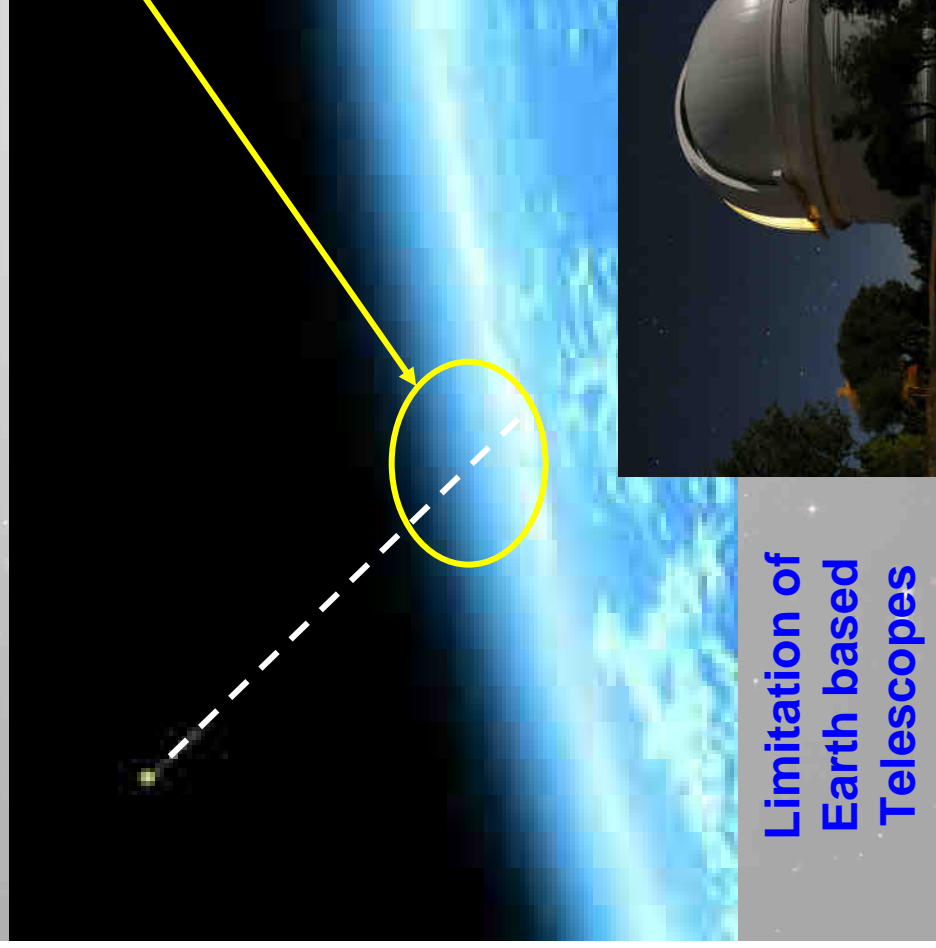
OBJECTIVE:
To study exo-planets and life
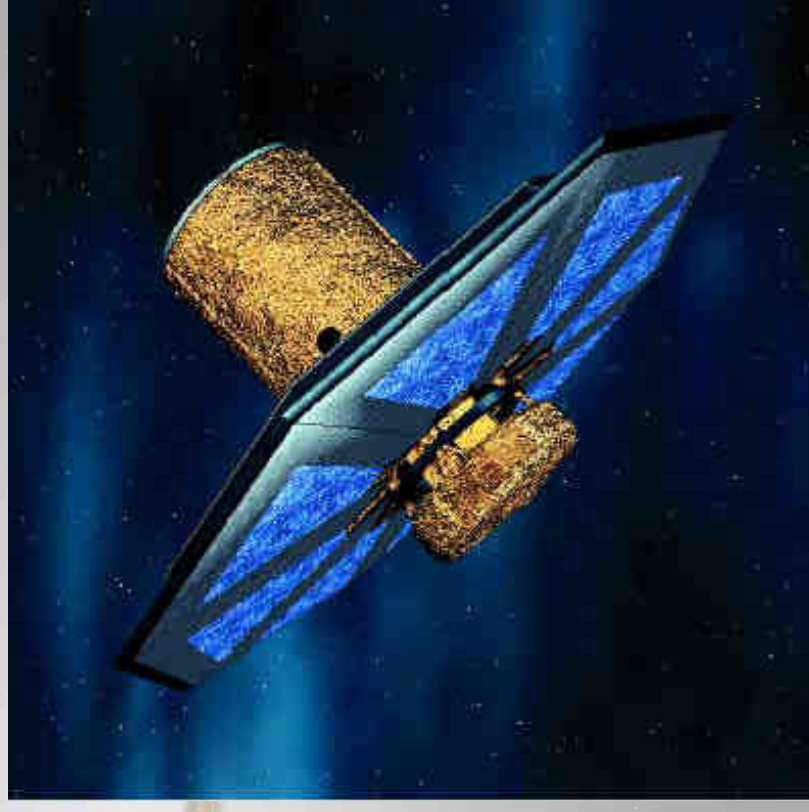
It is necessary

Infrared analysis

Instruments that work at temperature near zero Kelvin

Atmosphere absorbs infrared

Limitation of Earth based Telescopes

Darwin Mission Description (I)

- **ESA** cornerstone **mission**
  - Scheduled launch in 2015
  - Objectives:
    - ➤ Find Earth-like **Exo-planets**
    - ➤ Analyse their atmosphere to detect signs of life

- **Nulling interferometry**:
  - the light collected by the flying telescopes is recombined inside a central hub
    - ➤ from the star interfere destructively
    - ➤ from the planet interfere constructively
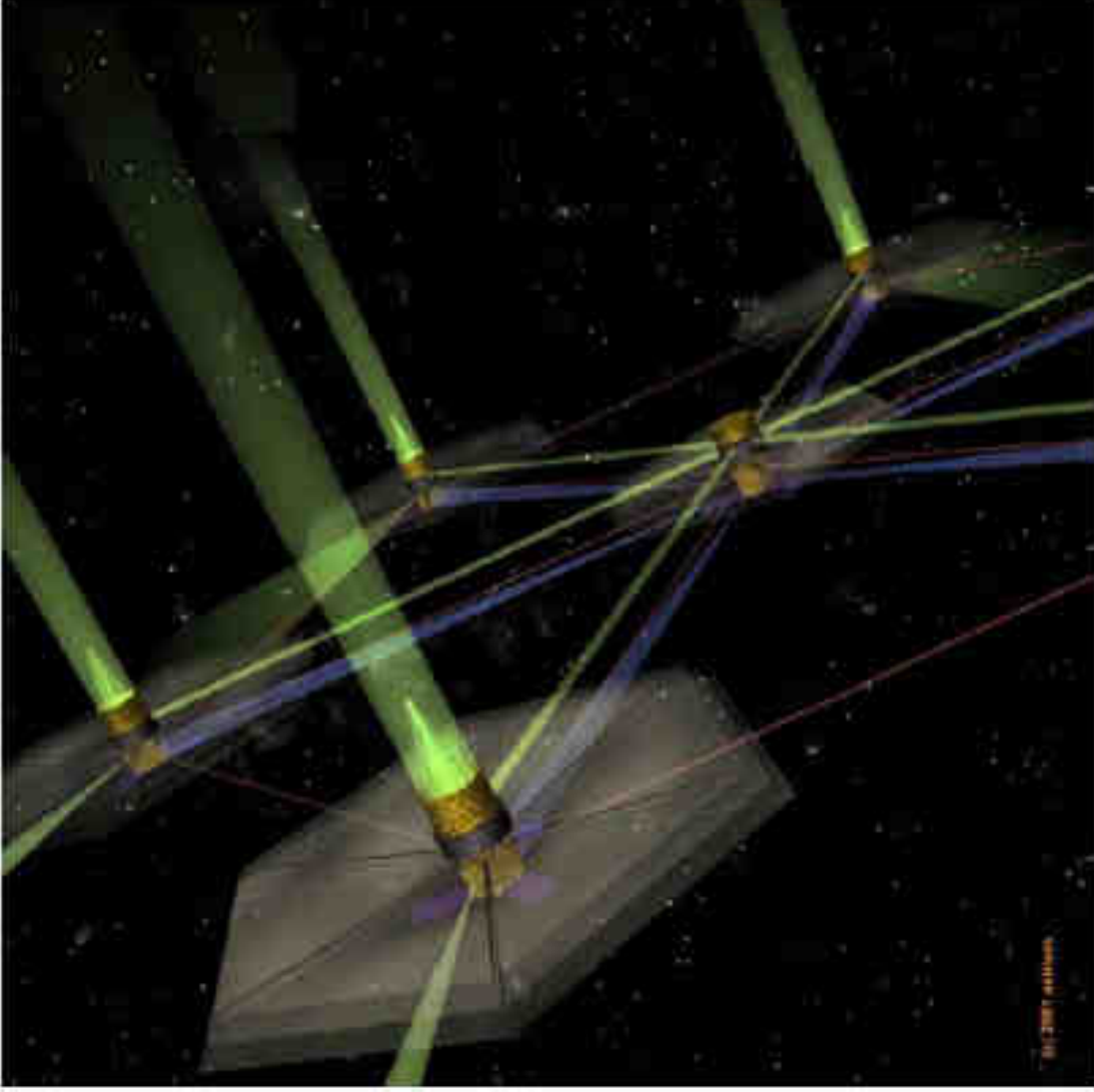
- **Constellation** of 3 to 6 Darwin-type satellites

Darwin Mission Description (II)
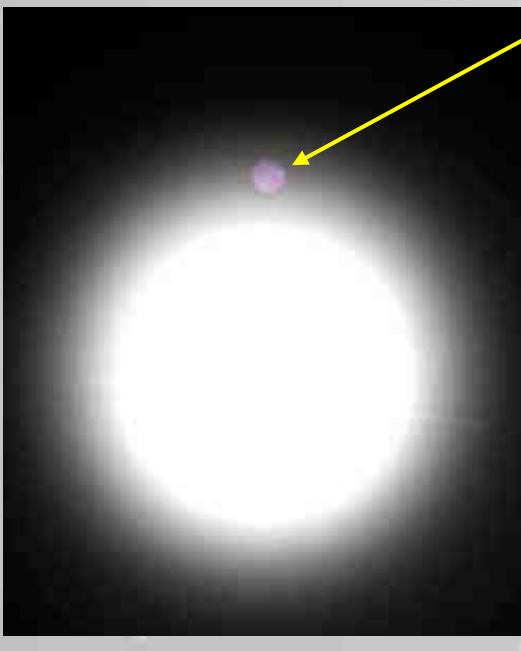
- **Exo-planets.**
  - The first one was discovered by Latham et al. in 1989.
  - and Mayor and Queloz (1995), Butler y Marcy (1996).
  - Nowadays (2007) we know more than 200 exo-planets in 140 external systems.

Currently we do not know exo-planets with signs or possibilities of life.

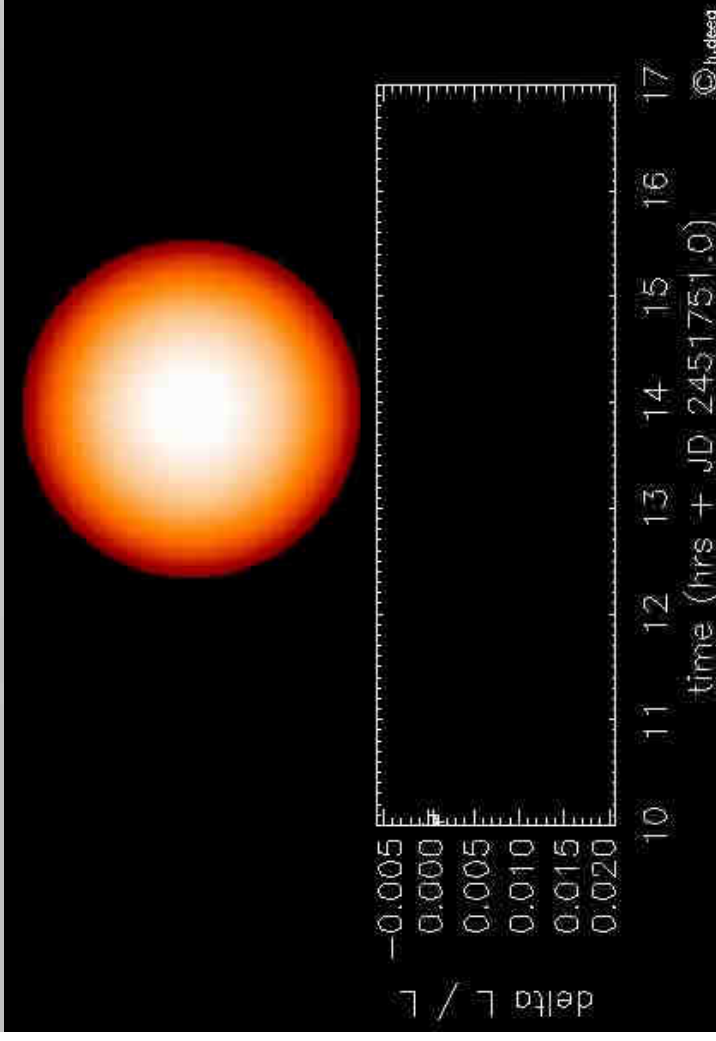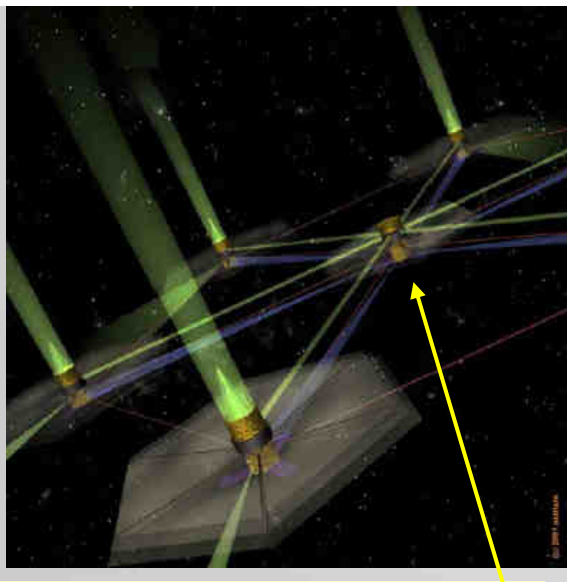*Ver difficult to observe. The near stars hides the exo-planets.*
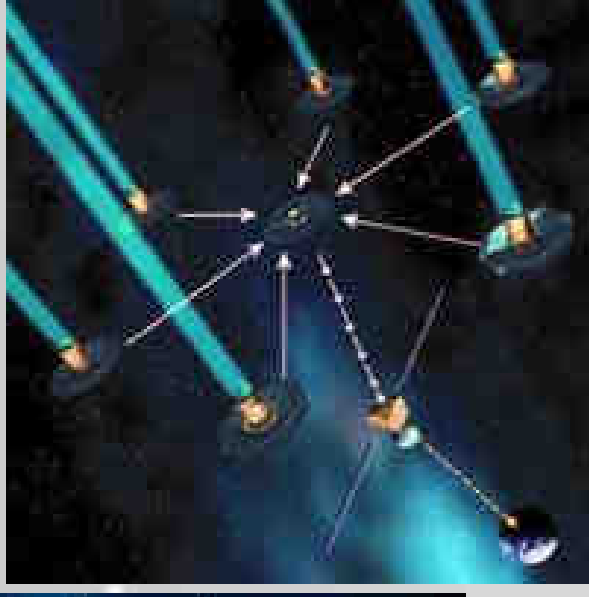
- **Destructive Interferometry**

Combining light from the telescopes

In the Hub

delta L / L

time (hrs + JD 2451751.0)

Darwin Satellite (I)

Telescope

Large shields parallels to (X,Y) plane
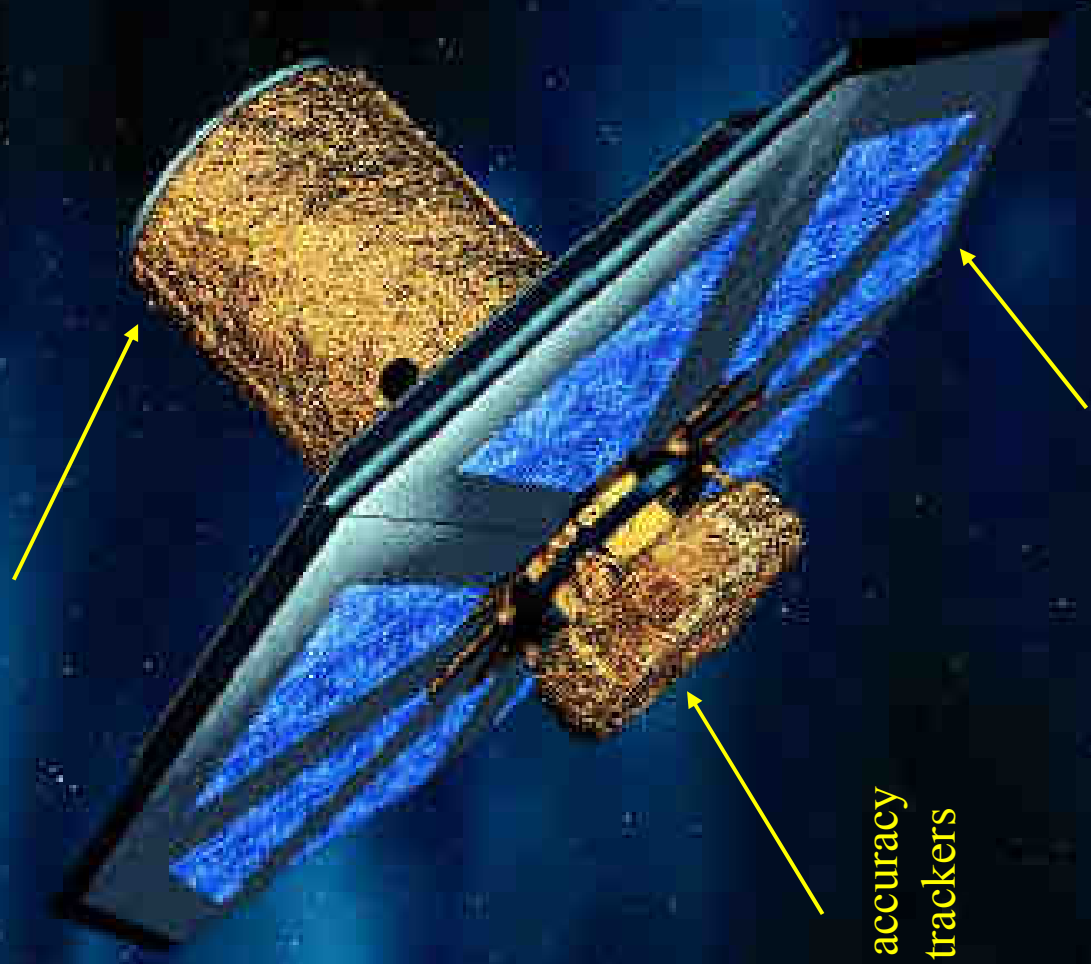
High accuracy star trackers

Darwin Satellite (II)

Thrusters and micro-actuators 6D (FEEPS)

–micro Newton ion thrusters + Magnetic field thrusters

Fine Pointing Metrology (FPM) for 3D fine attitude
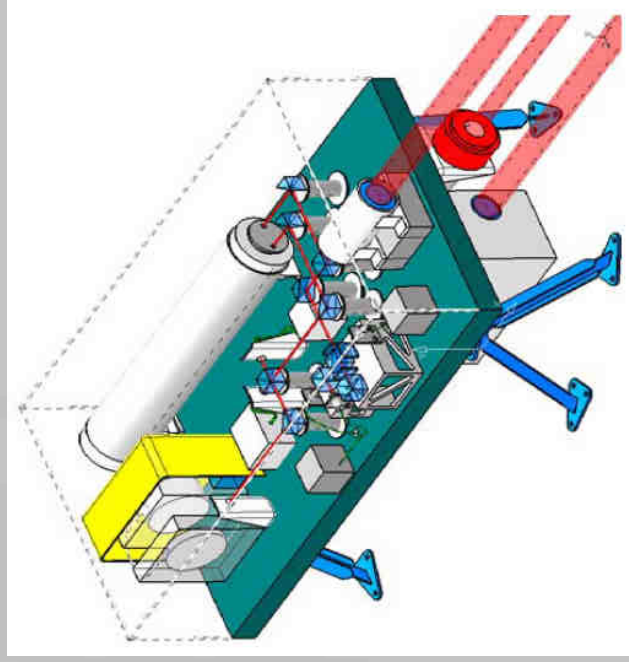
OPD (**Optical Pathlength Difference**) Fringe Tracker for fine position measures

Darwin Satellite (III)

primary mirror (M1)

optical bench

stowed sunshield

deployable M2 support arm

launch-lock bi-pods

secondary mirror (M2) assembly

support structure

lower stack interface points

payload radiator

optical beam cut-outs

thruster, RF metrology/ antenna boom

on-station bi-pods

stowed sunshield

EADS ASTRIUM
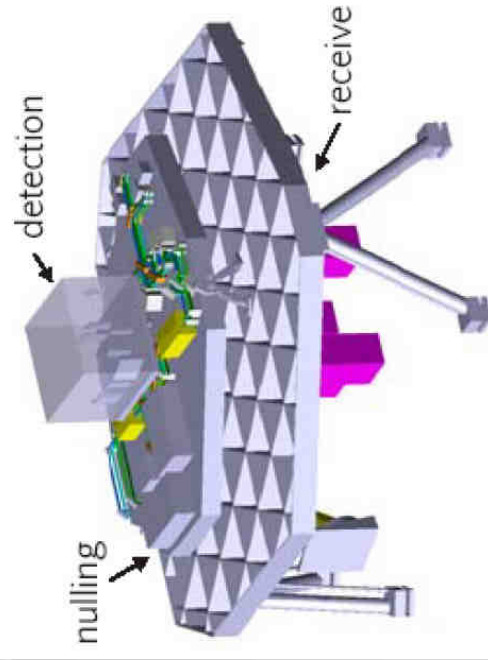
Hub satellite (Combinator)
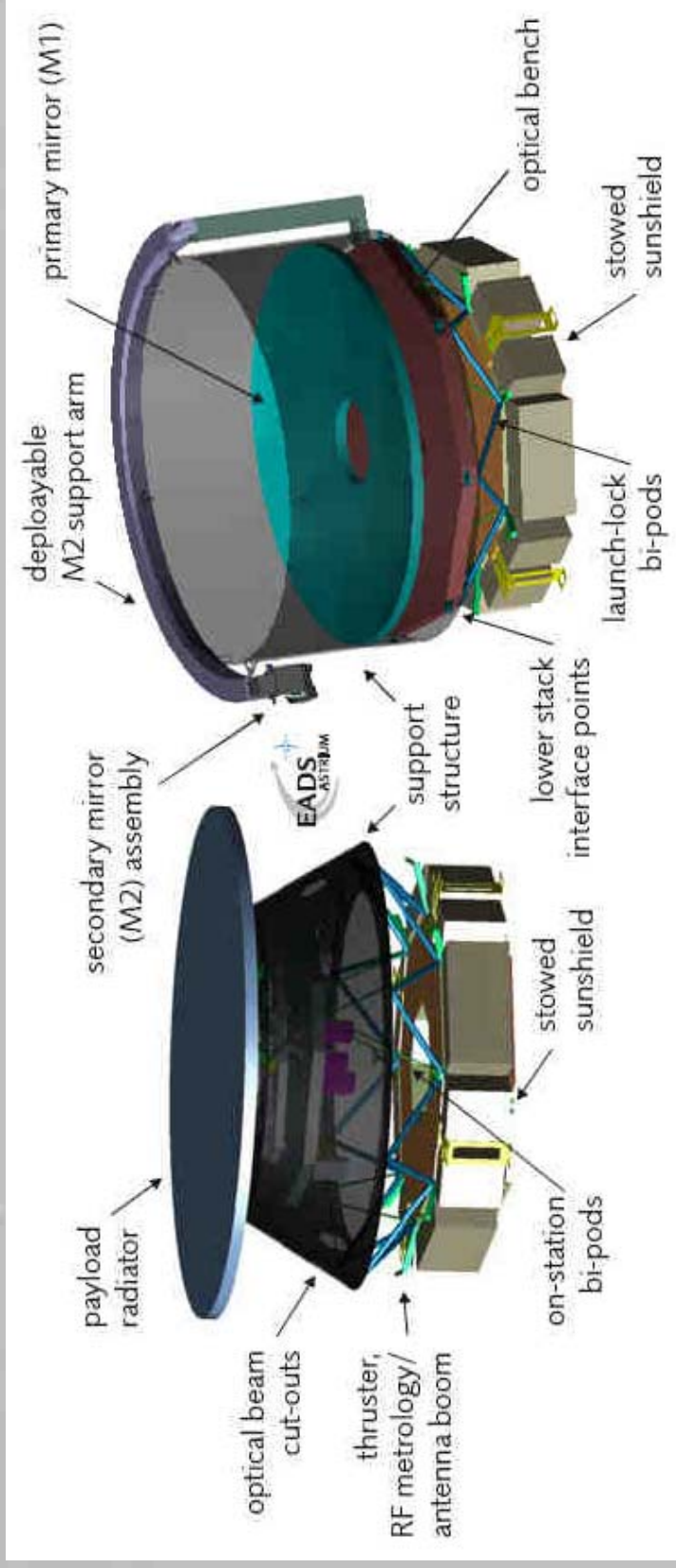
Darwin satellite (Collector)

Heigh: up to 52 m
Diameter: up to 5.4 m
Max. Liftoff mass : 746 tonnes
Max. Payload mass : 9.5 tonnes

operational orbit

L2

1.5x10^6 km

transfer orbit

earth

1.5x10^8 km

sun
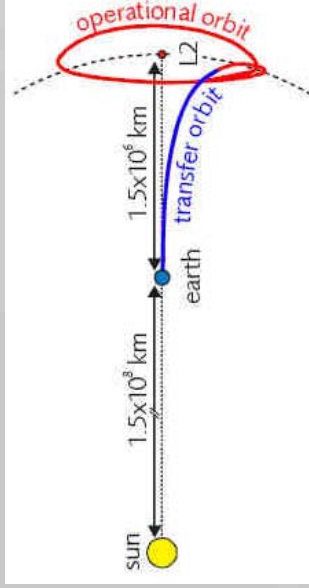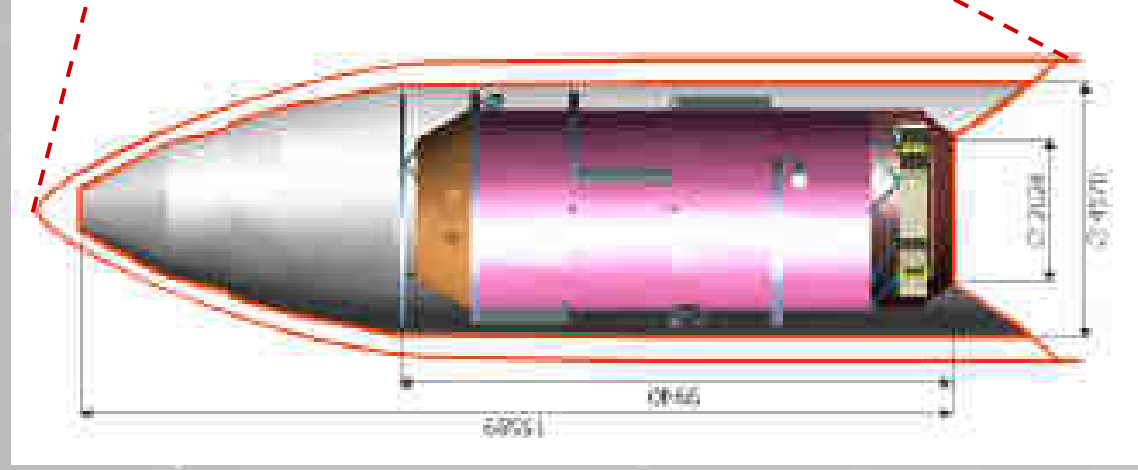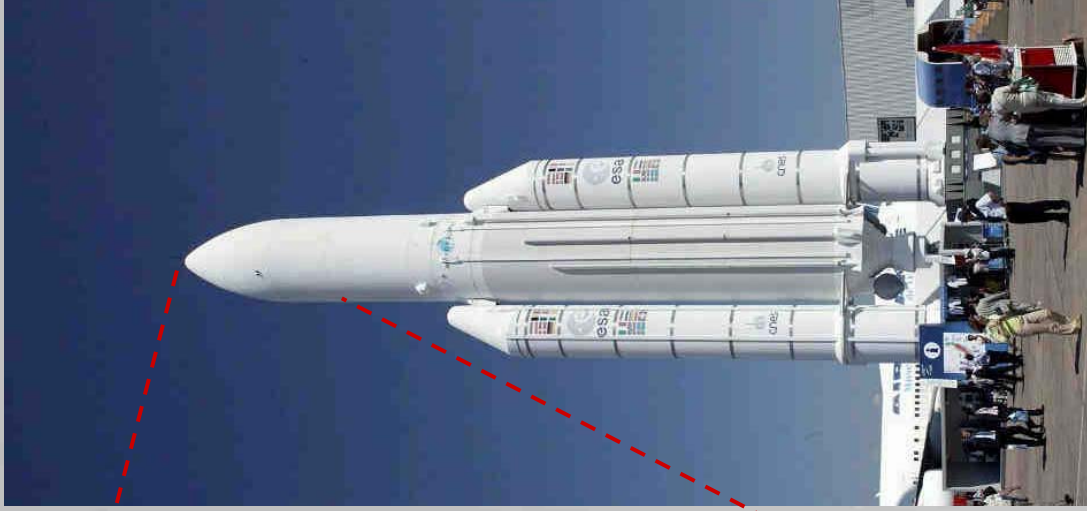
Launcher ARIANE V

with 4 Darwin sattelites
and a hub satellite

DARWIN

LISA

L_2

Earth

L_1

L_4

L_5

Sun

L_3

$\dot{\theta}$
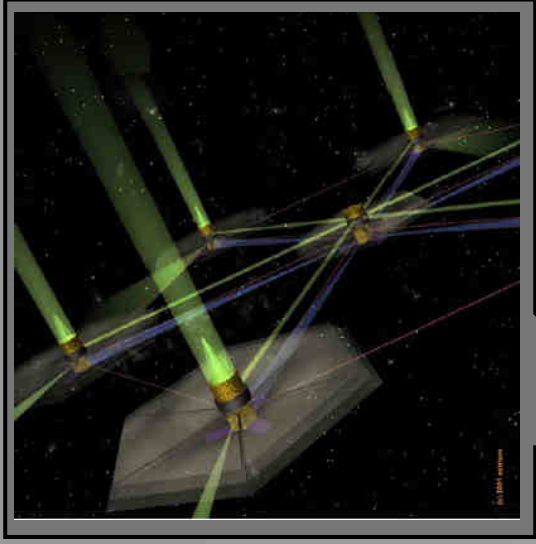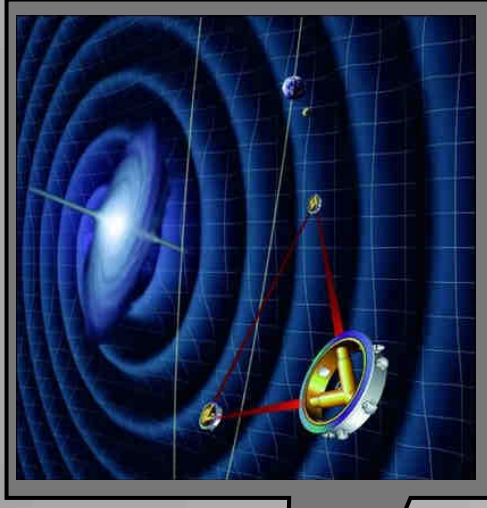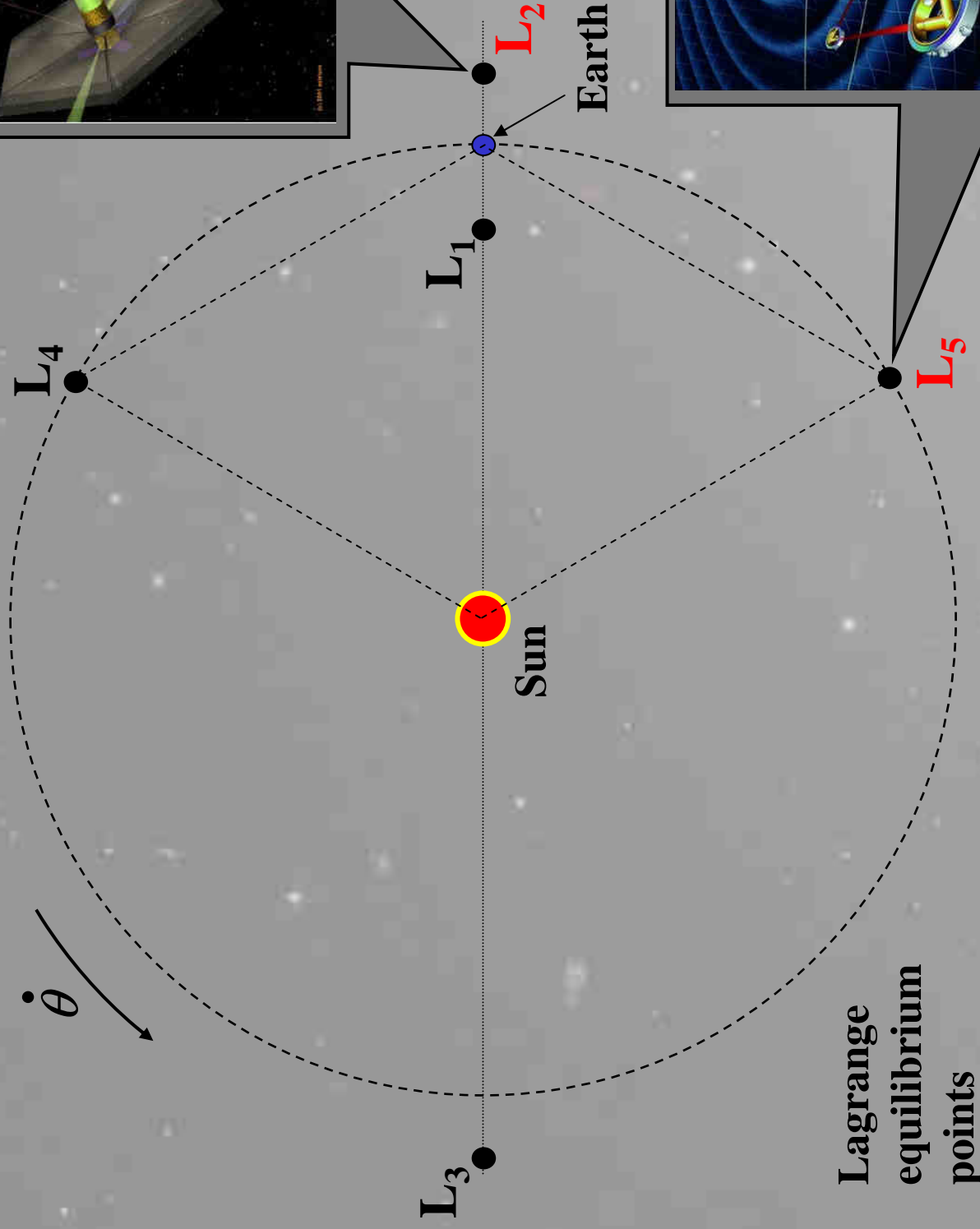
Lagrange
equilibrium
points

Sun-Earth Distance = 1 AU = 150 million km

Satellite Description (I)

- The large sun-shield protect the instruments from the sun-light

- Sun-shield characteristics:
  - Parallel to (X,Y) plan
  - Modelled with 6 large flexible beams attached to the rigid structure
    ⇒ FLIMSY APPENDAGES

Satellite Description (II)

- ## Satellite dimensions

  - body mass : 500 kg
  - cylinder with Zcont as revolution axis. 2 m diameter and 2 m height
  - beam mass : 7 kg * 6 beams = 42 kg
  - length of simple beam : 4 m

- ## Flexible modes

  - Validated with finite elements methods
  - 1st flexible mode has been considered for each beam and along its X and Y axes

  SYSTEM DYNAMICS UNCERTAINTY
  The satellite parameters vary within a certain range of uncertainty

Parameter	Uncertainty range
Frequency	[0.05 , 0.5] Hz
Damping	[0.1 , 1] %
Mass	5 %
Inertia	1 %

Mario Garcia-Sanz

Satellite Modeling (I)

$$
\begin{array}{c} \text{Position} \\ \left\{ \begin{array}{c} \\ \\ \\ \end{array} \right. \end{array}
\begin{bmatrix} x(s) \\ y(s) \\ z(s) \\ \varphi(s) \\ \theta(s) \\ \psi(s) \end{bmatrix}
=
\begin{bmatrix}
p_{11}(s) & p_{12}(s) & p_{13}(s) & p_{14}(s) & p_{15}(s) & p_{16}(s) \\
p_{21}(s) & p_{22}(s) & p_{23}(s) & p_{24}(s) & p_{25}(s) & p_{26}(s) \\
p_{31}(s) & p_{32}(s) & p_{33}(s) & p_{34}(s) & p_{35}(s) & p_{36}(s) \\
p_{41}(s) & p_{42}(s) & p_{43}(s) & p_{44}(s) & p_{45}(s) & p_{46}(s) \\
p_{51}(s) & p_{52}(s) & p_{53}(s) & p_{54}(s) & p_{55}(s) & p_{56}(s) \\
p_{61}(s) & p_{62}(s) & p_{63}(s) & p_{64}(s) & p_{65}(s) & p_{66}(s)
\end{bmatrix}
\begin{bmatrix} F_x(s) \\ F_y(s) \\ F_z(s) \\ T_\varphi(s) \\ T_\theta(s) \\ T_\psi(s) \end{bmatrix}
$$

Position
Attitude
Force
Torque

where every $p_{ij}(s)$, i, j = 1, 2, ... 6, is a **50 order** Laplace transfer function with **uncertainty**.

Rigid body
beams
CoM
Flyer
z_{cont}
x_{cont}
y_{cont}
2 m
2 m
1 m
1 m
4 m
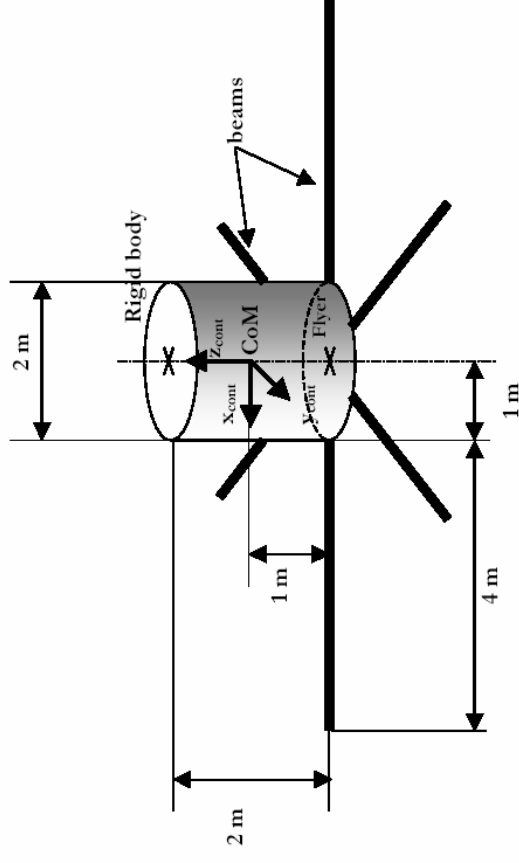
Satellite Modeling (II)

**Darwin Flyer
6DOF Dynamics**

Bode
plots of
the plant
matrix
elements

$$\begin{bmatrix} x(s) \\ y(s) \\ z(s) \\ \varphi(s) \\ \theta(s) \\ \psi(s) \end{bmatrix} = \begin{bmatrix} p_{11}(s) & p_{12}(s) & p_{13}(s) & p_{14}(s) & p_{15}(s) & p_{16}(s) \\ p_{21}(s) & p_{22}(s) & p_{23}(s) & p_{24}(s) & p_{25}(s) & p_{26}(s) \\ p_{31}(s) & p_{32}(s) & p_{33}(s) & p_{34}(s) & p_{35}(s) & p_{36}(s) \\ p_{41}(s) & p_{42}(s) & p_{43}(s) & p_{44}(s) & p_{45}(s) & p_{46}(s) \\ p_{51}(s) & p_{52}(s) & p_{53}(s) & p_{54}(s) & p_{55}(s) & p_{56}(s) \\ p_{61}(s) & p_{62}(s) & p_{63}(s) & p_{64}(s) & p_{65}(s) & p_{66}(s) \end{bmatrix} \begin{bmatrix} F_x(s) \\ F_y(s) \\ F_z(s) \\ T_\varphi(s) \\ T_\theta(s) \\ T_\psi(s) \end{bmatrix}$$

2.17
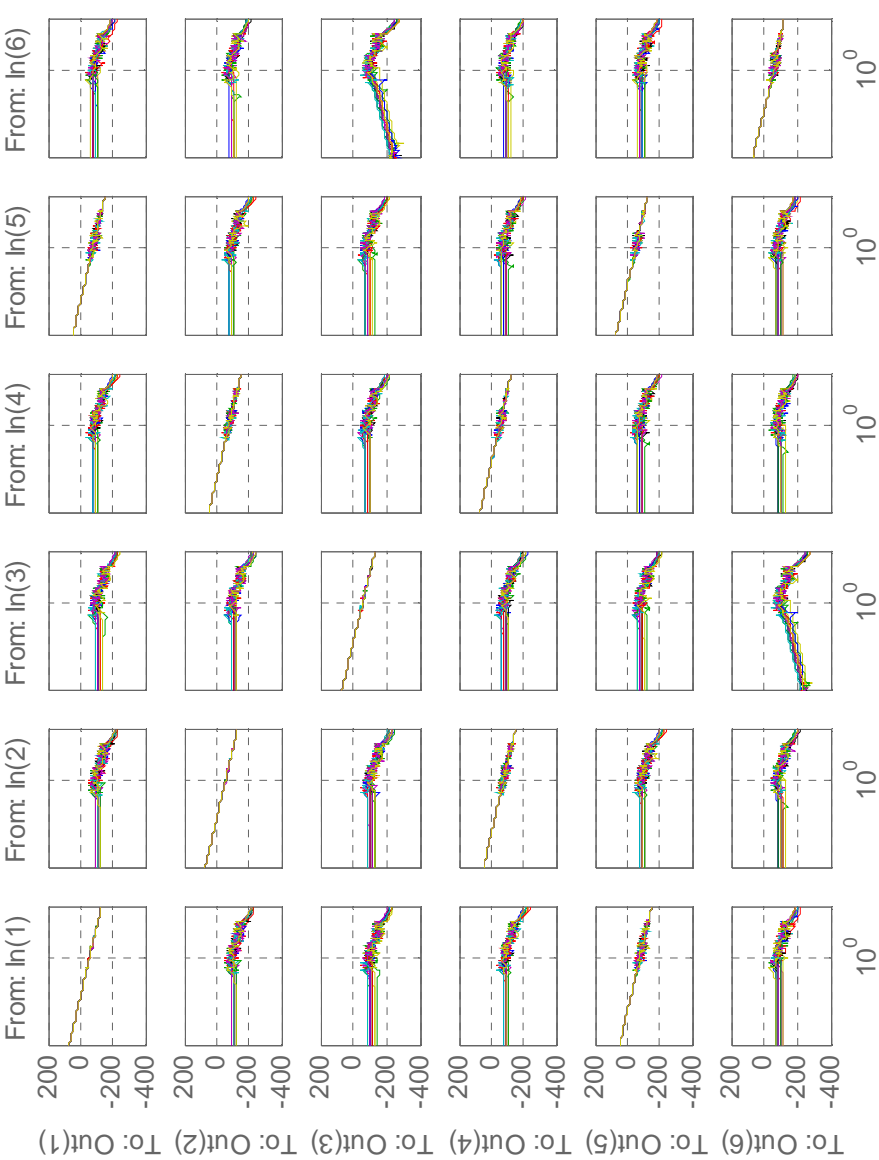
Specificacions

Darwin-type Flyer Requirements
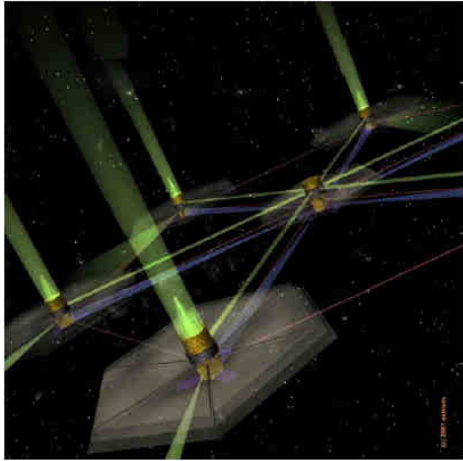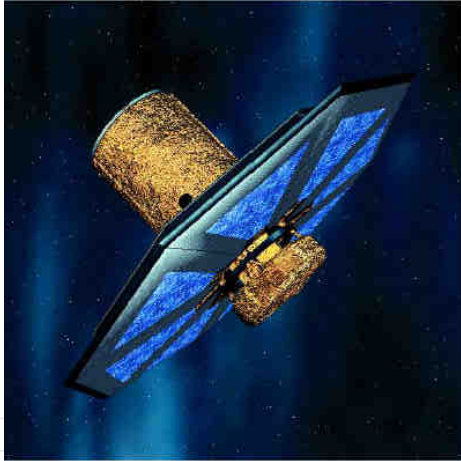
|	Objective	Numerical Requirement
Astronomical Requirements	Position accuracy	Maximum absolute value: 1 μm for all axes
		Standard deviation: 0.33 μm for all axes
	Pointing accuracy	Maximum absolute value: 25.5 mas for all axes (3 σ)
		Standard deviation: 8.5 mas for all axes (1 σ)
Engineering Requirements	Bandwidth	~ 0.01 Hz for all axes
	Saturation limits	Maximum force: 150 μN Maximum torque: 150 μNm
	Rejection of high frequency noises (from measurement and actuation)	High roll-off after the bandwidth
Control Requirements	Stability margins	$\max_{\omega}\|T(j\omega)\| < 2$ $\max_{\omega}\|S(j\omega)\| < 2$
	Loop interaction	Minimum
	Rejection of flexible modes	Maximum
	Controller complexity and order	Minimum

2.18

Mario Garcia-Sanz

Project Objetives

- **Analysis** of the new methodology:
  non-diagonal MIMO QFT robust control design:

- García-Sanz M., Egaña I. (2002).
  Quantitative Non-diagonal Controller Design for Multivariable Systems with Uncertainty.
  Int. J. Robust Nonlinear Control, Vol. 12, No. 4, pp. 321-333.

- García-Sanz M., Egaña I., Barreras M. (2005).
  Design of quantitative feedback theory non-diagonal controllers for use in uncertain multiple-input multiple-output systems.
  IEE Control Theory and Applications. Vol. 152, N. 02, pp. 177-187.

- García-Sanz M., Barreras M. (2006).
  Non-diagonal QFT controller design for a 3-input 3-output industrial Furnace.
  J. of Dynamic Systems, Measurement & Control, ASME, Vol. 128, pp. 319-329. USA.

- Garcia-Sanz M., Eguinoa I., Barreras M., Bennani S. (2008).
  Non-diagonal MIMO QFT Controller Design for Darwin-type Spacecraft with large flimsy appendages.
  *J.Dynamic Systems, Measurement & Control, ASME,USA.*Vol.130, January.

- **Application**: Control of Position + Attitude of a Darwin spacecraft with flexible appendages

- **Comparison** with previous studies (H-infinity and diagonal MIMO QFT)

BENCHMARK SIMULATOR

**AOCS for Large Flimsy Appendages
Benchmark 6 DOF
UPNA Evaluation**
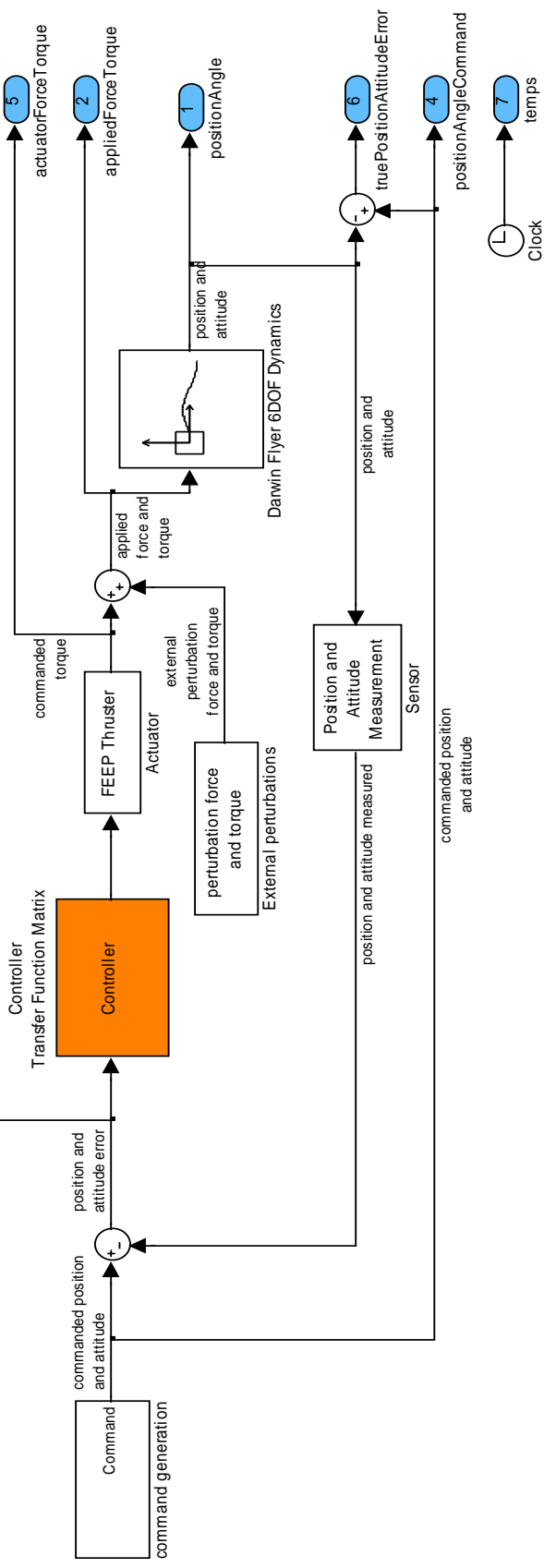
*Developed by Astrium Space
for ESA-ESTEC (Holland)*

300 different plants due
to uncertainty.
Monte-Carlo analysis

2.20

Mario Garcia-Sanz

COUPLING ANALYSIS AND CONTROLLER STRUCTURE (I)

RGA analysis of the Darwin-type satellite dynamic model performed for different frequencies
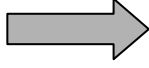
$$RGA(j\omega) =$$

$$= \begin{bmatrix} \lambda_{11} & \lambda_{12} & \cdots & \lambda_{1n} \\ \lambda_{21} & \lambda_{22} & \cdots & \lambda_{2n} \\ \cdots & \cdots & \cdots & \cdots \\ \lambda_{n1} & \lambda_{n2} & \cdots & \lambda_{mn} \end{bmatrix} =$$

$$= P(j\omega) \otimes (P^{-1}(j\omega))^T$$

Mario Garcia-Sanz

2.21

From low frequency up to 0.19 rad/sec
And from 3.51 rad/sec to infinity

$$\left|RGA_{(\omega=6.28\cdot10^{-4}\,\text{rad/sec})}\right| = \begin{bmatrix} 1.0064 & 0 & 0 & 0 & 0.0064 & 0 \\ 0 & 1.0064 & 0 & 0.0064 & 0 & 0 \\ 0 & 0 & 1 & 0 & 0 & 0 \\ 0 & 0.0064 & 0 & 1.0064 & 0 & 0 \\ 0.0064 & 0 & 0 & 0 & 1.0064 & 0 \\ 0 & 0 & 0 & 0 & 0 & 1 \end{bmatrix}$$

Other results

$$\left|RGA_{(\omega=0.8\,\text{rad/sec})}\right| = \begin{bmatrix} 1.1674 & 0.0001 & 0.0000 & 0.0012 & 0.3720 & 0.0001 \\ 0.0001 & 1.0180 & 0.0000 & 0.0305 & 0.0013 & 0.0004 \\ 0.0000 & 0.0000 & 4.8592 & 0.3468 & 4.1456 & 0.0000 \\ 0.0012 & 0.0305 & 0.3468 & 3.2030 & 2.3865 & 0.0006 \\ 0.3720 & 0.0013 & 4.1456 & 2.3865 & 7.2470 & 0.0008 \\ 0.0001 & 0.0004 & 0.0000 & 0.0006 & 0.0008 & 1.0009 \end{bmatrix}$$

$$\left|RGA_{(\omega=1\,\text{rad/sec})}\right| = \begin{bmatrix} 0.9899 & 0.0002 & 0.0000 & 0.0001 & 0.0003 & 0.0102 \\ 0.0002 & 0.9082 & 0.0000 & 0.0050 & 0.0009 & 0.0963 \\ 0.0000 & 0.0000 & 3.1307 & 2.3373 & 0.1110 & 0.0000 \\ 0.0001 & 0.0050 & 2.3373 & 12.5674 & 9.4613 & 0.0690 \\ 0.0003 & 0.0009 & 0.1110 & 9.4613 & 10.2042 & 0.0302 \\ 0.0102 & 0.0963 & 0.0000 & 0.0690 & 0.0302 & 0.7970 \end{bmatrix}$$

Results of the RGA matrix
for various frequencies
(significant values in bold)

First choice

$$|RGA|_{(\omega=6.28\cdot10^{-4}\ \text{rad/sec})} = \begin{bmatrix} 1.0064 & 0 & 0 & 0 & 0.0064 & 0 \\ 0 & 1.0064 & 0 & 0.0064 & 0 & 0 \\ 0 & 0 & 1 & 0 & 0 & 0 \\ 0 & 0.0064 & 0 & 1.0064 & 0 & 0 \\ 0.0064 & 0 & 0 & 0 & 1.0064 & 0 \\ 0 & 0 & 0 & 0 & 0 & 1 \end{bmatrix}$$

$$G(s) = \begin{bmatrix} g_{11}(s) & 0 & 0 & 0 & g_{15}(s) & 0 \\ 0 & g_{22}(s) & 0 & g_{24}(s) & 0 & 0 \\ 0 & 0 & g_{33}(s) & 0 & 0 & 0 \\ 0 & g_{42}(s) & 0 & g_{44}(s) & 0 & 0 \\ g_{51}(s) & 0 & 0 & 0 & g_{55}(s) & 0 \\ 0 & 0 & 0 & 0 & 0 & g_{66}(s) \end{bmatrix}$$

Control Subsystem	Controller Element	Corresponding Plant Description
SISO: loop 3	g_{33}	$\text{Force}_z \rightarrow \text{Position}_z$
SISO: loop 6	g_{66}	$\text{Torque}_z \rightarrow \text{Attitude}_z$
2x2 MIMO: loops 1 and 5	g_{11}	$\text{Force}_x \rightarrow \text{Position}_x$
	g_{55}	$\text{Torque}_y \rightarrow \text{Attitude}_y$
	g_{51}	$\text{Force}_x \rightarrow \text{Attitude}_y$
	g_{15}	$\text{Torque}_y \rightarrow \text{Position}_x$
2x2 MIMO: loops 2 and 4	g_{22}	$\text{Force}_y \rightarrow \text{Position}_y$
	g_{44}	$\text{Torque}_x \rightarrow \text{Attitude}_x$
	g_{42}	$\text{Force}_y \rightarrow \text{Attitude}_x$
	g_{24}	$\text{Torque}_x \rightarrow \text{Position}_y$

Mario Garcia-Sanz

If requirements are not fulfilled, Second choice:

$$G(s) = \begin{bmatrix} g_{11}(s) & 0 & 0 & 0 & g_{15}(s) & 0 \\ 0 & g_{22}(s) & 0 & g_{24}(s) & 0 & 0 \\ 0 & 0 & g_{33}(s) & g_{34}(s) & g_{35}(s) & 0 \\ 0 & g_{42}(s) & g_{43}(s) & g_{44}(s) & g_{45}(s) & 0 \\ g_{51}(s) & 0 & g_{53}(s) & g_{54}(s) & g_{55}(s) & 0 \\ 0 & 0 & 0 & 0 & 0 & g_{66}(s) \end{bmatrix}$$

$$\left| RGA \right|_{(\omega=0.8 \text{ rad/sec})} = \begin{bmatrix} \mathbf{1.1674} & 0.0001 & 0.0000 & 0.0012 & 0.3720 & 0.0001 \\ 0.0001 & \mathbf{1.0180} & 0.0000 & 0.0305 & 0.0013 & 0.0004 \\ 0.0000 & 0.0000 & \mathbf{4.8592} & 0.3468 & \mathbf{4.1456} & 0.0000 \\ 0.0012 & 0.0305 & 0.3468 & \mathbf{3.2030} & \mathbf{2.3865} & 0.0006 \\ 0.3720 & 0.0013 & \mathbf{4.1456} & \mathbf{2.3865} & \mathbf{7.2470} & 0.0008 \\ 0.0001 & 0.0004 & 0.0000 & 0.0006 & 0.0008 & \mathbf{1.0009} \end{bmatrix}$$

According to:

$$\left| RGA \right|_{(\omega=1 \text{ rad/sec})} = \begin{bmatrix} \mathbf{0.9899} & 0.0002 & 0.0000 & 0.0001 & 0.0003 & 0.0102 \\ 0.0002 & \mathbf{0.9082} & 0.0000 & 0.0050 & 0.0009 & 0.0963 \\ 0.0000 & 0.0000 & \mathbf{3.1307} & 2.3373 & 0.1110 & 0.0000 \\ 0.0001 & 0.0050 & 2.3373 & \mathbf{12.5674} & \mathbf{9.4613} & 0.0690 \\ 0.0003 & 0.0009 & 0.1110 & \mathbf{9.4613} & \mathbf{10.2042} & 0.0302 \\ 0.0102 & 0.0963 & 0.0000 & 0.0690 & 0.0302 & \mathbf{0.7970} \end{bmatrix}$$

$$\left| RGA \right|_{(\omega=6.28\cdot10^{-4} \text{ rad/sec})} = \begin{bmatrix} \mathbf{1.0064} & 0 & 0 & 0 & \mathbf{0.0064} & 0 \\ 0 & \mathbf{1.0064} & 0 & \mathbf{0.0064} & 0 & 0 \\ 0 & 0 & \mathbf{1} & 0 & \mathbf{1.0064} & 0 \\ 0 & \mathbf{0.0064} & 0 & \mathbf{1.0064} & 0 & 0 \\ \mathbf{0.0064} & 0 & \mathbf{1.0064} & 0 & \mathbf{1.0064} & 0 \\ 0 & 0 & 0 & 0 & 0 & \mathbf{1} \end{bmatrix}$$

Mario Garcia-Sanz

ROBUST SPECIFICATIONS (I)
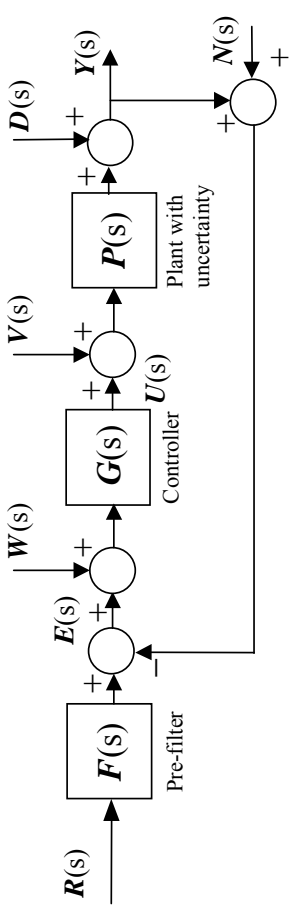
Transfer functions and specification models	Type	Description
$$\left|T_1(j\omega)\right| = \left|\frac{L(j\omega)}{1+L(j\omega)}\right| = \left|\frac{U(j\omega)}{V(j\omega)}\right| = \left|\frac{Y(j\omega)}{N(j\omega)}\right| = \left|\frac{Y(j\omega)}{W(j\omega)}\right| \le \delta_1(\omega), \omega \in \Omega_1$$	1	- Robust stability - Sensor noise attenuation - Attenuation of external perturbations and flexible modes
$$\left|T_2(j\omega)\right| = \left|\frac{1}{1+L(j\omega)}\right| = \left|\frac{Y(j\omega)}{D(j\omega)}\right| = \left|\frac{E(j\omega)}{N(j\omega)}\right| \le \delta_2(\omega), \ \omega \in \Omega_2$$	2	- Robust sensitivity - Sensor noise attenuation
$$\left|T_3(j\omega)\right| = \left|\frac{P(j\omega)}{1+L(j\omega)}\right| = \left|\frac{Y(j\omega)}{V(j\omega)}\right| = \left|\frac{E(j\omega)}{V(j\omega)}\right| \le \delta_3(\omega), \ \omega \in \Omega_3$$	3	- Robust disturbance rejection at plant input
$$\left|T_4(j\omega)\right| = \left|\frac{G(j\omega)}{1+L(j\omega)}\right| = \left|\frac{U(j\omega)}{D(j\omega)}\right| = \left|\frac{U(j\omega)}{N(j\omega)}\right| = \left|\frac{U(j\omega)}{W(j\omega)}\right| = \left|\frac{U(j\omega)}{R(j\omega)F(j\omega)}\right| \le \delta_4(\omega), \omega \in \Omega_4$$	4	- Robust control effort attenuation of actuator noise, sensor noise and external perturbations

ROBUST SPECIFICATIONS (II)
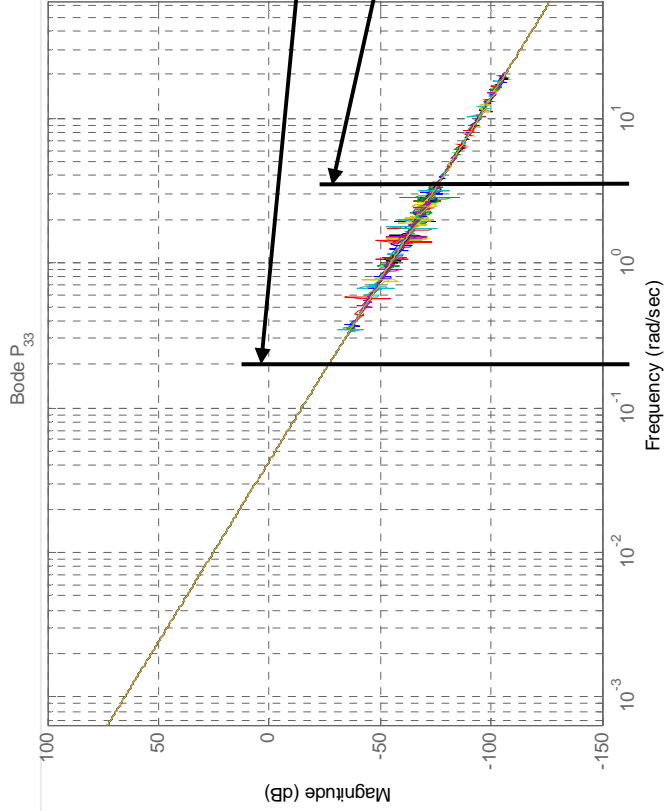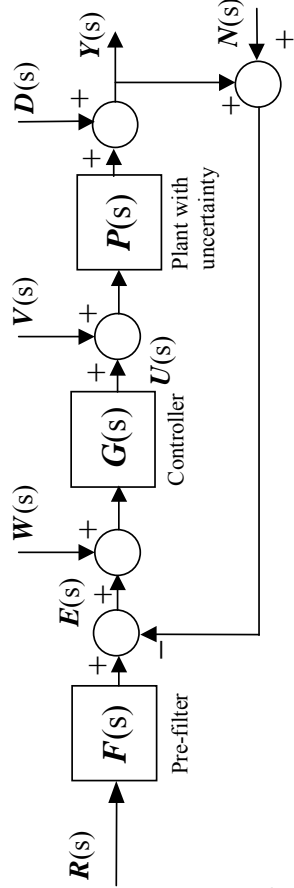
$10^{-4} = 0.0001$ Hz $= 0.00062$ rad/s

$10^{-1.5} = 0.0316$ Hz $= 0.2$ rad/s

$10^{-0.25} = 0.562$ Hz $= 3.53$ rad/s

$10^1 = 10$ Hz $= 62.8$ rad/s
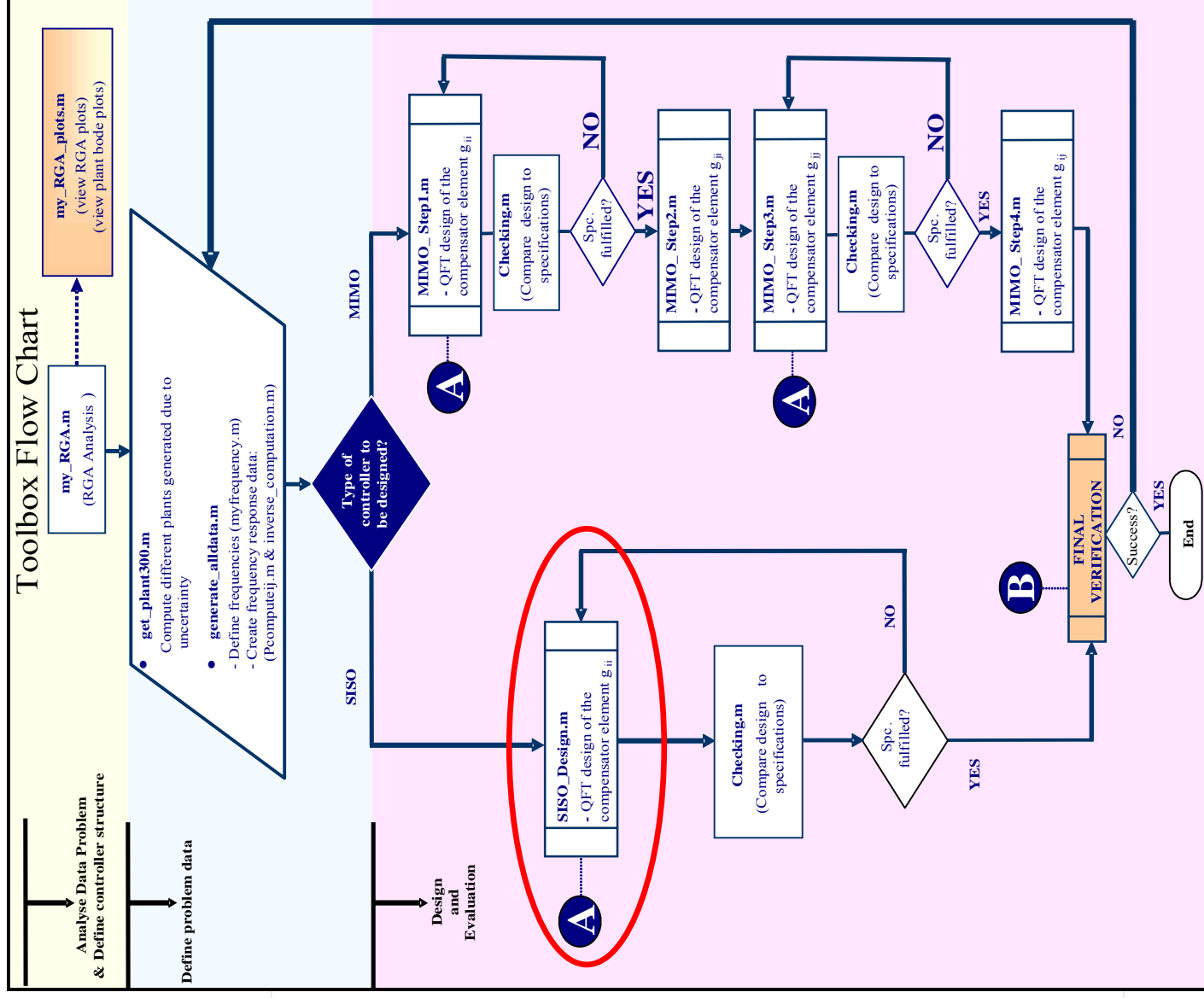
Bode P$_{33}$

Frequencies of interest (Hz)	
freq1	logspace(-4, -1.5, 4)
freq2 (Problematic range of frequencies)	logspace(-1.5, -0.25, 12)
freq3	logspace(-0.25, 1, 3)

Mario Garcia-Sanz

2.26

SISO DESIGNS

Classical QFT robust control design for SISO subsystems:

– Loop 3

– Loop 6

Steps 1a and 1b

Toolbox Flow Chart

Analyse Data Problem & Define controller structure

my_RGA.m
(RGA Analysis)

my_RGA_plots.m
(view RGA plots)
(view plant bode plots)

Define problem data

- **get_plant300.m**
  Compute different plants generated due to uncertainty

- **generate_alldata.m**
  - Define frequencies (myfrequency.m)
  - Create frequency response data:
    (Pcomputeij.m & inverse_computation.m)

Type of controller to be designed?

MIMO

SISO

Design and Evaluation

MIMO_ Step1.m
- QFT design of the compensator element g_{ii}

Checking.m
(Compare design to specifications)

A

Spc. fulfilled?

NO

YES

MIMO_ Step2.m
- QFT design of the compensator element g_{ji}

MIMO_ Step3.m
- QFT design of the compensator element g_{jj}

A

Checking.m
(Compare design to specifications)

Spc. fulfilled?

NO

YES

MIMO_ Step4.m
- QFT design of the compensator element g_{ij}

SISO_Design.m
- QFT design of the compensator element g_{ii}

A

Checking.m
(Compare design to specifications)

Spc. fulfilled?

NO

YES

B

FINAL VERIFICATION

NO

Success?

YES

End

SISO DESIGNS

Robust Performance Specifications

Step 1a) : design of the diagonal controller $g_{33}(s)$

Robust stability (Type 1)

$$\left| \frac{P(s)\,G(s)}{1+P(s)\,G(s)} \right| = |T(s)| \le 1.85$$

Robust disturbance rejection at plant input (Type 3)

Bode Diagram Filter F_{3b} - δ_{3b}, Loop 3.
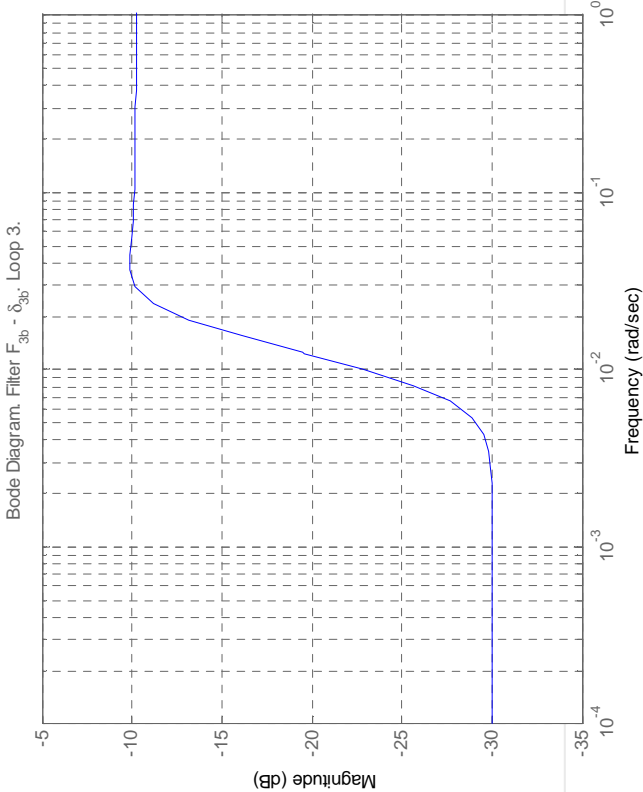
Robust sensitivity (Type 2)

$$\left| \frac{1}{1+P(s)\,G(s)} \right| = |S(s)| \le 2$$

Robust control effort attenuation (Type 4)

Bode Diagram Filter F_{4b} - δ_{4b}, Loop 3.

2.28

Mario Garcia-Sanz
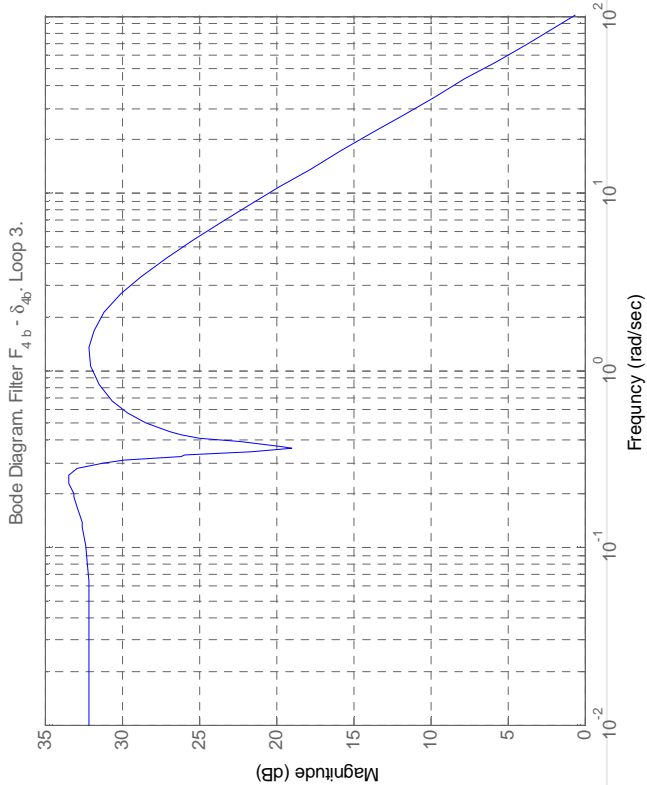
SISO DESIGNS

Step 1a) : design of the diagonal controller $g_{33}(s)$

Templates of the plant $p_{33}(s)$

Loop-shaping $L_{33}(s)=p_{33}(s)\ g_{33}(s)$

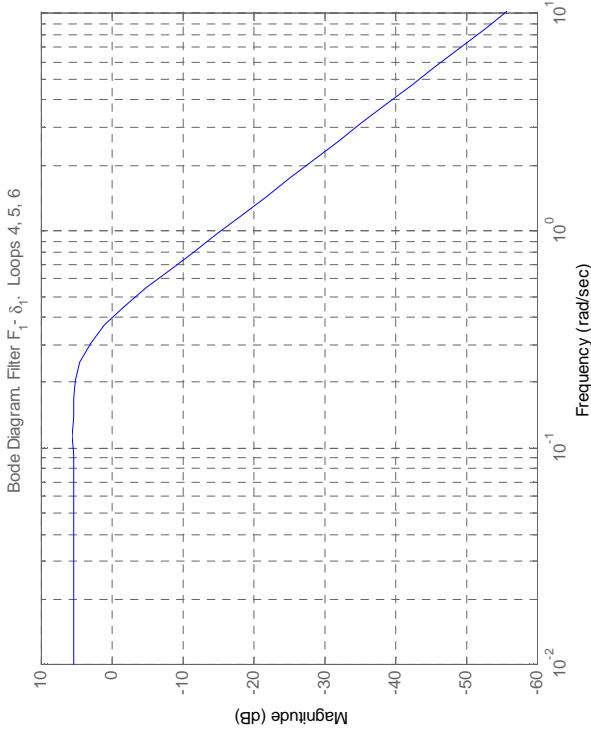The subsystem is found to be **stable** according to the sufficient stability conditions (a and b).

Mario Garcia-Sanz

2.29
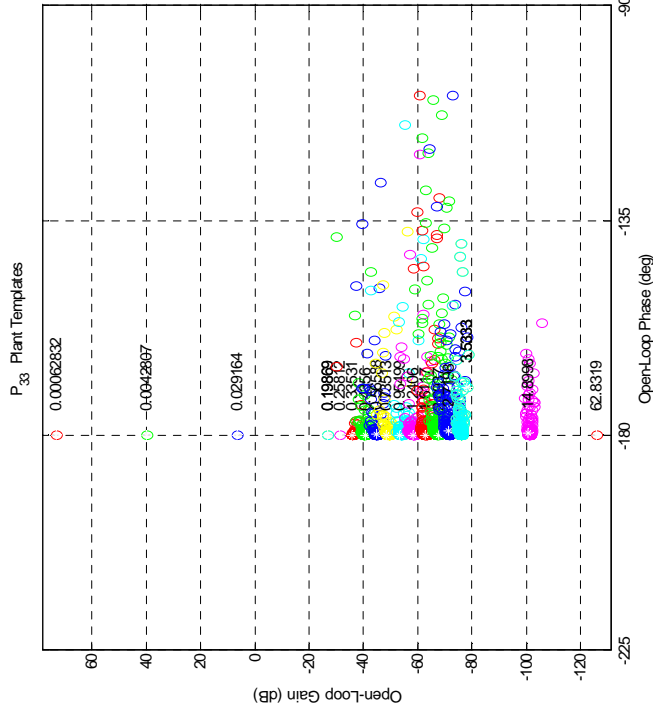
SISO DESIGNS

Step 1b) : design of the diagonal controller $g_{66}(s)$
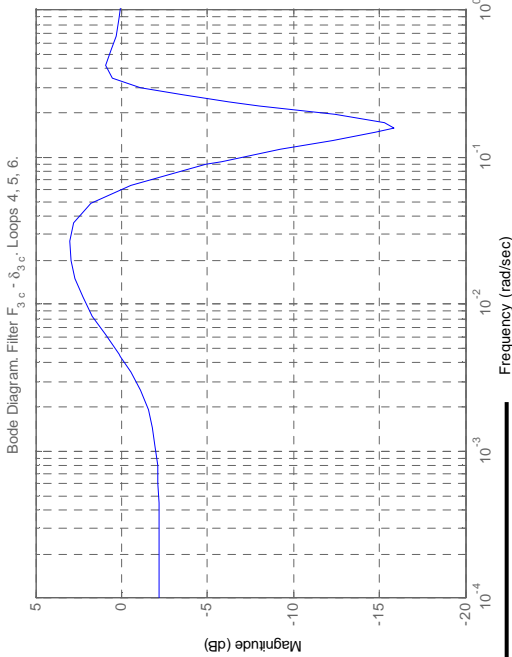
Robust Performance Specifications

Robust disturbance rejection
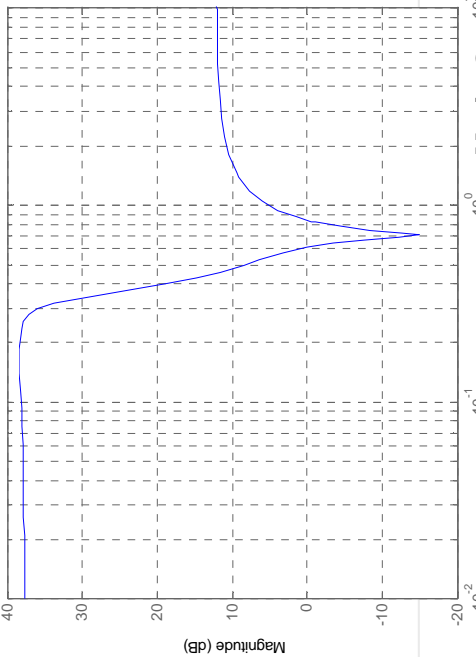at plant input (Type 3)

Robust stability (Type 1)

Bode Diagram. Filter $F_1 - \delta_1$, Loops 4, 5, 6

Bode Diagram. Filter $F_{3c} - \delta_{3c}$, Loops 4, 5, 6.

Robust control effort attenuation (Type 4)

Robust sensitivity (Type 2)

$$\left| \frac{1}{1 + P(s)\,G(s)} \right| = |S(s)| \leq 2$$

SISO DESIGNS

Step 1b) : design of the diagonal controller $g_{66}(s)$

Loop-shaping $L_{66}(s) = p_{66}(s)\,g_{66}(s)$

Templates of the plant $p_{66}(s)$

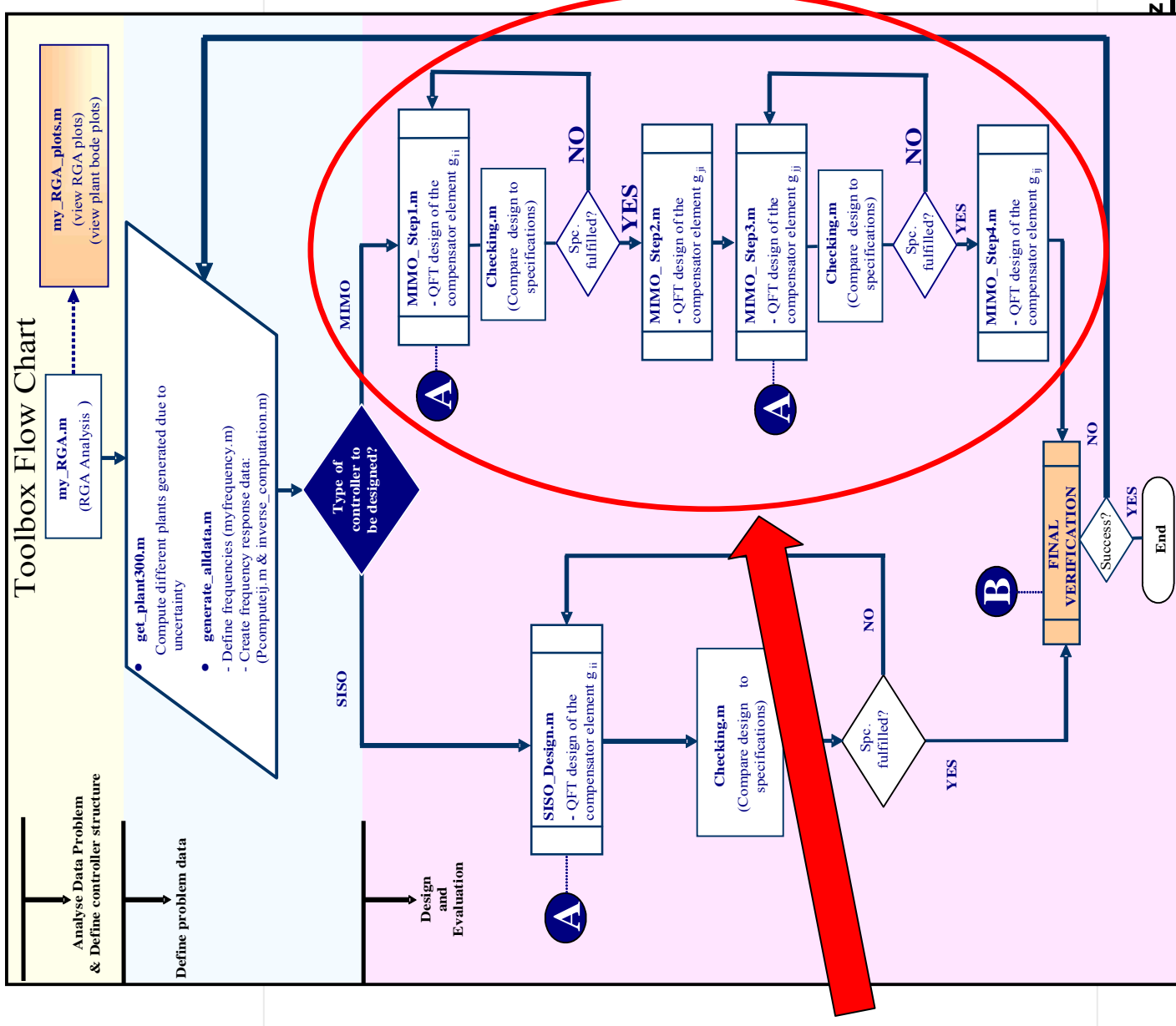The subsystem is found to be **stable** according to the sufficient stability conditions (a and b).

MIMO DESIGNS

Non-diagonal MIMO
QFT design
methodology for
MIMO subsystems:

– Loops 1 and 5

– Loops 2 and 4

**Steps 2 a
and 2 b**

Toolbox Flow Chart

**Analyse Data Problem
& Define controller structure**

Define problem data

**Design
and
Evaluation**

my_RGA_plots.m
(view RGA plots)
(view plant bode plots)

my_RGA.m
(RGA Analysis)

get_plant300.m
Compute different plants generated due to
uncertainty

generate_alldata.m
- Define frequencies (myfrequency.m)
- Create frequency response data:
(Pcomputeij.m & inverse_computation.m)

**Type of
controller to
be designed?**

MIMO

SISO

MIMO_Step1.m
- QFT design of the
compensator element g$_{ii}$

Checking.m
(Compare design to
specifications)

Spc.
fulfilled?

NO

YES

MIMO_Step2.m
- QFT design of the
compensator element g$_{ji}$

MIMO_Step3.m
- QFT design of the
compensator element g$_{jj}$

Checking.m
(Compare design to
specifications)

Spc.
fulfilled?

NO

YES

MIMO_Step4.m
- QFT design of the
compensator element g$_{ij}$

SISO_Design.m
- QFT design of the
compensator element g$_{ii}$

Checking.m
(Compare design to
specifications)

Spc.
fulfilled?

NO

YES

**FINAL
VERIFICATION**

NO

Success?

YES

End

A

A

A

B

$$G = \begin{bmatrix} g_{11} & 0 \\ g_{51} & 0 \end{bmatrix} \Rightarrow \begin{bmatrix} g_{11} & g_{15} \\ g_{51} & g_{55} \end{bmatrix}$$
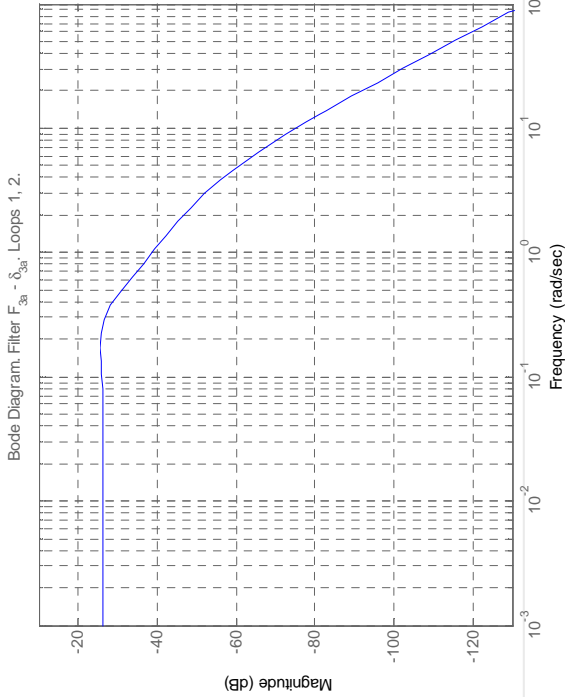
Step 2a) : MIMO subsystem loops 1 and 5

Design of the diagonal controller $g_{11}(s)$

Robust Performance Specifications

Robust stability (Type 1)

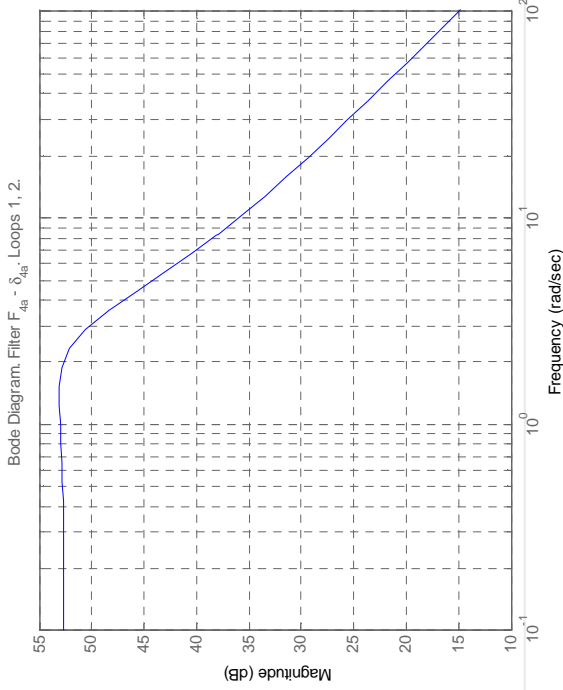$$\left| \frac{P(s)G(s)}{1+P(s)G(s)} \right| = |T(s)| \leq 1.85$$

Robust sensitivity (Type 2)

$$\left| \frac{1}{1+P(s)G(s)} \right| = |S(s)| \leq 2$$

Robust disturbance rejection at plant input (Type 3)

Bode Diagram. Filter F_{3a} - δ_{3a}, Loops 1, 2.

Robust control effort attenuation (Type 4)

Bode Diagram. Filter F_{4a} - δ_{4a}, Loops 1, 2.

2.33

Mario Garcia-Sanz

MIMO DESIGNS

Step 2a) : MIMO subsystem loops 1 and 5

$$G = \begin{bmatrix} g_{11} & 0 \\ g_{51} & 0 \end{bmatrix} \Rightarrow \begin{bmatrix} g_{11} & g_{15} \\ g_{51} & g_{55} \end{bmatrix}$$
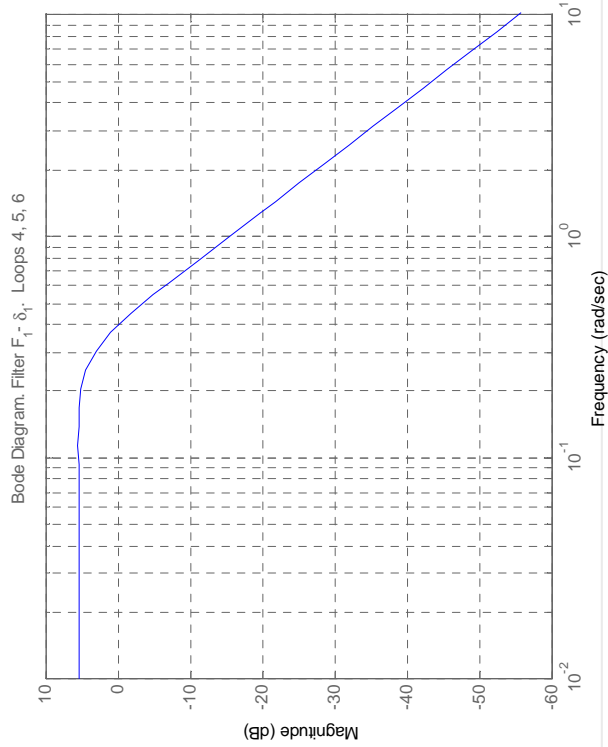
Design of the diagonal controller $g_{11}(s)$

Templates of the plant $(p_{11}{}^{*e}(s))^{-1}$

Loop-shaping $L_{11}(s)= (p_{11}{}^{*e}(s))^{-1}\, g_{11}(s)$

The subsystem is found to be **stable** according to the sufficient stability conditions (a and b).

Mario Garcia-Sanz

2.34
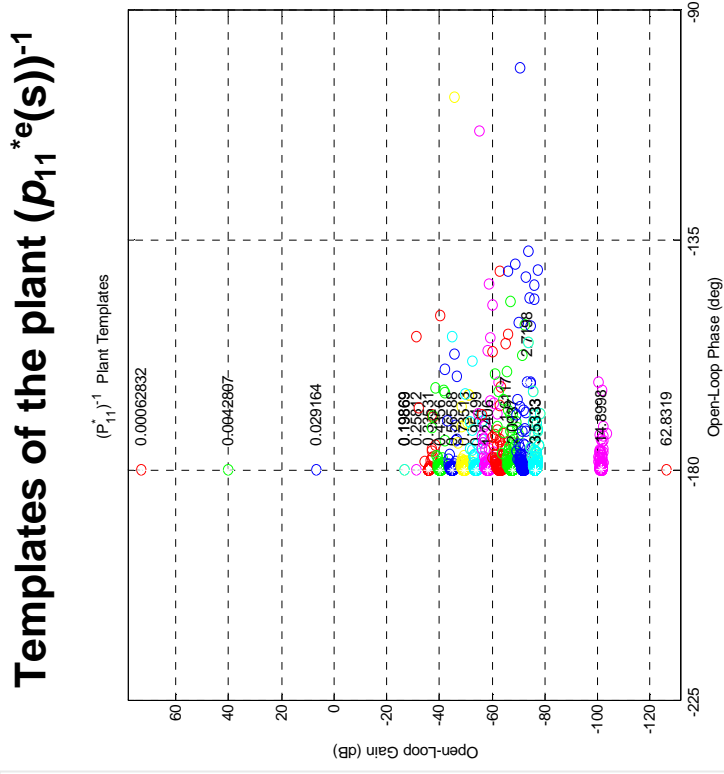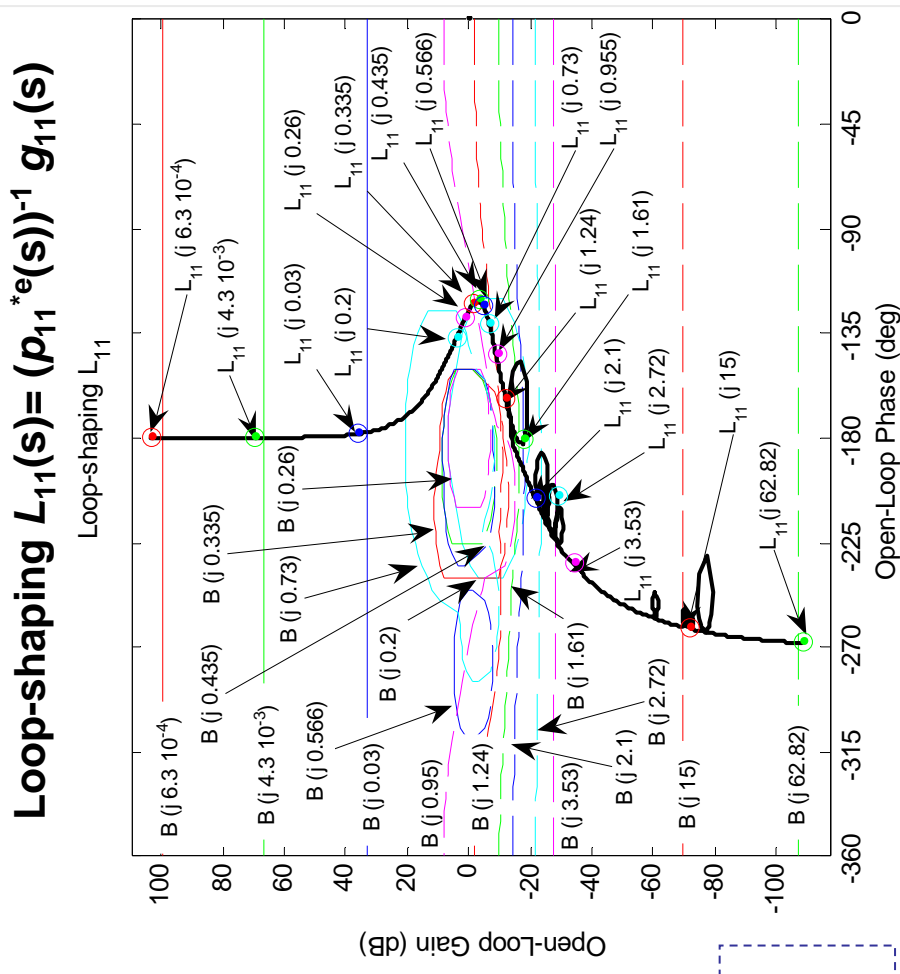
$$G = \begin{bmatrix} g_{11} & 0 \\ g_{51} & 0 \end{bmatrix} \Rightarrow \begin{bmatrix} g_{11} & g_{15} \\ g_{51} & g_{55} \end{bmatrix}$$

MIMO DESIGNS

Step 2a) : MIMO subsystem loops 1 and 5

Design the off-diagonal controller g_{51}(s)

- Element designed to reduce the coupling

- Calculated according to the expression: $\longrightarrow$ $g_{51}^{opt}(s) = -p_{51}^{*\,N}(s)$
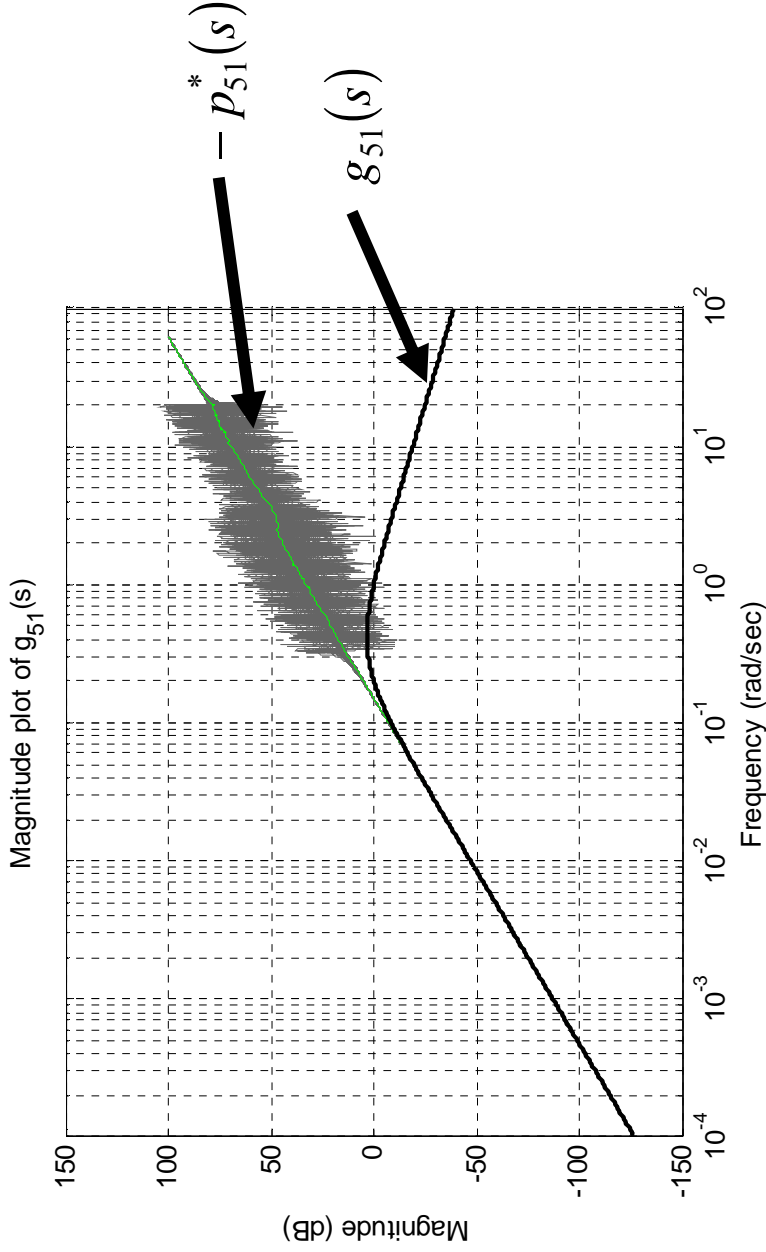
Magnitude plot of g_{51}(s)
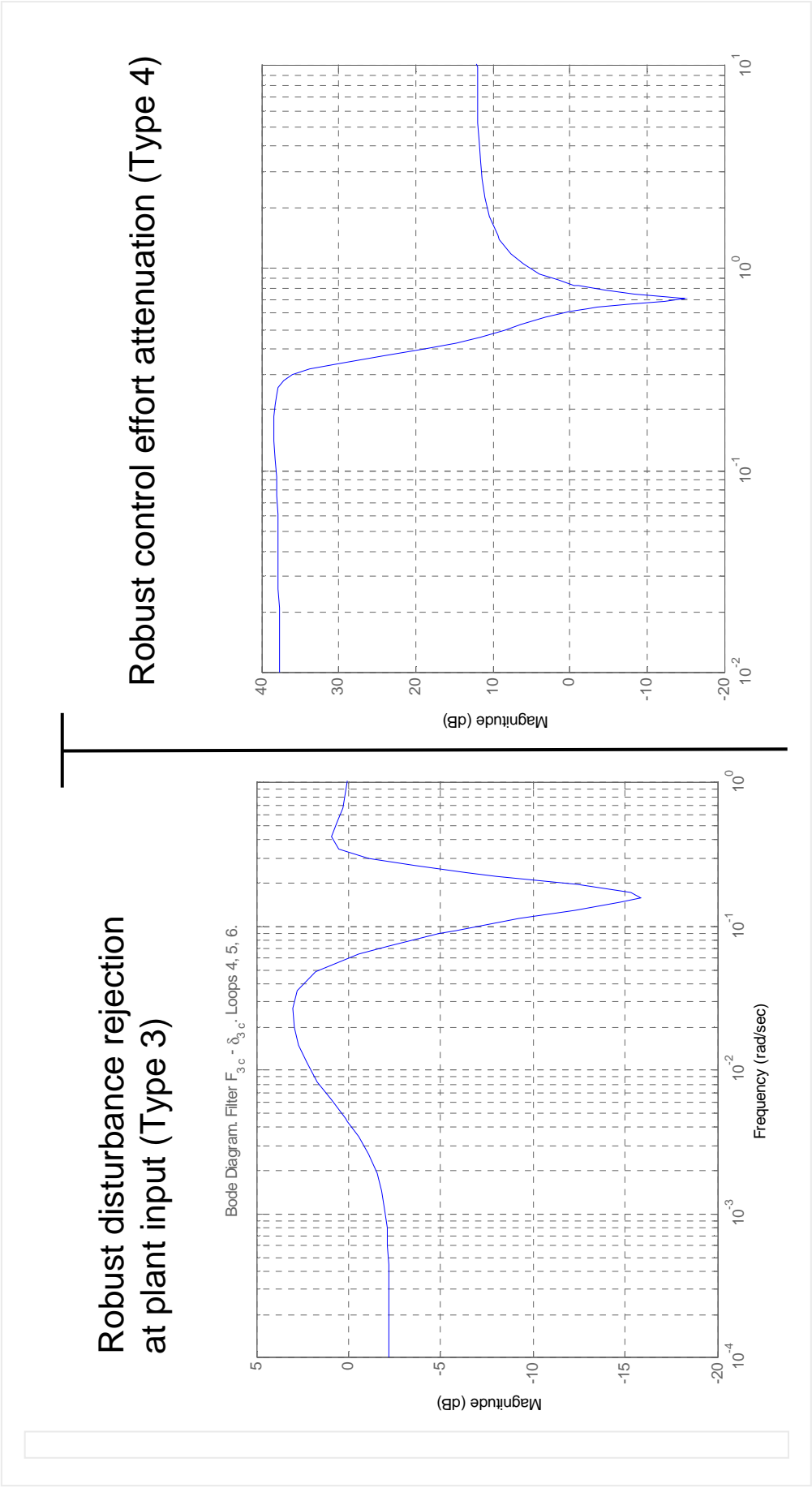
$-p_{51}^{*}(s)$

$g_{51}(s)$

2.35

MIMO DESIGNS

Step 2a) : MIMO subsystem loops 1 and 5

$$G = \begin{bmatrix} g_{11} & 0 \\ g_{51} & 0 \end{bmatrix} \Rightarrow \begin{bmatrix} g_{11} & g_{15} \\ g_{51} & g_{55} \end{bmatrix}$$

Design the diagonal controller g_{55}(s)

Controller element designed for the **equivalent plant** computed with :

$$\left[p_{55}^{*e}(s) \right]_2 = \left[p_{55}^{*e}(s) \right]_1 - \frac{\left(\left[p_{51}^{*e}(s) \right]_1 + \left[g_{51}(s) \right]_1 \right) \left(\left[p_{15}^{*e}(s) \right]_1 \right)}{\left[p_{11}^{*e}(s) \right]_1 + \left[g_{11}(s) \right]_1}$$

<u>Robust Performance Specifications</u>

Robust stability (Type 1)

Bode Diagram. Filter F_1 – δ_1. Loops 4, 5, 6

Robust sensitivity (Type 2)

$$\left| \frac{1}{1 + P(s)\,G(s)} \right| = |S(s)| \le 2$$

MIMO DESIGNS

Step 2a) : MIMO subsystem loops 1 and 5

$$G = \begin{bmatrix} g_{11} & 0 \\ g_{51} & 0 \end{bmatrix} \Rightarrow \begin{bmatrix} g_{11} & g_{15} \\ g_{51} & g_{55} \end{bmatrix}$$

Design the diagonal controller g_{55}(s)

Robust disturbance rejection at plant input (Type 3)

Robust control effort attenuation (Type 4)

Bode Diagram. Filter F_{3c} - δ_{3c}. Loops 4, 5, 6.

Mario Garcia-Sanz

MIMO DESIGNS

Step 2a) : MIMO subsystem loops 1 and 5

$$G = \begin{bmatrix} g_{11} & 0 \\ g_{51} & 0 \end{bmatrix} \Rightarrow \begin{bmatrix} g_{11} & g_{15} \\ g_{51} & g_{55} \end{bmatrix}$$
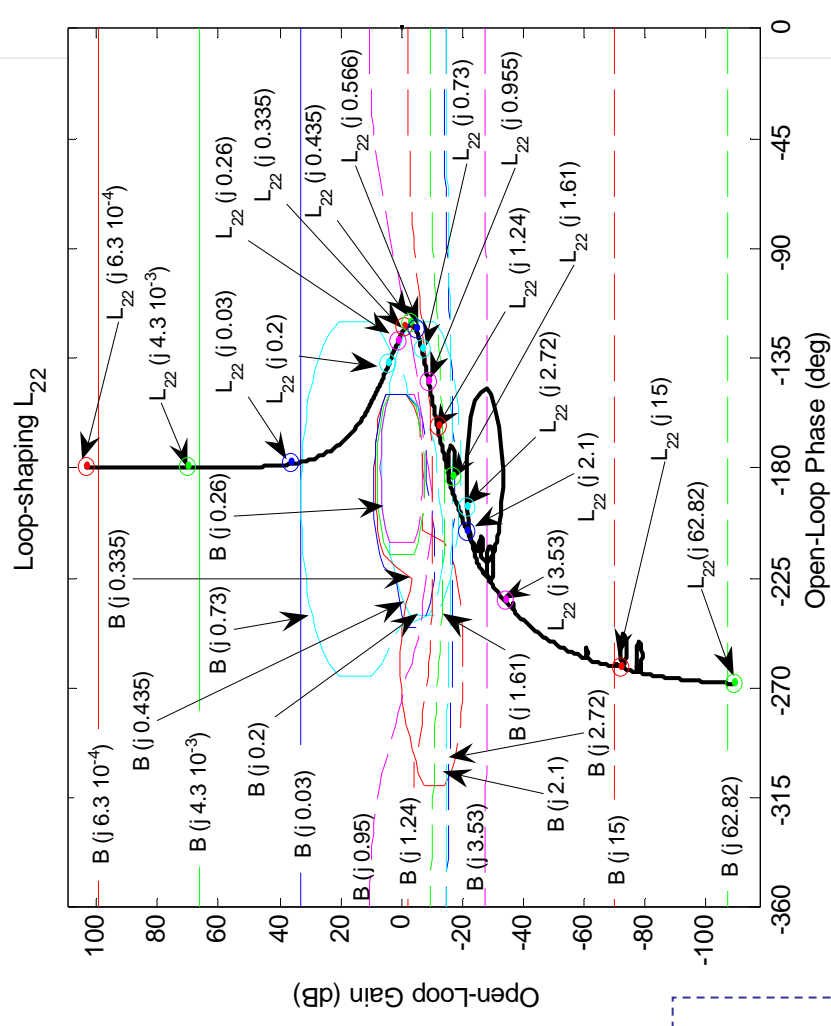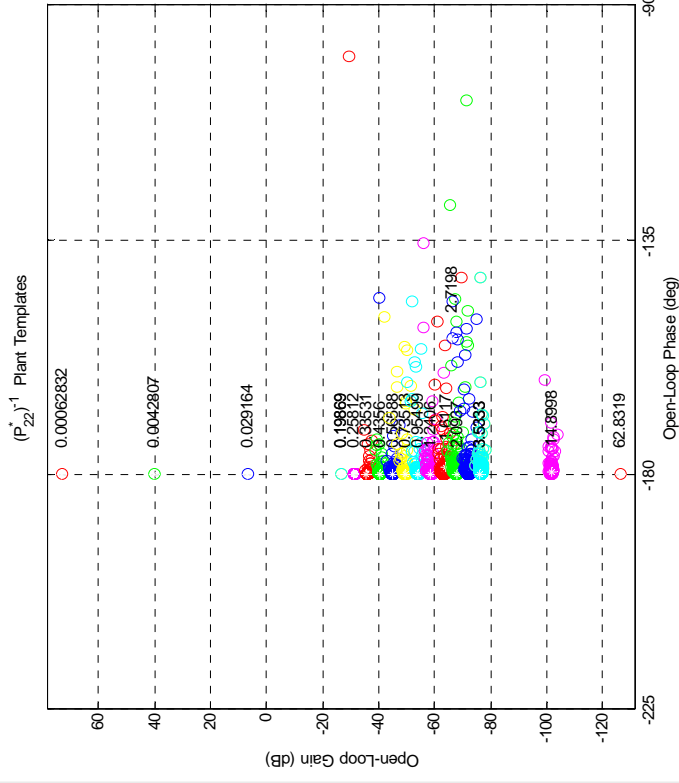
Design the diagonal controller $g_{55}(s)$

Templates of the plant $(p_{55}{}^{*}e(s))^{-1}$
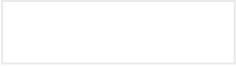
Loop-shaping $L_{55}(s)= (p_{55}{}^{*}e(s))^{-1} g_{55}(s)$

The subsystem is found to be **stable** according to the sufficient stability conditions (a and b).

Mario Garcia-Sanz

2.38

MIMO DESIGNS

Step 2a) : MIMO subsystem loops 1 and 5

$$G = \begin{bmatrix} g_{11} & 0 \\ g_{51} & 0 \end{bmatrix} \Rightarrow \begin{bmatrix} g_{11} & g_{15} \\ g_{51} & g_{55} \end{bmatrix}$$

Design the off-diagonal controller g_{15}(s)

- Element designed to reduce the coupling

- Calculated according to the expression:

$$g_{15}^{opt}(s) = -p_{15}^{*} \, ^{N}(s)$$
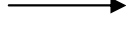
$$\longrightarrow \quad g_{15}(s) = 0$$

But due to requirement of minimum controller complexity and order

The 2x2 MIMO subsystem is found to be **stable** according to the sufficient stability conditions (c and d).

Finally, it is also checked that **no additional RHP zeros** have been introduced by the compensator

$$G = \begin{bmatrix} g_{22} & 0 \\ g_{42} & 0 \end{bmatrix} \Rightarrow \begin{bmatrix} g_{22} & g_{24} \\ g_{42} & g_{44} \end{bmatrix}$$
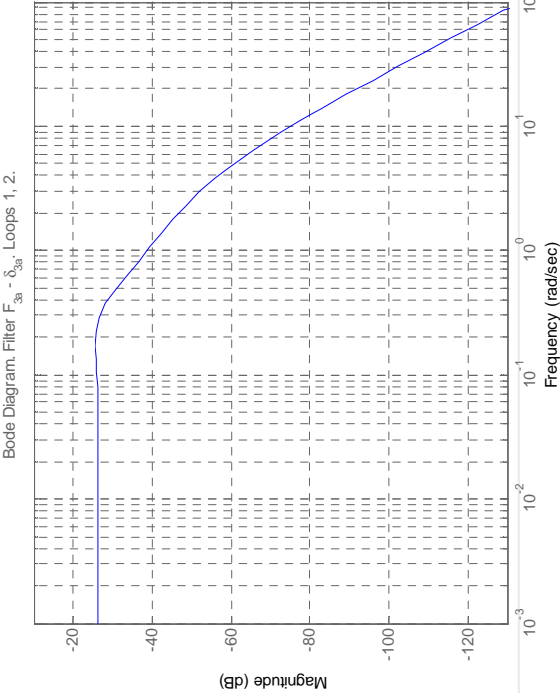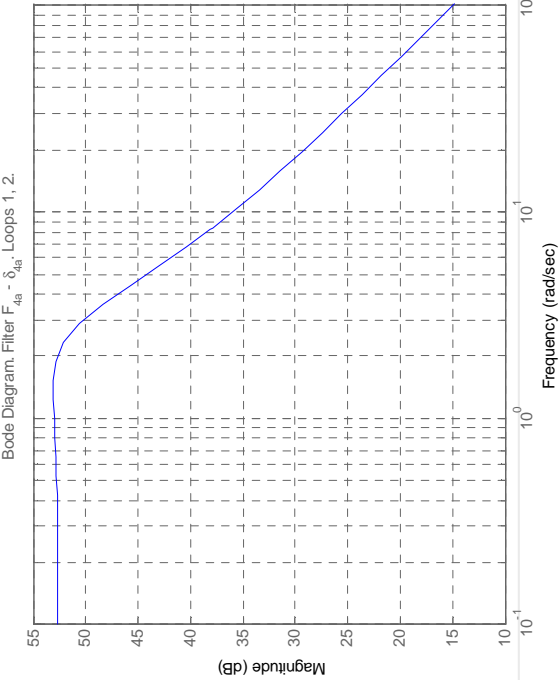
MIMO DESIGNS

Step 2b) : MIMO subsystem loops 2 and 4

Design of the diagonal controller $g_{22}(s)$

Robust Performance Specifications

Robust stability (Type 1)

$$\left| \frac{P(s)\,G(s)}{1+P(s)\,G(s)} \right| = |T(s)| \le 1.85$$

Robust sensitivity (Type 2)

$$\left| \frac{1}{1+P(s)\,G(s)} \right| = |S(s)| \le 2$$

Robust disturbance rejection at plant input (Type 3)

Bode Diagram. Filter F_{3a} - δ_{3a}. Loops 1, 2.

Robust control effort attenuation (Type 4)

Bode Diagram. Filter F_{4a} - δ_{4a}. Loops 1, 2.

Mario Garcia-Sanz

MIMO DESIGNS

Step 2b) : MIMO subsystem loops 2 and 4

$$G = \begin{bmatrix} g_{22} & 0 \\ g_{42} & 0 \end{bmatrix} \Rightarrow \begin{bmatrix} g_{22} & g_{24} \\ g_{42} & g_{44} \end{bmatrix}$$
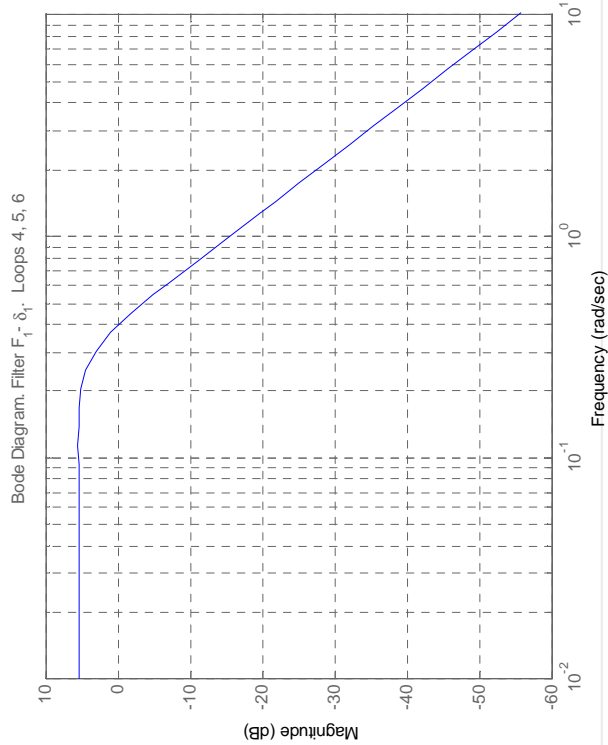
Design of the diagonal controller $g_{22}(s)$

Loop-shaping $L_{22}(s) = (p_{22} * e(s))^{-1} g_{22}(s)$

Templates of the plant $(p_{22} * e(s))^{-1}$

The subsystem is found to be **stable** according to the sufficient stability conditions (a and b).

Mario Garcia-Sanz

2.41

MIMO DESIGNS

Step 2b) : MIMO subsystem loops 2 and 4

$$G = \begin{bmatrix} g_{22} & 0 \\ g_{42} & 0 \end{bmatrix} \Rightarrow \begin{bmatrix} g_{22} & g_{24} \\ g_{42} & g_{44} \end{bmatrix}$$

Design the off-diagonal controller $g_{42}(s)$

- Element designed to reduce the coupling

- Calculated according to the expression: $\longrightarrow$ $g_{42}^{opt}(s) = -p_{42}^{*\,N}(s)$
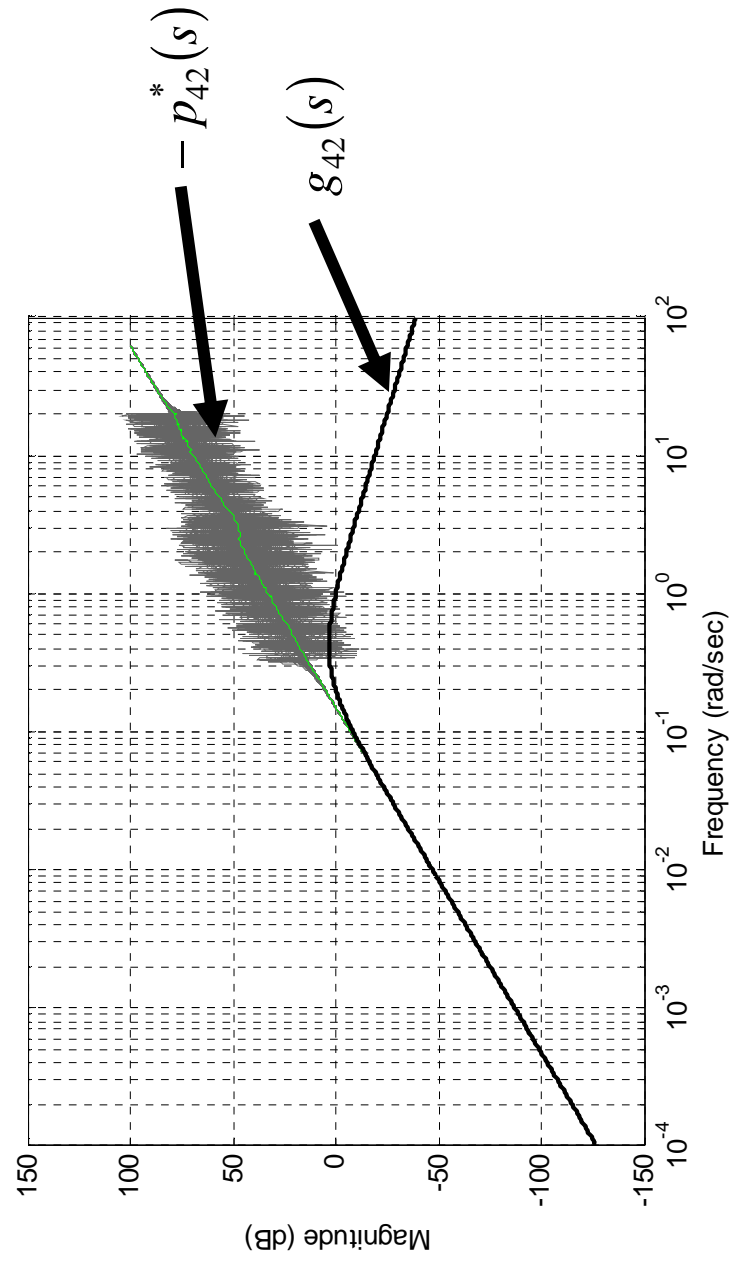
$-p_{42}^{*}(s)$

$g_{42}(s)$

Frequency (rad/sec)

Magnitude (dB)

2.42

Step 2b) : MIMO subsystem loops 2 and 4

$$G = \begin{bmatrix} g_{22} & 0 \\ g_{42} & 0 \end{bmatrix} \Rightarrow \begin{bmatrix} g_{22} & g_{24} \\ g_{42} & g_{44} \end{bmatrix}$$

Design of the diagonal controller g_{44}(s)

Controller element designed for the **equivalent plant** computed with :

$$[p_{44}^{*e}(s)]_2 = [p_{44}^{*e}(s)]_1 - \frac{\left([p_{42}^{*e}(s)]_1 + [g_{42}(s)]_1\right)\left([p_{24}^{*e}(s)]_1\right)}{[p_{22}^{*e}(s)]_1 + [g_{22}(s)]_1}$$

<u>Robust Performance Specifications</u>

Robust stability (Type 1)

Bode Diagram. Filter $F_1 - \delta_1$. Loops 4, 5, 6

Robust sensitivity (Type 2)

$$\left| \frac{1}{1 + P(s)\,G(s)} \right| = |S(s)| \le 2$$

Mario Garcia-Sanz

2.43

MIMO DESIGNS

Step 2b) : MIMO subsystem loops 2 and 4

$$G = \begin{bmatrix} g_{22} & 0 \\ g_{42} & 0 \end{bmatrix} \Rightarrow \begin{bmatrix} g_{22} & g_{24} \\ g_{42} & g_{44} \end{bmatrix}$$

Design of the diagonal controller $g_{44}(s)$

Robust disturbance rejection at plant input (Type 3)

Robust control effort attenuation (Type 4)

Bode Diagram. Filter F_{3c} - δ_{3c}. Loops 4, 5, 6.

Mario Garcia-Sanz

2.44

MIMO DESIGNS

Step 2b) : MIMO subsystem loops 2 and 4

$$G = \begin{bmatrix} g_{22} & 0 \\ g_{42} & 0 \end{bmatrix} \Rightarrow \begin{bmatrix} g_{22} & g_{24} \\ g_{42} & g_{44} \end{bmatrix}$$

Design of the diagonal controller $g_{44}(s)$

Loop-shaping $L_{44}(s) = (p_{44}{}^{*}e(s))^{-1} g_{44}(s)$
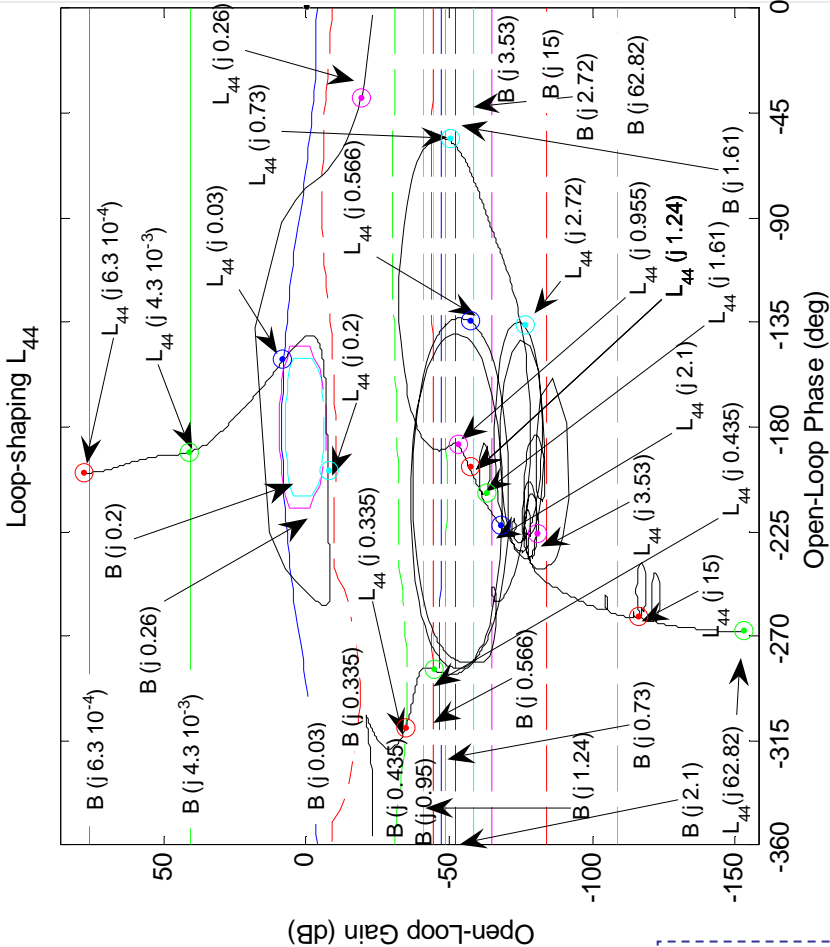
Templates of the plant $(p_{44}{}^{*}e(s))^{-1}$

The subsystem is found to be **stable** according to the sufficient stability conditions (a and b).

Mario Garcia-Sanz

2.45

$$G = \begin{bmatrix} g_{22} & 0 \\ g_{42} & 0 \end{bmatrix} \Rightarrow \begin{bmatrix} g_{22} & g_{24} \\ g_{42} & g_{44} \end{bmatrix}$$

MIMO DESIGNS

Step 2b) : MIMO subsystem loops 2 and 4

Design the off-diagonal controller g_{24}(s)

- Element designed to reduce the coupling

- Calculated according to the expression:

$$g_{24}^{opt}(s) = -p_{24}^{*N}(s)$$

$$g_{24}(s) = 0$$

But due to requirement of minimum controller complexity and order

The 2x2 MIMO subsystem is found to be **stable** according to the sufficient stability conditions (c and d).

Finally, it is also checked that **no additional RHP zeros** have been introduced by the compensator

Controller evaluation and comparison (I)

- **Non-diagonal MIMO QFT** (introduced here)
- **H-infinity** (provided by ESA)
- **Diagonal MIMO QFT** (for comparision)
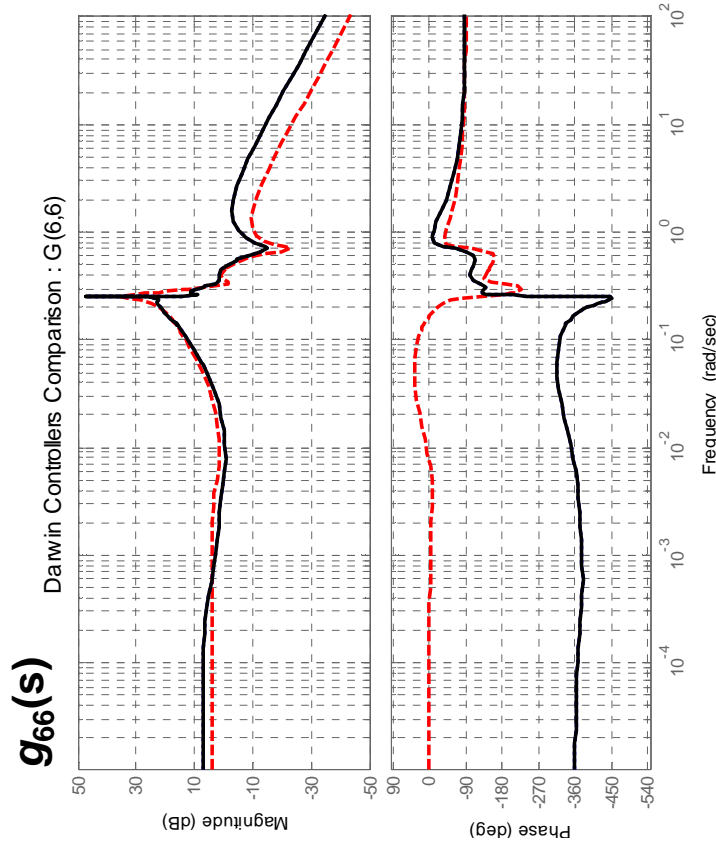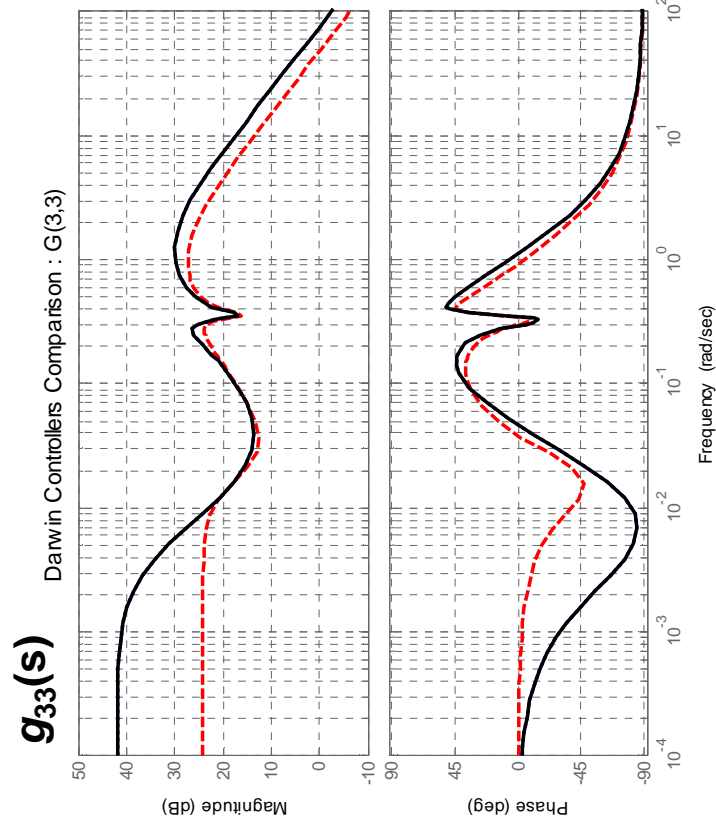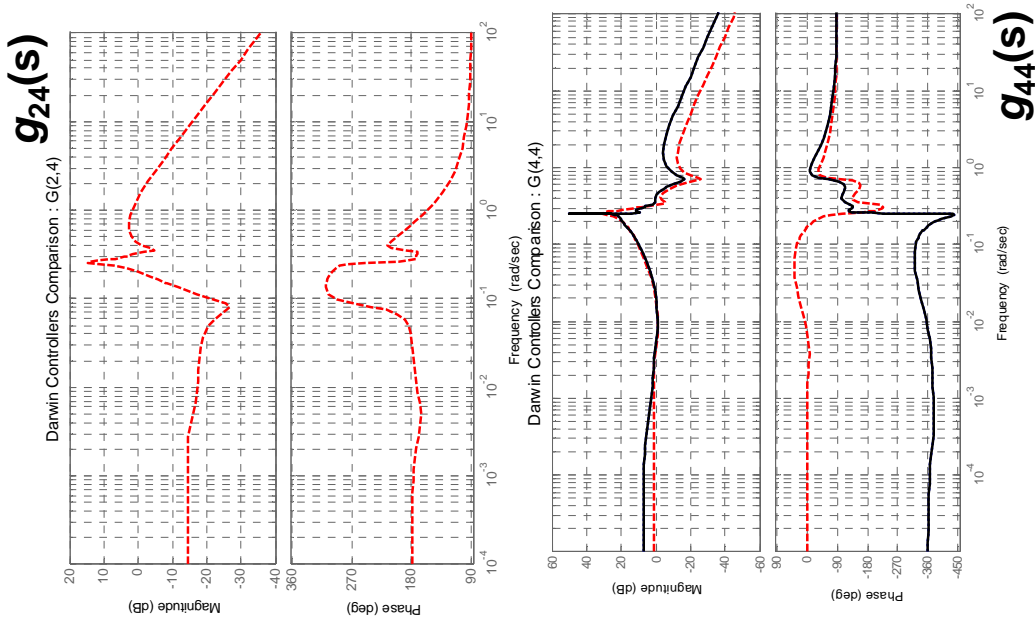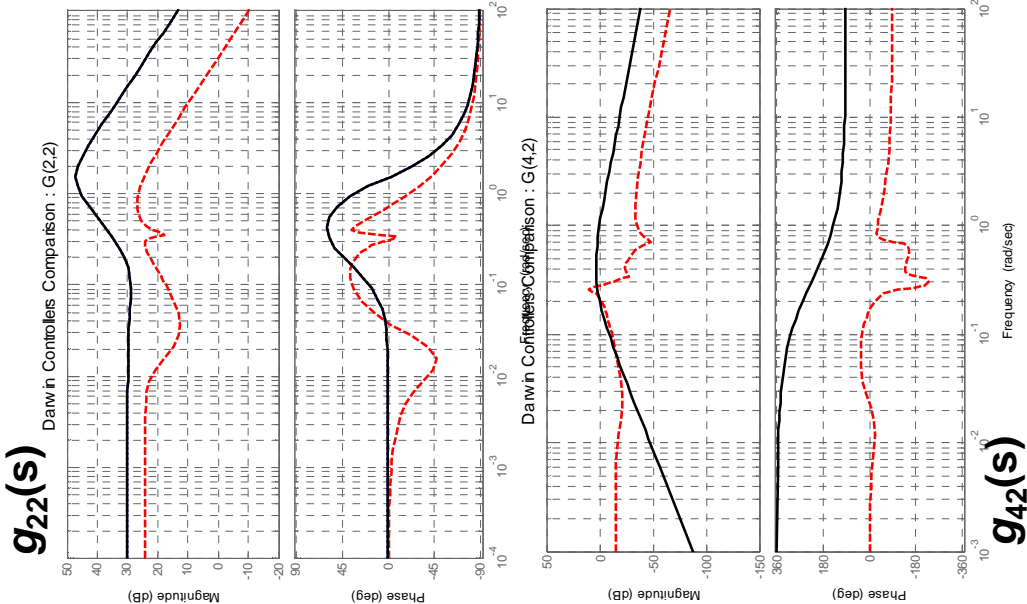
Bode Diagram Compensators:
Non-diagonal and Diagonal MIMO QFT in solid line,
H-infinity in dashed line.
(a) $g33(s)$, (b) $g66(s)$

$g_{33}(s)$

$g_{66}(s)$

Controller evaluation and comparison (II)

- **Non-diagonal MIMO QFT** (introduced here)
- H-infinity (provided by ESA)
- Diagonal MIMO QFT (for comparision)
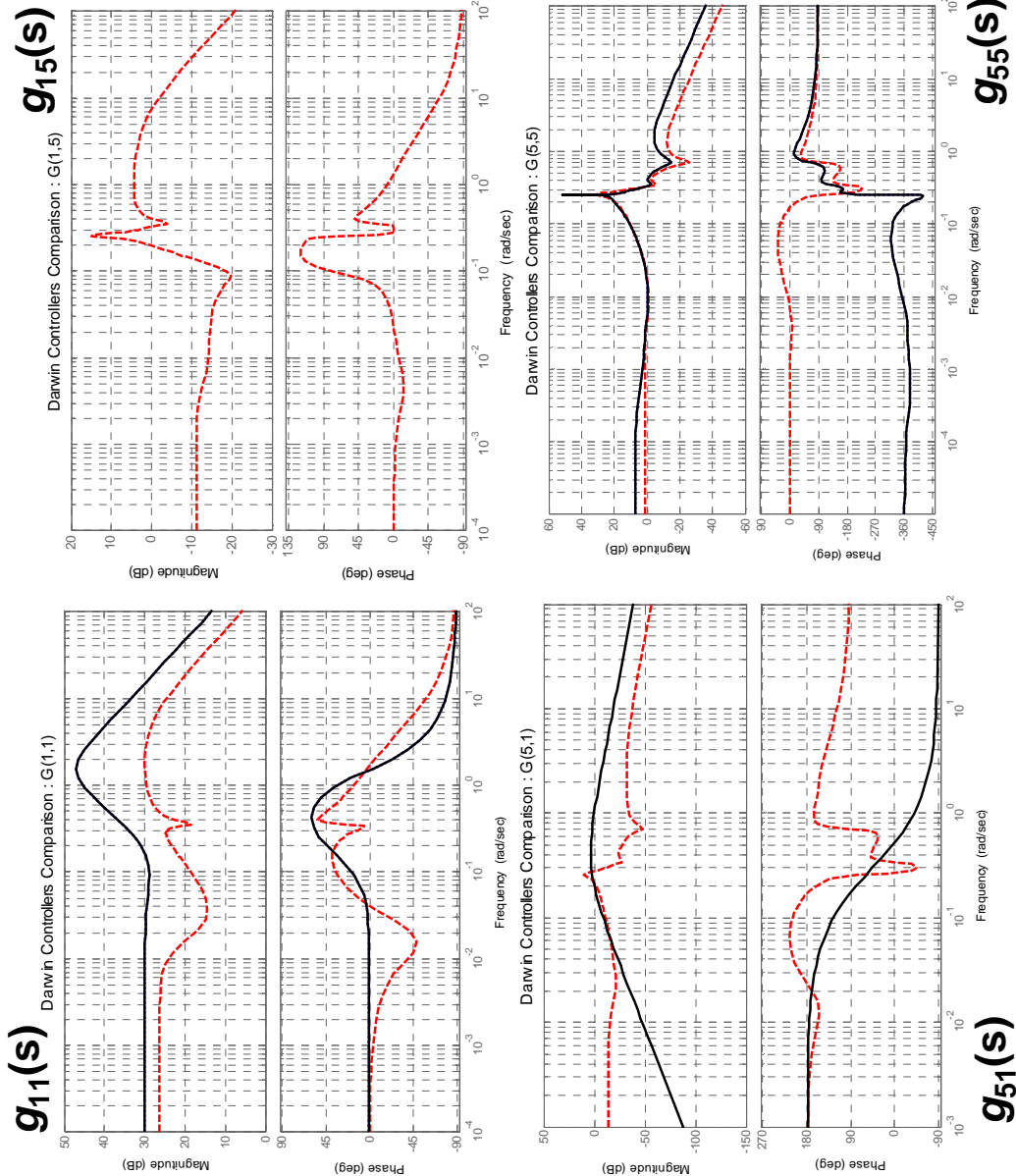
Bode Diagram Compensators:

Non-diagonal MIMO QFT in solid line

[also diagonal MIMO QFT for $g11(s)$ and $g55(s)$],

H-infinity in dashed line.

(a) $g11(s)$, (b) $g15(s)$, (c) $g51(s)$, (d) $g55(s)$

$g_{15}(s)$

$g_{55}(s)$

$g_{11}(s)$

$g_{51}(s)$

Controller evaluation and comparison (III)

- **Non-diagonal MIMO QFT** (introduced here)
- **H-infinity** (provided by ESA)
- **Diagonal MIMO QFT** (for comparision)

Bode Diagram Compensators:

Non-diagonal MIMO QFT in solid line

[also diagonal MIMO QFT for $g22(s)$ and $g44(s)$],

H-infinity in dashed line.

(a) $g22(s)$, (b) $g24(s)$,
(c) $g42(s)$, (d) $g44(s)$

$g_{24}(s)$

$g_{44}(s)$

$g_{22}(s)$

$g_{42}(s)$

Controller evaluation and comparison (IV)

- **Non-diagonal MIMO QFT** (introduced here)
- H-infinity (provided by ESA)
- Diagonal MIMO QFT (for comparision)

Element (5,1)
of the coupling matrix $C2$:

non-diagonal MIMO QFT in solid line

diagonal MIMO QFT in dotted line

H-infinity in dashed line

$$\left| c_{2ij} \right|_{g_{ij}=g_{ij}^{opt}} = \left| \psi_{ij} \, \Delta_{ij} \right|$$

$$\psi_{ij} = \frac{p_{ij}^{*N}}{\left(1 + \Delta_{jj}\right) p_{jj}^{*N} + g_{jj}}$$

Coupling matrix for disturbance rejection at plant input: $C_2(5,1)$
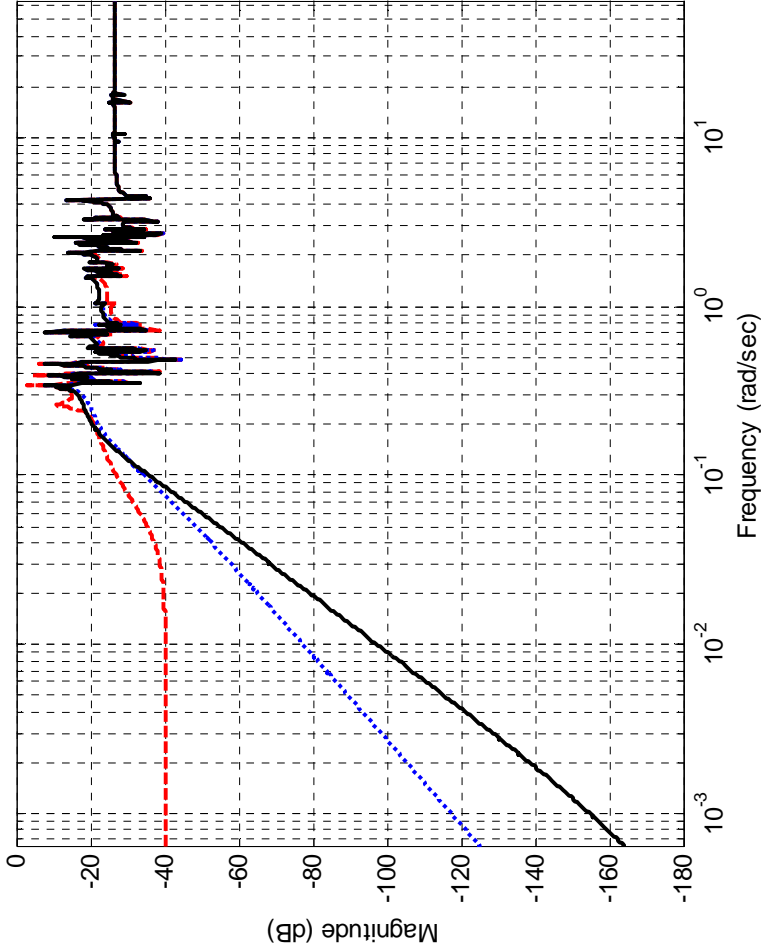
For $\omega \in [0, 0.1]$ rad/sec: $C_2(5,1)_{\text{non-diag QFT}} < C_2(5,1)_{\text{diag QFT}} < C_2(5,1)_{\text{H-infinity}}$,

which explains results under low frequency external disturbances

- **Non-diagonal MIMO QFT** (introduced here)
- H-infinity (provided by ESA)
- Diagonal MIMO QFT (for comparision)

Non-diagonal MIMO QFT has **8 elements** of order: from **3** to **14**.

$$\mathbf{G}(s) = \begin{bmatrix} g_{11}(s) & 0 & 0 & 0 & 0 & 0 \\ 0 & g_{22}(s) & 0 & 0 & 0 & 0 \\ 0 & 0 & g_{33}(s) & 0 & 0 & 0 \\ 0 & g_{42}(s) & 0 & g_{44}(s) & 0 & 0 \\ g_{51}(s) & 0 & 0 & 0 & g_{55}(s) & 0 \\ 0 & 0 & 0 & 0 & 0 & g_{66}(s) \end{bmatrix}$$

H-infinity expressed as transfer functions has **36 elements** of order **42**.

$$\mathbf{G}(s) = \begin{bmatrix} g_{11}(s) & g_{12}(s) & g_{13}(s) & g_{14}(s) & g_{15}(s) & g_{16}(s) \\ g_{21}(s) & g_{22}(s) & g_{23}(s) & g_{24}(s) & g_{25}(s) & g_{26}(s) \\ g_{31}(s) & g_{32}(s) & g_{33}(s) & g_{34}(s) & g_{35}(s) & g_{36}(s) \\ g_{41}(s) & g_{42}(s) & g_{43}(s) & g_{44}(s) & g_{45}(s) & g_{46}(s) \\ g_{51}(s) & g_{52}(s) & g_{53}(s) & g_{54}(s) & g_{55}(s) & g_{56}(s) \\ g_{61}(s) & g_{62}(s) & g_{63}(s) & g_{64}(s) & g_{65}(s) & g_{66}(s) \end{bmatrix}$$

**Diagonal MIMO QFT** has **6 elements** of order: from **5** to **14**.

$$\mathbf{G}(s) = \begin{bmatrix} g_{11}(s) & 0 & 0 & 0 & 0 & 0 \\ 0 & g_{22}(s) & 0 & 0 & 0 & 0 \\ 0 & 0 & g_{33}(s) & 0 & 0 & 0 \\ 0 & 0 & 0 & g_{44}(s) & 0 & 0 \\ 0 & 0 & 0 & 0 & g_{55}(s) & 0 \\ 0 & 0 & 0 & 0 & 0 & g_{66}(s) \end{bmatrix}$$

Controller	Number of Multiplications	Number of Sums
Non-diagonal MIMO QFT	130	124
H-infinity	2994	2988
Diagonal MIMO QFT	116	110

2.51

Mario Garcia-Sanz

Benchmark Simulator (I)

- **Non-diagonal MIMO QFT** (introduced here)
- H-infinity (provided by ESA)
- Diagonal MIMO QFT (for comparision)

AOCS for Large Flimsy Appendages
Benchmark 6 DOF
UPNA Evaluation
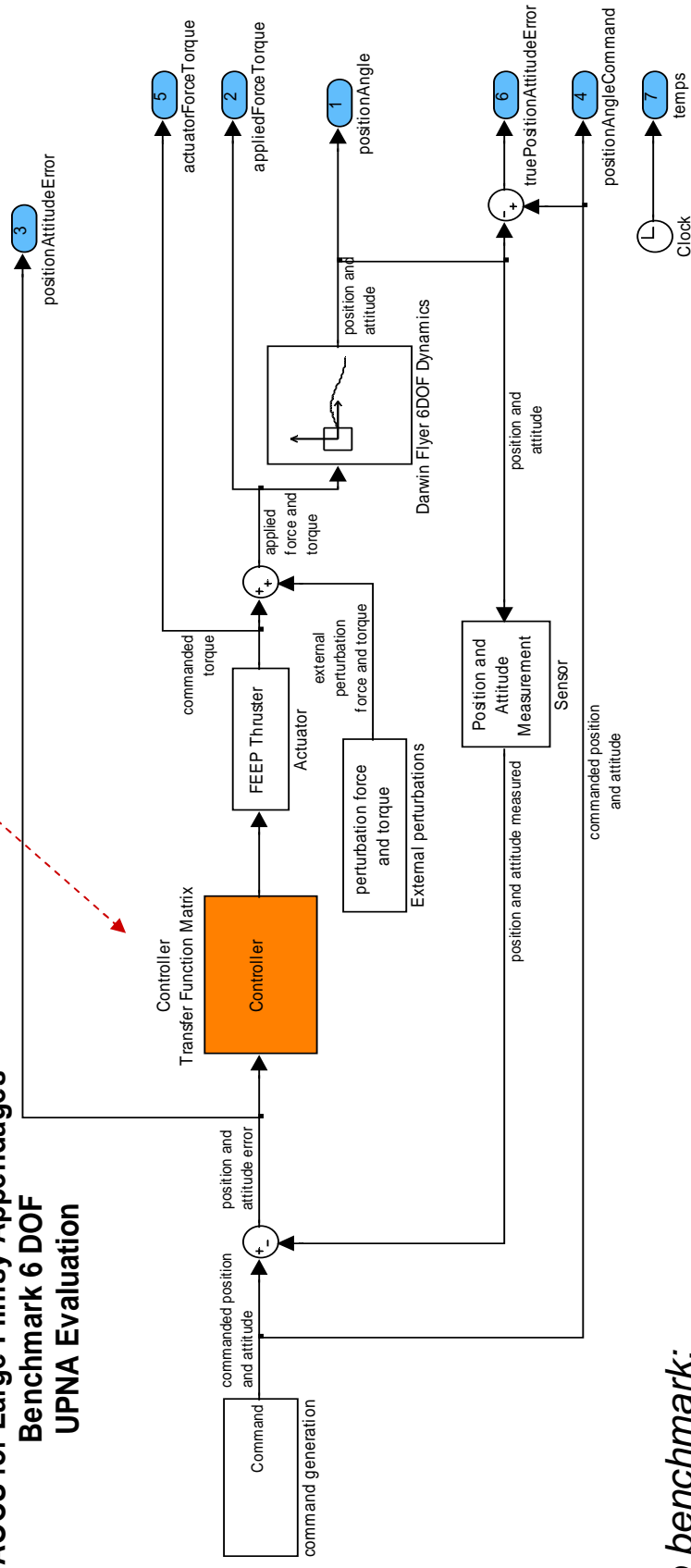
Two benchmark:

B1.- *Developed by Astrium Space for ESA-ESTEC*

B2.- *B1 + Low freq. disturbances*

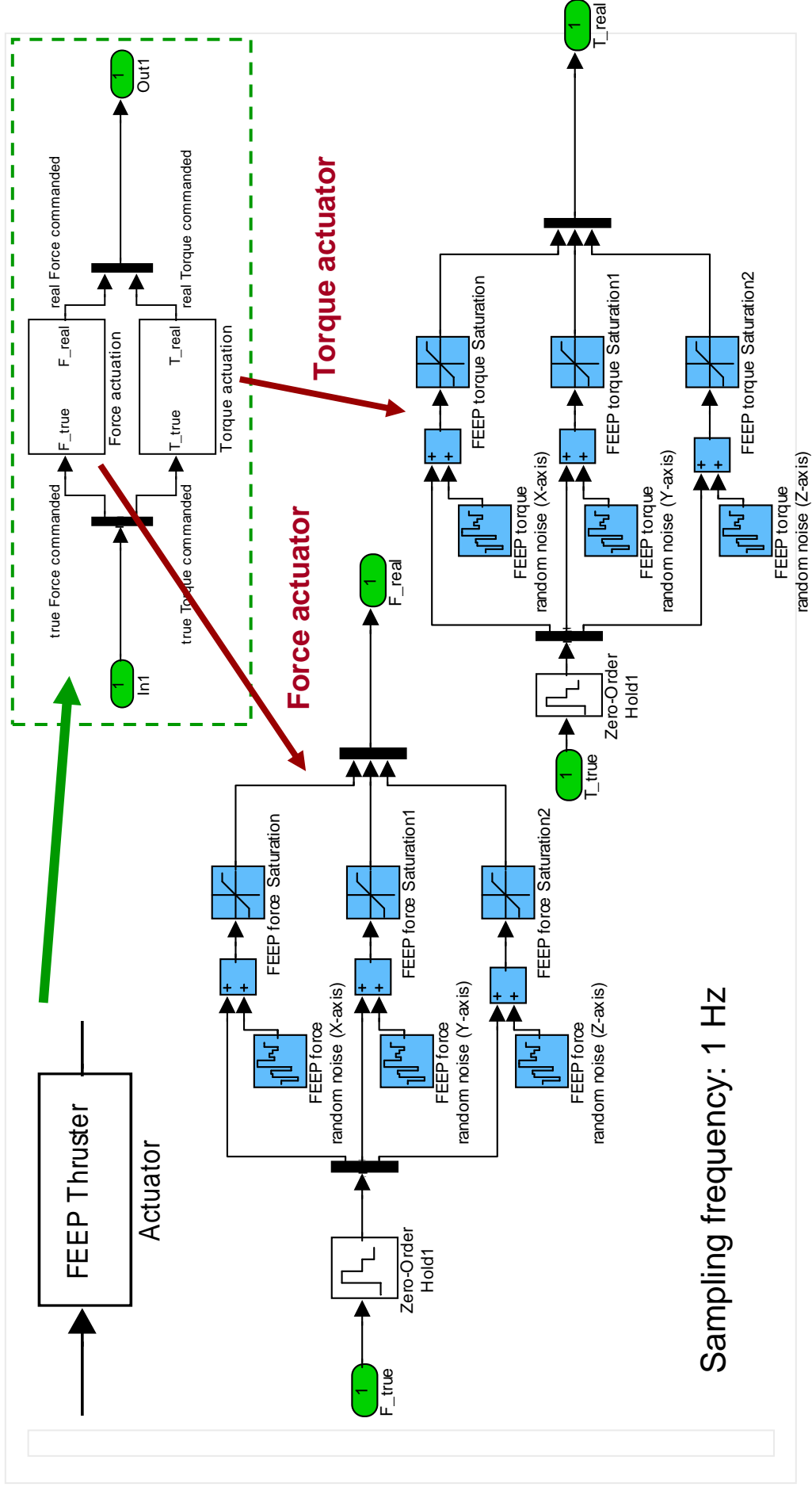300 different plants due to uncertainty. Monte-Carlo analysis

Sampling frequency: 1 Hz

Mario Garcia-Sanz

2.52

Benchmark Simulator (II)

Position and attitude sensors

- **Non-diagonal MIMO QFT** (introduced here)
- **H-infinity** (provided by ESA)
- **Diagonal MIMO QFT** (for comparision)

Sampling frequency: 1 Hz

Mario Garcia-Sanz

2.53
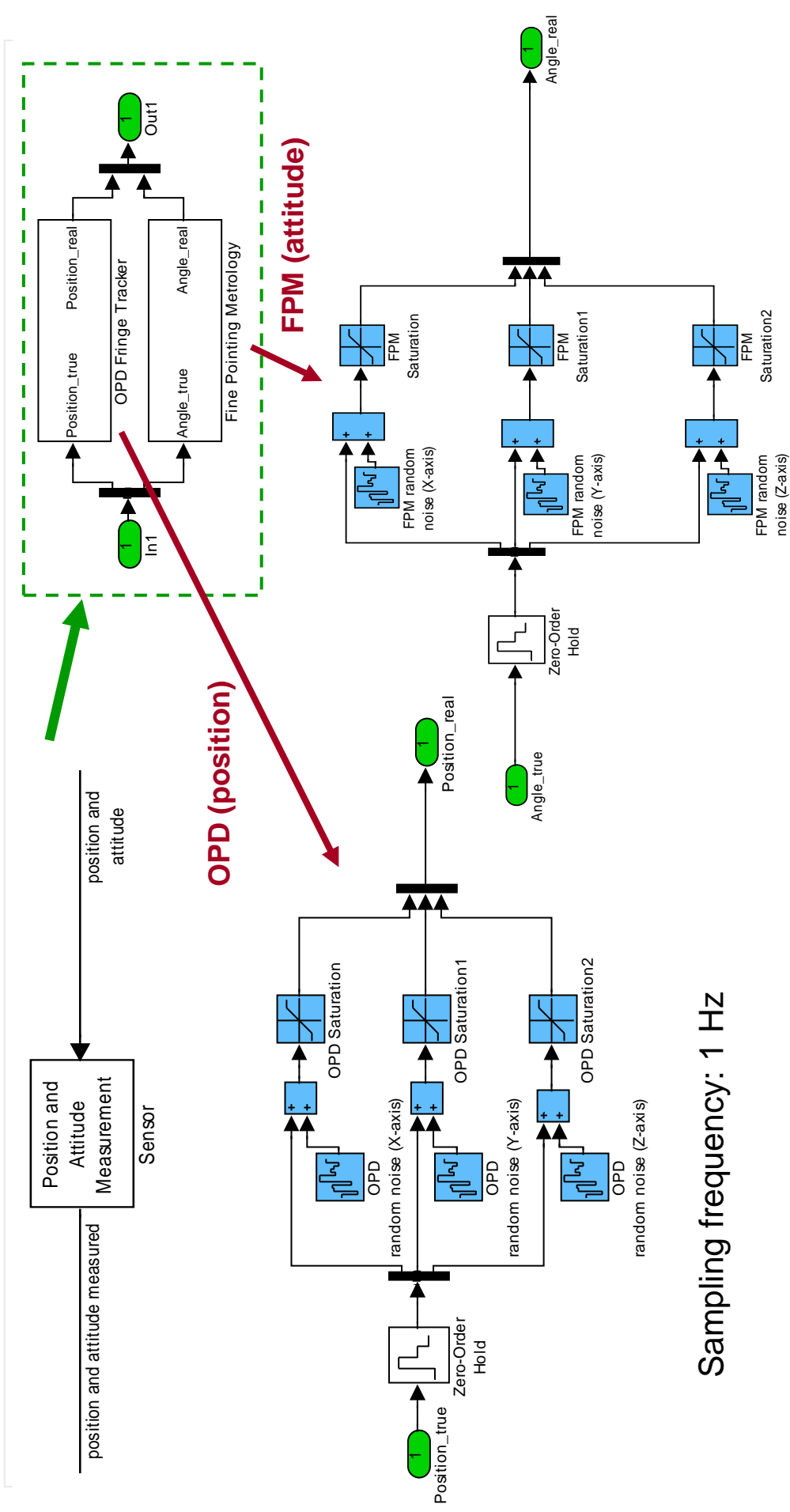
Benchmark Simulator (III)

FEEP Thrusters Actuators

- **Non-diagonal MIMO QFT** (introduced here)
- H-infinity (provided by ESA)
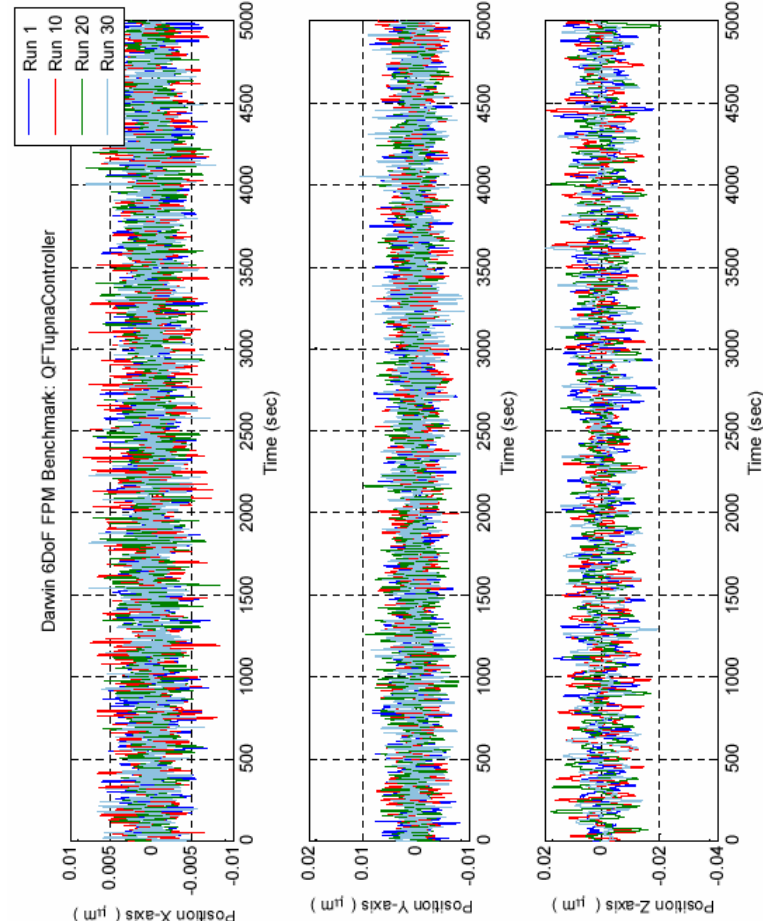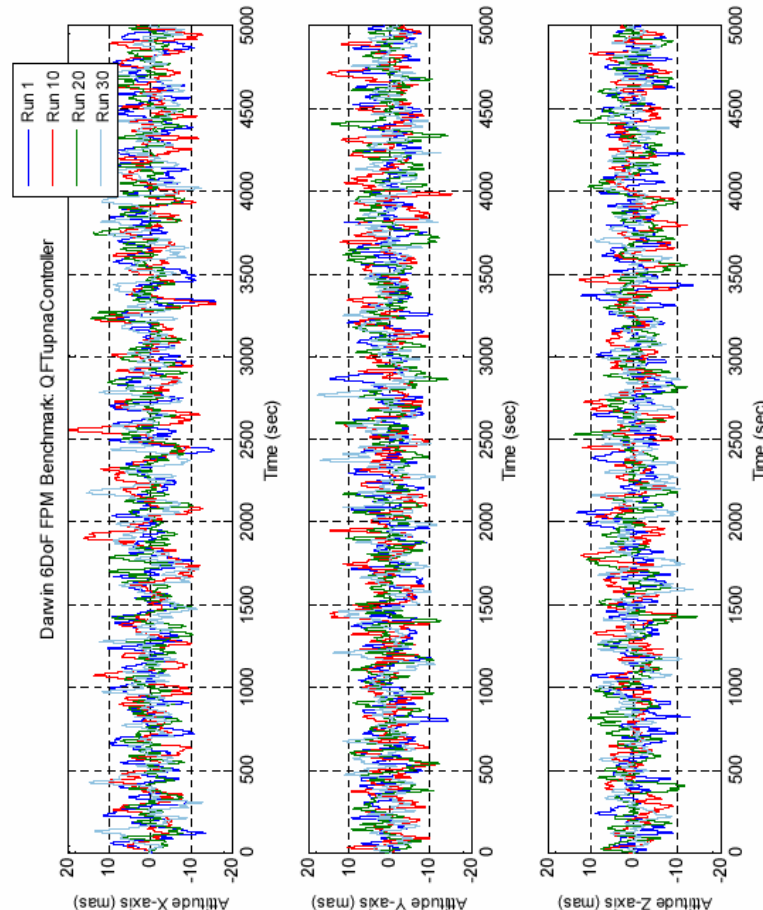- Diagonal MIMO QFT (for comparision)

Force actuator

Torque actuator

Sampling frequency: 1 Hz

Mario Garcia-Sanz

2.54

Benchmark Simulator (IV)

External Perturbations at the plant input

- **Non-diagonal MIMO QFT** (introduced here)
- **H-infinity** (provided by ESA)
- **Diagonal MIMO QFT** (for comparision)

B2 = B1 + low frequency disturbance force at plant input along the X-axis

2 μN, 0.05 rad/sec

Solar pressure

Gravity gradient

2.55

Mario Garcia-Sanz

Time-domain Analysis. Results (I)

- **Non-diagonal MIMO QFT** (introduced here)
- **H-infinity** (provided by ESA)
- **Diagonal MIMO QFT** (for comparision)

Position and attitude responses

Position outputs for several run cases

Attitude outputs for several run cases

Mario Garcia-Sanz

2.56

- **Non-diagonal MIMO QFT** (introduced here)
  - H-infinity (provided by ESA)
  - Diagonal MIMO QFT (for comparision)

Evaluation Criteria

For each controller:

the **greatest value** over the 300 uncertain cases is shown for:

- **Position errors**: the maximum

  the standard deviation

- **Attitude errors**: the maximum

  the standard deviation

- Actuator commands: the maximum

in all axes.

Time-domain Analysis. Results (III)

Specification	Requirement	Benchmark	Non-diagonal MIMO QFT Controller	Diagonal MIMO QFT Controller	H-infinity Controller
1 Maximum Position Error X (μm)	< 1 μm	B1	**0.0131**	**0.0131**	0.0293
		B2	**0.0816**	**0.0816**	0.511
2 Maximum Position Error Y (μm)	< 1 μm	B1	**0.0120**	**0.0120**	0.0299
		B2	**0.0120**	**0.0120**	0.0299
3 Maximum Position Error Z (μm)	< 1 μm	B1	**0.0288**	**0.0288**	0.0292
		B2	**0.0288**	**0.0288**	0.0292
4 Maximum Attitude Error X (mas)	< 25.5 mas	B1	**25.27**	25.31	25.95
		B2	**25.27**	25.31	25.95
5 Maximum Attitude Error Y (mas)	< 25.5 mas	B1	**22.91**	22.99	23.21
		B2	**22.55**	23.75	28.91
6 Maximum Attitude Error Z (mas)	< 25.5 mas	B1	**21.15**	**21.15**	22.84
		B2	**21.15**	**21.15**	22.84

2.58

Mario Garcia-Sanz

Time-domain Analysis. Results (IV)

	Specification	Requirement	Benchmark	Non-diagonal MIMO QFT Controller	Diagonal MIMO QFT Controller	H-infinity Controller
7	Std. Deviation of Position Error X (μm)	< 0.33 μm	B1	**0.00275**	0.00276	0.00686
			B2	**0.0511**	**0.0511**	0.341
8	Std. Deviation of Position Error Y (μm)	< 0.33 μm	B1	**0.00265**	0.00266	0.00722
			B2	**0.00265**	0.00266	0.00722
9	Std. Deviation of Position Error Z (μm)	< 0.33 μm	B1	**0.00668**	**0.00668**	0.00691
			B2	**0.00668**	**0.00668**	0.00691
10	Std. Deviation of Attitude Error X (mas)	< 8.5 mas	B1	**5.57**	**5.57**	5.68
			B2	**5.57**	**5.57**	5.68
11	Std. Deviation of Attitude Error Y (mas)	< 8.5 mas	B1	**5.76**	**5.76**	6.01
			B2	**5.80**	5.85	8.23
12	Std. Deviation of Attitude Error Z (mas)	< 8.5 mas	B1	**4.83**	**4.83**	5.00
			B2	**4.83**	**4.83**	5.00

	Specification	Requirement	Benchmark	Non-diagonal MIMO QFT Controller	Diagonal MIMO QFT Controller	H-infinity Controller
13	Max. Actuator Force Command X (N)	< 1.5e-4 N	B1	1.94e-6	1.94e-6	**7.42e-7**
			B2	3.94e-6	3.94e-6	**3.31e-6**
14	Max. Actuator Force Command Y (N)	< 1.5e-4 N	B1	1.86e-6	1.86e-6	**6.68e-7**
			B2	1.86e-6	1.86e-6	**6.68e-7**
15	Max. Actuator Force Command Z (N)	< 1.5e-4 N	B1	5.94e-7	5.94e-7	**5.61e-7**
			B2	5.94e-7	5.94e-7	**5.61e-7**
16	Max. Actuator Torque Command X (Nm)	< 1.5e-4 N m	B1	**8.68e-7**	8.71e-7	1.03e-6
			B2	**8.68e-7**	8.71e-7	1.03e-6
17	Max. Actuator Torque Command Y (Nm)	< 1.5e-4 N m	B1	**1.05e-6**	1.05e-6	1.15e-6
			B2	**1.06e-6**	1.06e-6	1.16e-6
18	Max. Actuator Torque Command Z (Nm)	< 1.5e-4 N m	B1	**1.08e-6**	1.08e-6	1.27e-6
			B2	**1.08e-6**	1.08e-6	1.27e-6

Mario Garcia-Sanz

4.3.- Conclusions

- A **Non-diagonal MIMO QFT** Controller Design methodology

  to design fully populated matrix controllers

  to solve:

  the reference tracking problem

  the external disturbance rejection problem at both, plant input and output,

  in the presence of model plant uncertainty,

  has been presented.

- The technique has been **validated** with a Darwin-type spacecraft

  with flexible appendages

2.61

4.4.- Some References
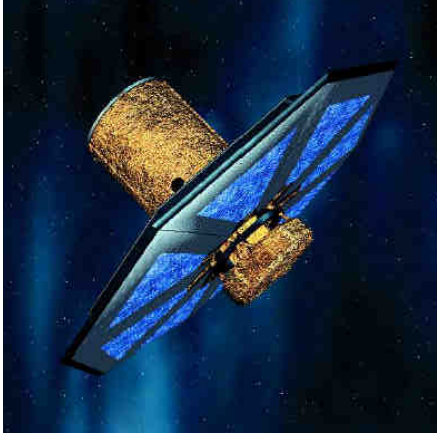
ESA-ESTEC
Noordwijk (Holland)

⇧ *Complex MIMO model*

⇧ *Demanding Spec.*

⇧ *Comparison: H-infinity, Diagonal MIMO QFT, Non-diagonal MIMO QFT*

Ref: M. Garcia-Sanz, I. Eguinoa, M. Barreras, S. Bennani

"Non-diagonal MIMO QFT Controller Design for Darwin-type Spacecraft with large flimsy appendages".

Journal of Dynamic Systems, Measurement and Control, **ASME**, USA. Vol. 130, January 2008.
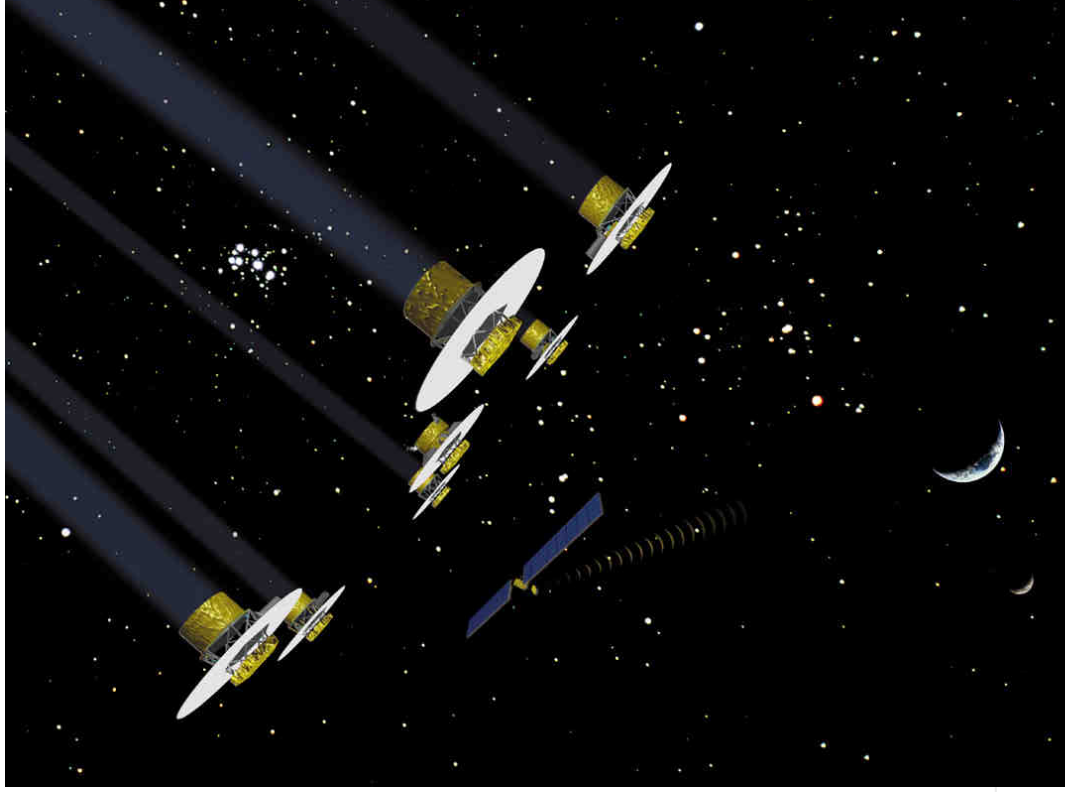
Special Issue: COOPERATIVE CONTROL OF MULTIPLE SPACECRAFT FLYING IN FORMATION

M. Garcia-Sanz (Guest Editor)

IET Control Theory and Applications, Vol. 1, Issue 2 , March 2007, UK.
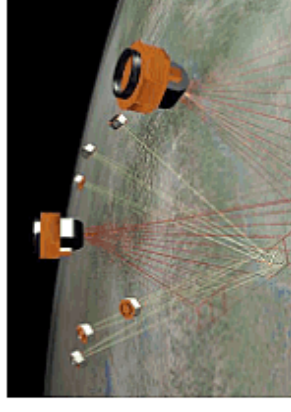
LOAD-SHARING ROBUST CONTROL OF SPACECRAFT FORMATIONS: Deep Space and Low Earth Elliptic Orbits

M. Garcia-Sanz, F. Y. Hadaegh

IET Control Theory and Applications, Vol. 1, Issue 2 , pp. 475-484, March 2007, UK

Mario Garcia-Sanz

2.63

Outline

1.- QFT Controller Design Technique Fundamentals

2.- Real-world QFT control applications and examples

3.- Non-diagonal MIMO QFT controller design methodologies

4.- Application: Robust QFT control for a MIMO Spacecraft with flexible sunshield

5.- Switching robust control: Beyond the linear limitations.

6.- Example: Switching control for Unmanned Vehicles

5.- Switching robust control: Beyond the linear limitations

Serious Design

amplification

attenuation

Log Magnitude

Frequency

Classical linear limitations of feedback systems
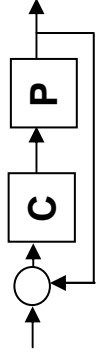
- Bode integrals 1945,
- Freudenberg, Looze 80...

$$\frac{1}{\pi}\int_0^\infty \frac{1}{\omega^2}\log_e \left|T(j\omega)\right| d\omega = -\frac{1}{2}K_v^{-1} + \frac{1}{2}\tau + \sum_{z_i \in CRHP} \frac{1}{z_i}$$

where $K_v = \lim_{s\to 0}\{sC(s)P(s)\}$ *is the system velocity constant,* τ *is the time delay in the loop, and* z_i *are the zeros in the loop.*

$$\int_{\omega=0}^{\omega=\infty}\log_e\left|S(j\omega)\right|d\omega = \pi\left(\sum_{p_i\in CRHP}p_i\right) - \frac{\pi}{2}k_{HF}$$

where $p_i \in CRHP$ are the poles of $L(s)=C(s)P(s)$ in the closed right half plane, and $k_{HF}=\lim_{s\to\infty}\{sL(s)\}$ (with units of radians/sec), and

Sensitivity

"waterbed effect"
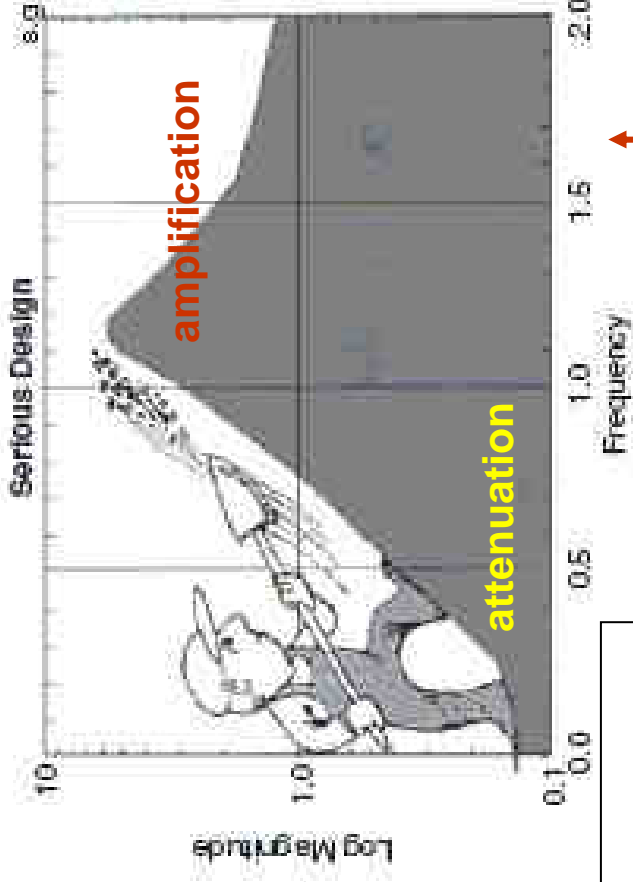
$$S(s)=\frac{1}{1+C(s)P(s)}$$

$$T(s)=1-S(s)=\frac{C(s)P(s)}{1+C(s)P(s)}$$

Complementary Sensitivity

Mario Garcia-Sanz

2.65

Example: X-29
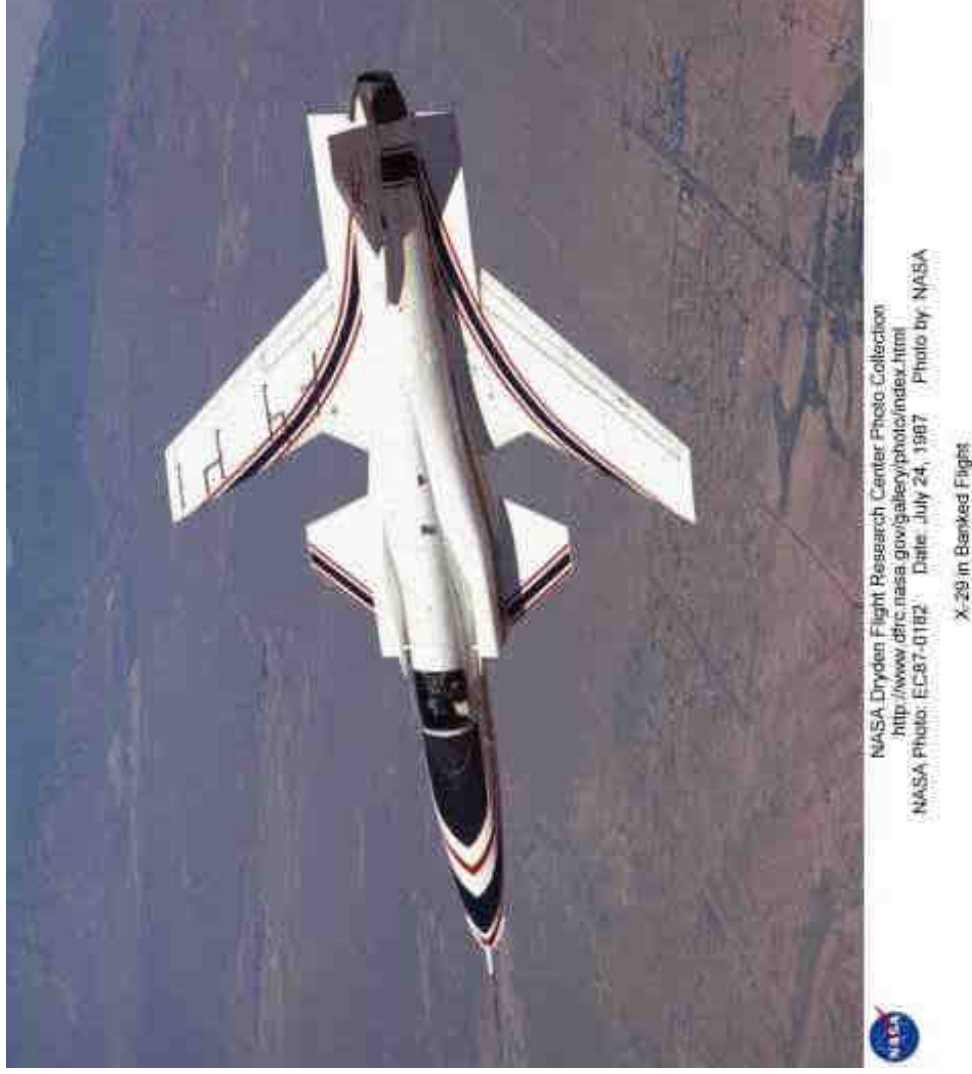
Unstable
(pole RHP)

Non-minimum phase
(zero RHP)

Linear limitations

<u>In practice</u>:

-Objective Phase Margin = 45^0

- Result ONLY Phase Margin = 39^0

NASA Dryden Flight Research Center Photo Collection
http://www.dfrc.nasa.gov/gallery/photo/index.html
NASA Photo: EC87-0182   Date: July 24, 1987   Photo by: NASA

X-29 in Banked Flight

Mario Garcia-Sanz

2.66

García-Sanz M., Elso J. (2008). **Beyond the linear limitations by combining switching and QFT: Application to wind turbines pitch control systems.** *Int. J. Robust Nonlinear Control*, Vol. 18, N.12.

To go beyond the linear limitations:

SWITCHING

Nonlinear control

Even for linear systems

Problem to be solved:

system **stability** is not assured *a priori*, even if the switching is made between stable controllers
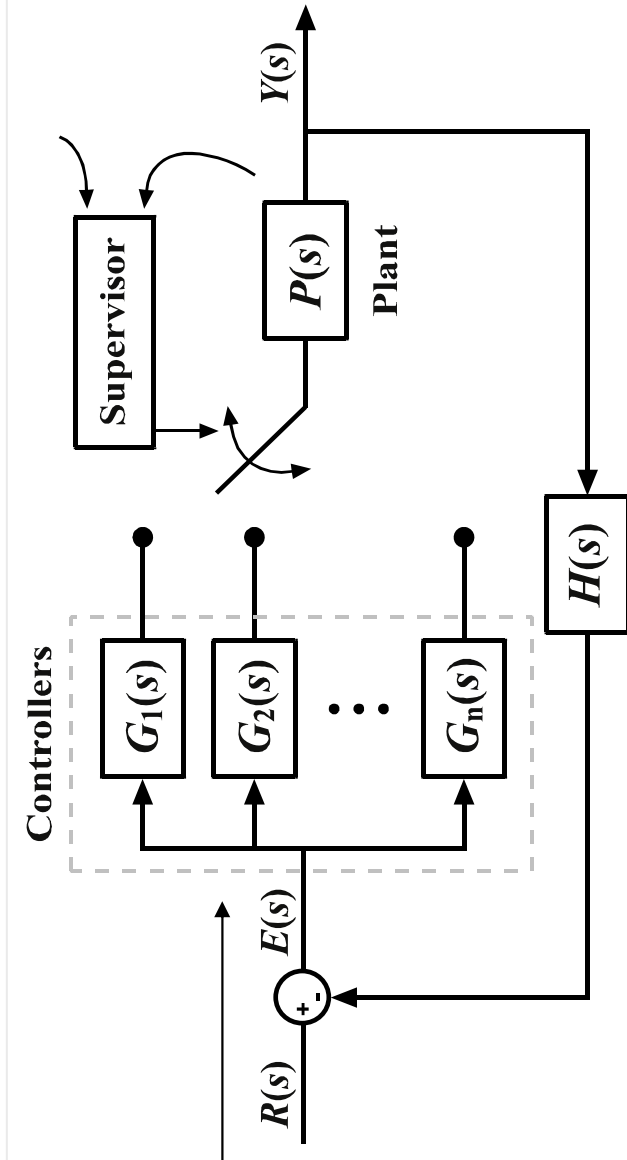
SWITCHING

System stability analysis (I)
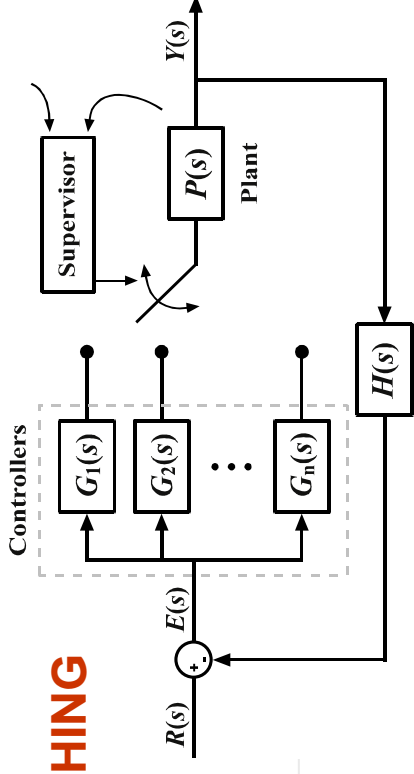
it has been proved that a system

$$\dot{x}(t) = A(t)x(t), \quad A(t) \in \mathcal{A} = \{A_1,...,A_m\}, \quad A_i \text{ Hurwitz,}$$

with arbitrary switching within the set of matrices A

is exponentially **stable**

if there exists a **Common Lyapunov Function** (CLF) for all $A_i \in \mathcal{A}$

It has also been proved that the existence of a

Common Quadratic Lyapunov Function (CQLF) for all $A_i \in \mathcal{A}$

is a sufficient condition for exponential stability

SWITCHING

System stability analysis (II)
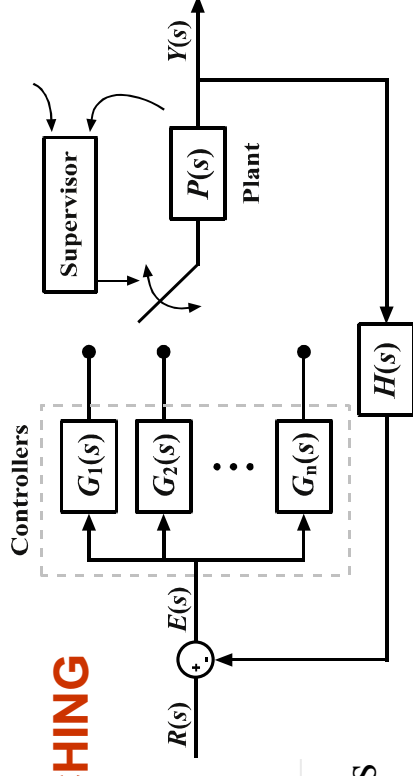
it has been proved that the **circle criterion** provides

necessary and sufficient conditions

for the **existence of a CQLF** for two systems in companion form

In particular the systems $\quad \dot{x}(t) = \mathbf{A}x(t) \qquad \dot{x}(t) = (\mathbf{A} - \mathbf{g}\Delta^T)x(t)$

both Hurwitz, with

$$A = \begin{bmatrix} 0 & 1 & 0 & \cdots & 0 & 0 \\ 0 & 0 & 1 & \cdots & 0 & 0 \\ 0 & 0 & 0 & \cdots & 0 & 0 \\ \vdots & \vdots & \vdots & \ddots & \vdots & \vdots \\ 0 & 0 & 0 & \cdots & 0 & 1 \\ -e_0 & -e_1 & -e_2 & \cdots & -e_{n-2} & -e_{n-1} \end{bmatrix}, \quad \mathbf{g} = \begin{bmatrix} 0 \\ 0 \\ 0 \\ \cdots \\ 0 \\ 1 \end{bmatrix}, \quad \Delta = \begin{bmatrix} \Delta e_0 \\ \Delta e_1 \\ \Delta e_2 \\ \cdots \\ \Delta e_{n-2} \\ \Delta e_{n-1} \end{bmatrix}$$

have a **CQLF** if and only if

$$1 + \text{Re}\{\Delta^T(s\mathbf{I} - \mathbf{A})^{-1}\mathbf{g}\} > 0, \quad s = j\omega, \text{ for all frequency } \omega$$

System stability analysis (III)

Now we consider stability for arbitrary switching between **two closed-loop systems** with transfer functions

$$T_1(s) = \frac{L_1(s)}{1 + L_1(s)} = \frac{N(s)}{D(s) + N(s)}$$

$$T_2(s) = \frac{L_2(s)}{1 + L_2(s)} = \frac{N(s) + \Delta N(s)}{D(s) + \Delta D(s) + N(s) + \Delta N(s)},$$

$$L_1(s) = \frac{b_{n-1}s^{n-1} + \ldots + b_0}{s^n + a_{n-1}s^{n-1} + \ldots + a_0} = \frac{N(s)}{D(s)}$$

$$L_2(s) = \frac{(b_{n-1} + \Delta b_{n-1})s^{n-1} + \ldots + (b_0 + \Delta b_0)}{s^n + (a_{n-1} + \Delta a_{n-1})s^{n-1} + \ldots + (a_0 + \Delta a_0)} =$$

$$= \frac{N(s) + \Delta N(s)}{D(s) + \Delta D(s)}.$$
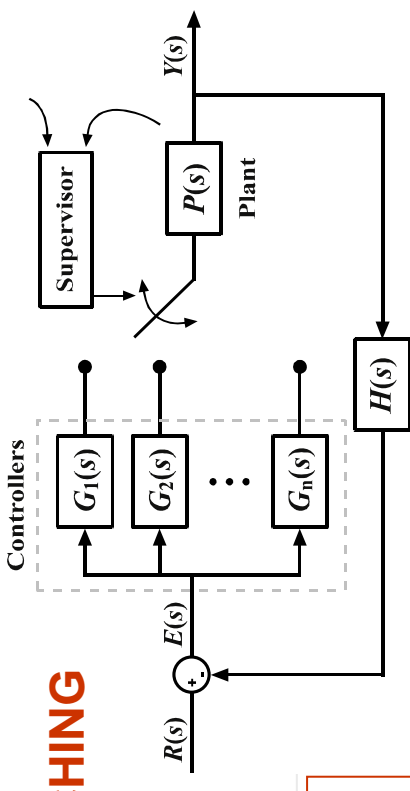
where: $L_1(s) = P(s)G_1(s)$ and
$L_2(s) = P(s)G_2(s)$

are proper, have the same number of poles, and the same number of zeros.

$$e_i = a_i + b_i$$
$$\Delta e_i = \Delta a_i + \Delta b_i.$$

where the characteristic equations are

$$D(s) + N(s) =$$

$$= s^n + e_{n-1}s^{n-1} + \ldots + e_1 s + e_0$$

$$D(s) + \Delta D(s) + N(s) + \Delta N(s) =$$

$$= s^n + (e_{n-1} + \Delta e_{n-1})s^{n-1} + \ldots + (e_0 + \Delta e_0),$$

System stability analysis (IV)
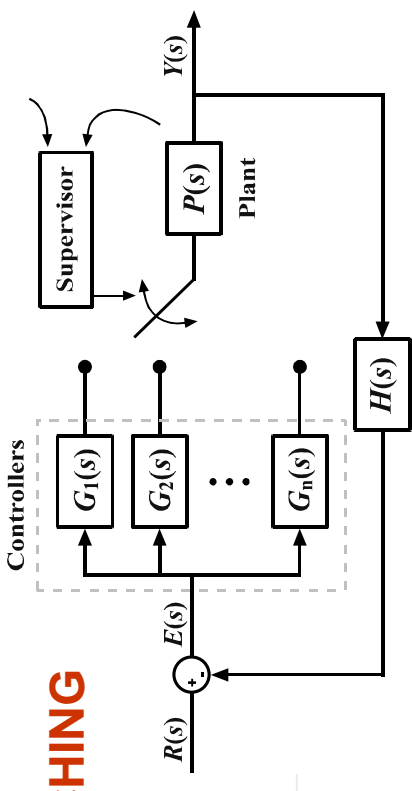
Now, the previous stability condition

$$1 + \text{Re}\{\mathbf{\Delta}^T (s\mathbf{I} - \mathbf{A})^{-1} \mathbf{g}\} > 0, \quad s = j\omega, \text{ for all frequency } \omega$$

becomes

$$1 + \text{Re}\left\{ \frac{\Delta e_{n-1} s^{n-1} + \ldots + \Delta e_1 s + \Delta e_0}{s^n + e_{n-1} s^{n-1} + \ldots + e_1 s + e_0} \right\} > 0, \quad s = j\omega, \text{ for all frequency } \omega$$
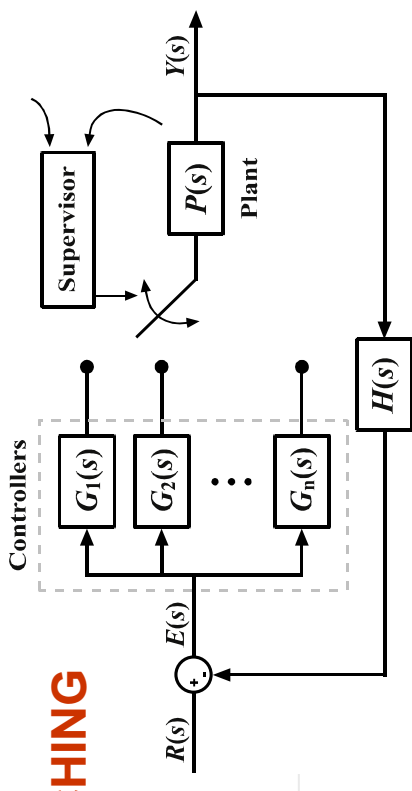
and then

$$\text{Re}\left\{ \frac{1 + L_2(s)}{1 + L_1(s)} \left(\frac{D(s) + \Delta D(s)}{D(s)} \right) \right\} > 0, \quad s = j\omega, \text{ for all frequency } \omega$$

which, due to symmetry, is

$$\left| \arg\{1 + L_2(j\omega)\} - \arg\{1 + L_1(j\omega)\} + \arg\left\{ \frac{D(j\omega) + \Delta D(j\omega)}{D(j\omega)} \right\} \right| < \frac{\pi}{2} \text{ for all } \omega > 0$$

SWITCHING

System stability analysis (V)

$$\left| \left| \arg\{1 + L_2(j\omega)\} - \arg\{1 + L_1(j\omega)\} + \arg\left\{ \frac{D(j\omega) + \Delta D(j\omega)}{D(j\omega)} \right\} \right| \right| < \frac{\pi}{2} \text{ for all } \omega > 0$$
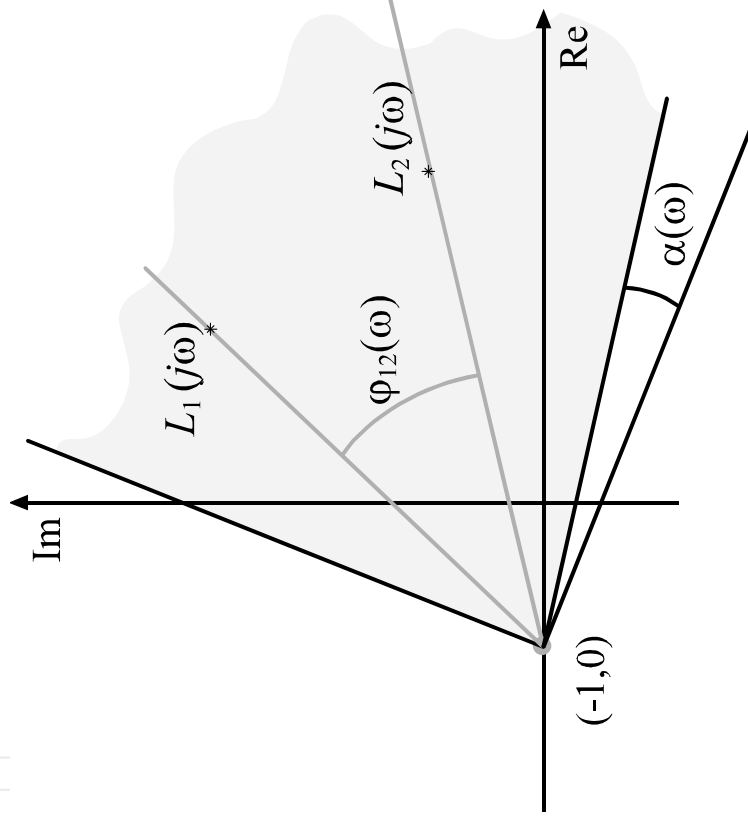
denoting

$$\varphi_{12}(\omega)[\text{deg}] = \left| \arg\{1 + L_2(j\omega)\} - \arg\{1 + L_1(j\omega)\} \right|,$$

$$\alpha(\omega)[\text{deg}] = \left| \arg\left\{ \frac{D(j\omega) + \Delta D(j\omega)}{D(j\omega)} \right\} \right|.$$

and applying the triangle inequality

$$\varphi_{12}(\omega) < 90 - \alpha(\omega) \text{ deg for all } \omega \geq 0$$

System stability analysis (VI)
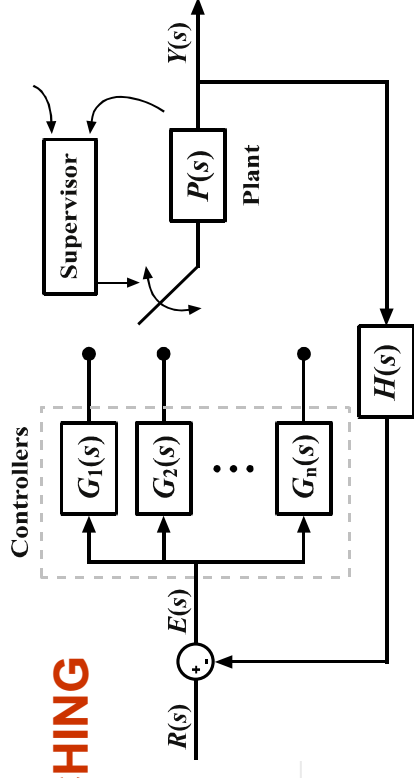
The criterion can be applied graphically in the **Nyquist diagram**

$$\varphi_{12}(\omega) < 90 - \alpha(\omega) \text{ deg for all } \omega \geq 0$$

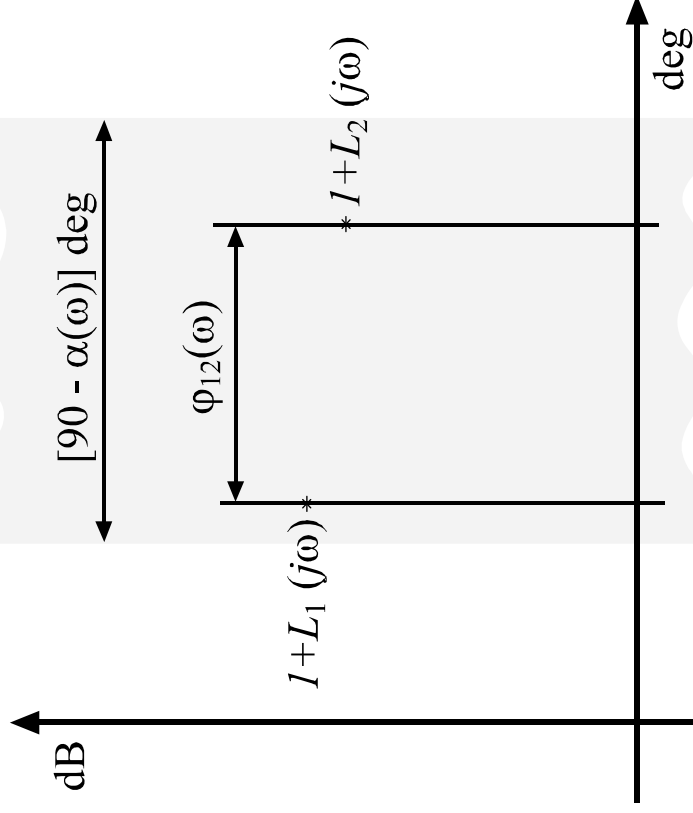$$\varphi_{12}(\omega)[\deg] = \left| \arg\{1 + L_2(j\omega)\} - \arg\{1 + L_1(j\omega)\} \right|,$$

$$\alpha(\omega)[\deg] = \left| \arg\left\{ \frac{D(j\omega) + \Delta D(j\omega)}{D(j\omega)} \right\} \right|.$$

For **stable switching**:

$L_1(j\omega)$ and $L_2(j\omega)$

must be **inside** of an arc of $[90 - \alpha(\omega)]$ deg

around the point $(-1,0)$ at each frequency

2.73

SWITCHING

The criterion can be applied graphically in the **Nichols diagram**

$$\varphi_{12}(\omega) < 90 - \alpha(\omega) \text{ deg for all } \omega \geq 0$$

$$\varphi_{12}(\omega)[\text{deg}] = \left|\arg\{1 + L_2(j\omega)\} - \arg\{1 + L_1(j\omega)\}\right|,$$

$$\alpha(\omega)[\text{deg}] = \left|\arg\left\{\frac{D(j\omega) + \Delta D(j\omega)}{D(j\omega)}\right\}\right|.$$
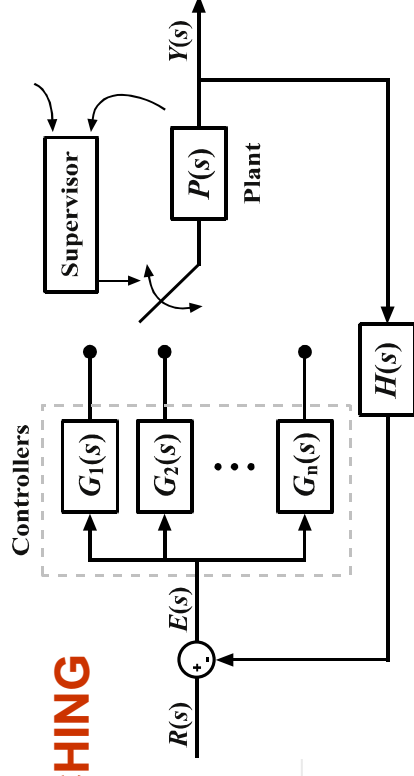
For stable switching:

plot $[1 + L_1(j\omega)]$ and $[1 + L_2(j\omega)]$,

the distance $\varphi_{12}(\omega)$ on the horizontal axis at each frequency

must be less than $[90 - \alpha(\omega)]$ deg

System stability analysis (VIII)
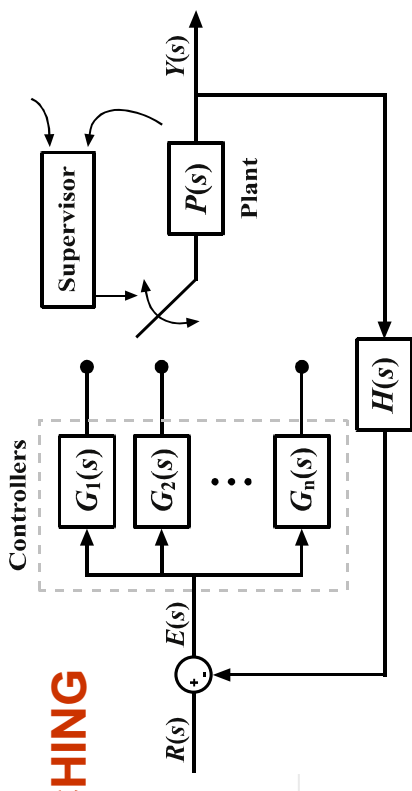
$\alpha(\omega)$ may be considered as a measurement of the **controller poles change**
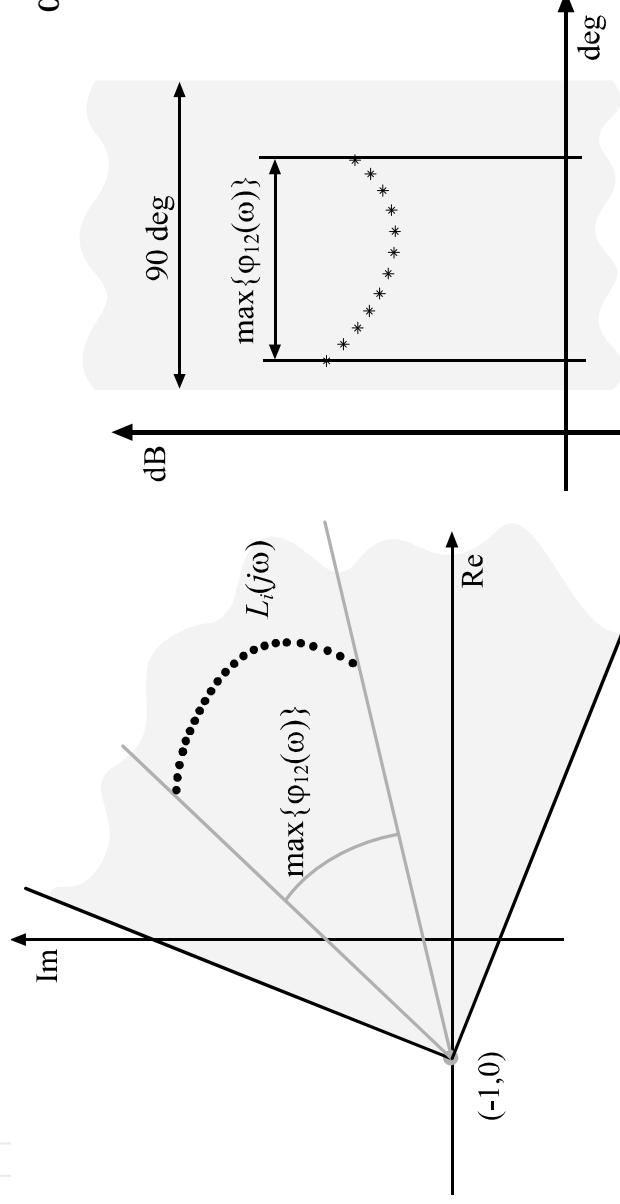
$$\boxed{\varphi_{12}(\omega) < 90 - \alpha(\omega) \text{ deg for all } \omega \geq 0}$$

$$\varphi_{12}(\omega)[\text{deg}] = \left|\arg\{1 + L_2(j\omega)\} - \arg\{1 + L_1(j\omega)\}\right|,$$
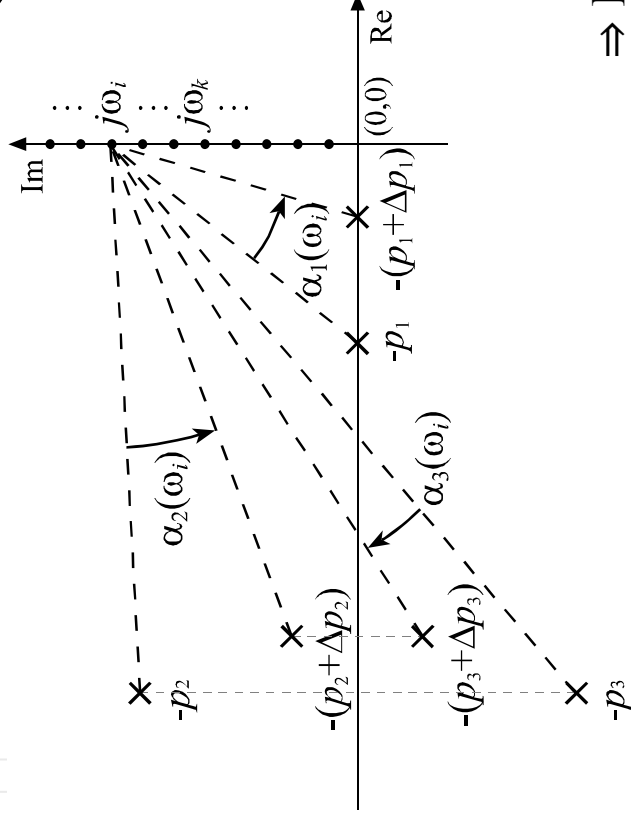
$$\alpha(\omega)[\text{deg}] = \left|\arg\left\{\frac{D(j\omega) + \Delta D(j\omega)}{D(j\omega)}\right\}\right|.$$
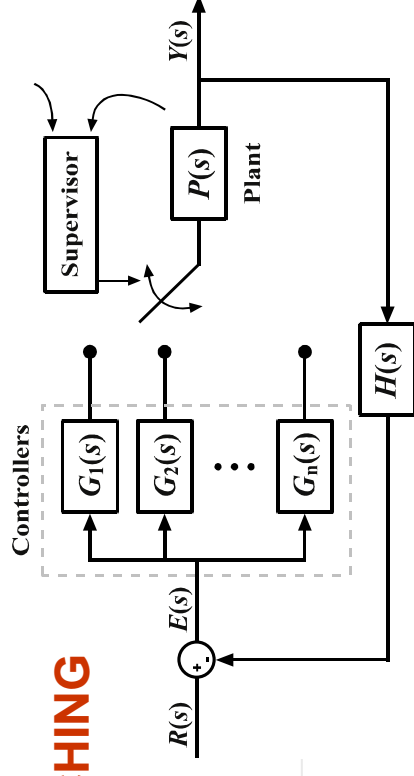
$$\alpha(\omega) = \left|\arg\left\{\frac{D(j\omega) + \Delta D(j\omega)}{D(j\omega)}\right\}\right| = \left|\arg\left\{\frac{\prod\limits_{j=1}^{n}(j\omega + p_j + \Delta p_j)}{\prod\limits_{j=1}^{n}(j\omega + p_j)}\right\}\right| =$$

$$= \left|\sum\limits_{j=1}^{n}\arg\{j\omega + p_j + \Delta p_j\} - \arg\{j\omega + p_j\}\right|$$

$\Rightarrow$ If there aren't moving poles, the angle $\alpha(\omega)$ is null.

SWITCHING

System stability analysis (IX)

Note 1: Switching among an infinite number of systems (LPV)

Easy if we only move gain and zeros $\Rightarrow \alpha(\omega) = 0$

$$\varphi_{12}(\omega) < 90 - \alpha(\omega) \text{ deg for all } \omega \geq 0$$

$$\varphi_{12}(\omega)[\deg] = \left| \arg\{1 + L_2(j\omega)\} - \arg\{1 + L_1(j\omega)\} \right|,$$

$$\alpha(\omega)[\deg] = \left| \arg\left\{ \frac{D(j\omega) + \Delta D(j\omega)}{D(j\omega)} \right\} \right|.$$

the angle between any two possible systems $L_i(j\omega)$ (or $[1 + L_1(j\omega)]$) is **less than 90 deg**

Block diagram labels

Supervisor · $P(s)$ Plant · $Y(s)$ · $H(s)$ · Controllers · $G_1(s)$ · $G_2(s)$ · $\cdots$ · $G_n(s)$ · $E(s)$ · $R(s)$

Plot labels

$L_i(j\omega)$ · $\max\{\varphi_{12}(\omega)\}$ · Im · Re · $(-1,0)$ · 90 deg · dB · deg

SWITCHING

$$\varphi_{12}(\omega) < 90 - \alpha(\omega) \text{ deg for all } \omega \geq 0$$
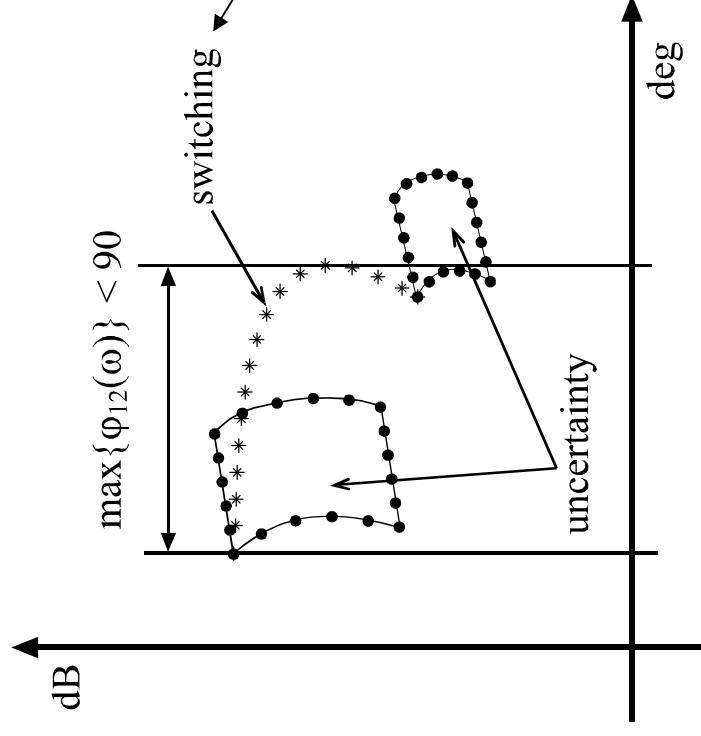
<u>**Note 2**</u>: To deal with Uncertainty

switching = modifies position and shape of templates of $[1 + L_i(j\omega)]$

$$\varphi_{12}(\omega)[\deg] = \left| \arg\{1 + L_2(j\omega)\} - \arg\{1 + L_1(j\omega)\} \right|,$$

$$\alpha(\omega)[\deg] = \left| \arg\left\{ \frac{D(j\omega) + \Delta D(j\omega)}{D(j\omega)} \right\} \right|.$$

criterion applied to

path from each point of the *departure template* to its corresponding point in the *arrival template*

uncertainty changes the plant slowly in comparison with the system dynamics
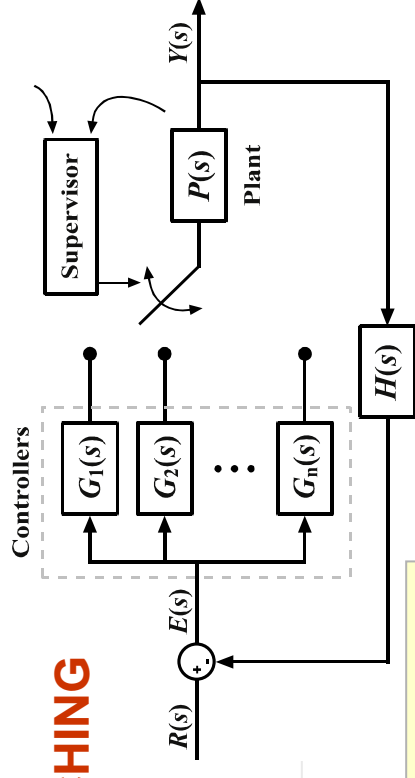
SWITCHING

The switching criterion

Signal: the error amplitude

Criteria:

i) *Large error*: large bandwidth (speed), loop gain not very high

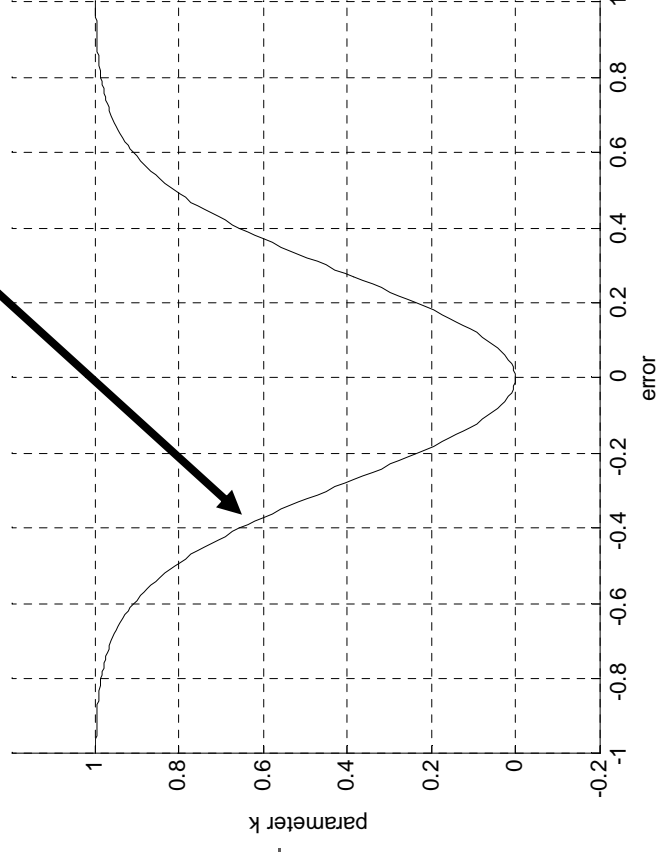ii) *Small errors*: reduced bandwidth (noise), increased low frequency gain (jitter, tracking error)

LARGE ERROR
↑ STABILITY MARGINS
↑ SPEED, ↓PRECISION
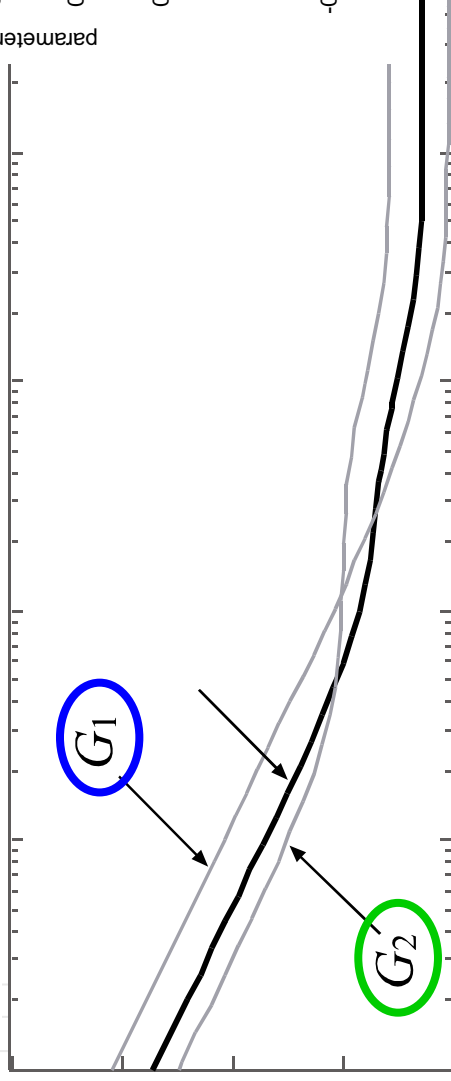
SMALL ERROR
↓ STABILITY MARGINS
↑ LOW FREQUENCY GAIN
(⇒↑ PRECISION & DISTURBANCE REJECTION)

Switching Function:

for example

G_1 G_2

Mario Garcia-Sanz

SWITCHING

Controller Design Methodology
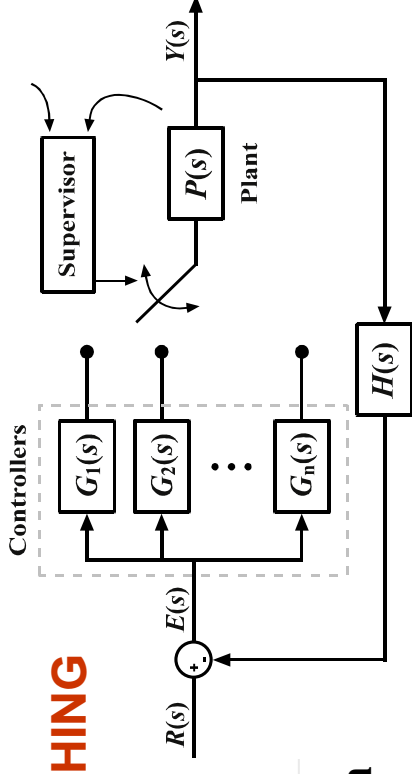
Step 1: **Preliminary QFT linear controller design**
- parametric and/or non-parametric uncertainty,
- stability and performance specifications,
- Templates and QFT-bounds
- design a linear controller by loop-shaping

Step 2: **Design two extreme controllers with the same structure.**
- Gain and zeros vary freely, but poles stand still.
- Their characteristics must be related with the *error amplitude*:
  i) **Large error**: large bandwidth (speed), loop gain not very high
  ii) **Small errors**: reduced bandwidth (noise), increased low freq.gain (jitter, tracking error)

Step 3: **Check Stability.**
- robust stability of extreme designs guaranteed by QFT.
- stability with switching is assured by new graphical criterion.

Step 4: **Design the Switching function.**
- Simulations of the system governed by each extreme controller.
- Design the function that relates the error amplitude with the controller parameters.

6.- Example: Switching control for Unmanned Vehicles

Remotely Controlled
Reconnaissance Vehicle   (Dorf)

<u>Plant & parametric uncertainty</u>

$$P(s) = \frac{1}{\left(s^2 + a_1 s + a_0\right)}$$

where $a_1 \in [1.8, 2.2]$, and $a_0 \in [3.6, 4.4]$

Step 1: **Preliminary linear controller design**
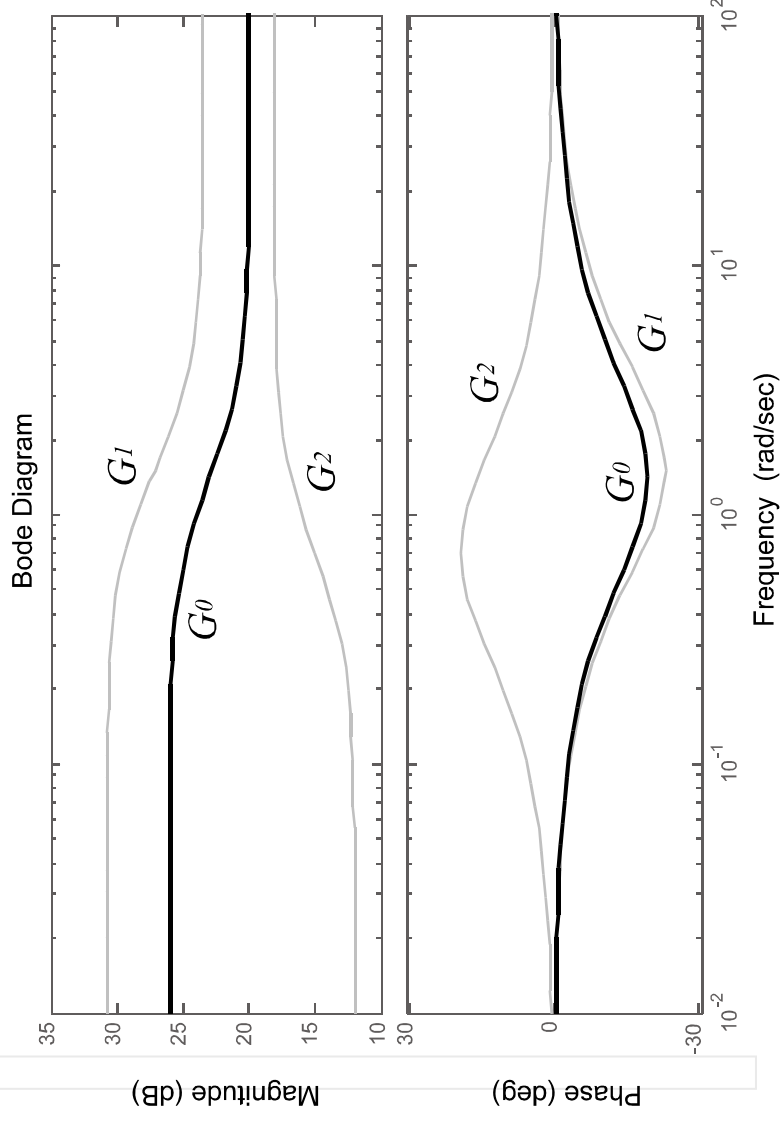
$$G_0(s) = \frac{10(s+2)}{(s+1)}$$

(Designed by Dorf)

Mario Garcia-Sanz

$$G_0(s) = \frac{10(s+2)}{(s+1)}$$

Step 2: **Design two extreme controllers with the same structure.**

- Gain and zeros vary freely, but poles stand still.
- Their characteristics must be related with the *error amplitude*:
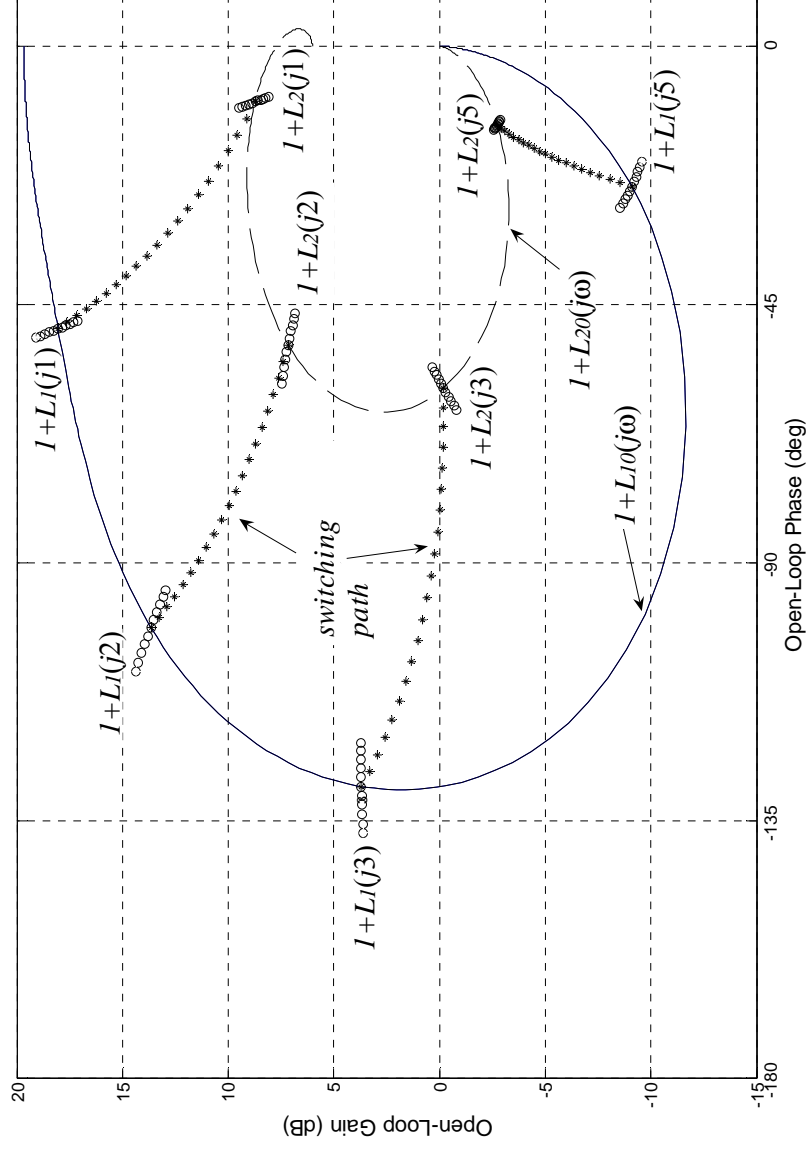
$$G_1(s) = \frac{15(s+2.3)}{(s+1)}$$

$$G_2(s) = \frac{8(s+0.5)}{(s+1)}$$

Bode Diagram

$$G_1(s) = \frac{15(s+2.3)}{(s+1)}$$

$$G_2(s) = \frac{8(s+0.5)}{(s+1)}$$

Step 3: **Check Stability.**

- robust stability of extreme designs guaranteed by QFT.
- stability with switching is assured by new graphical criterion.

UNCERTAINTY
in the path from each point of the first template to its corresponding point of the second template, the maximum horizontal distance between two points is not higher than 90 deg
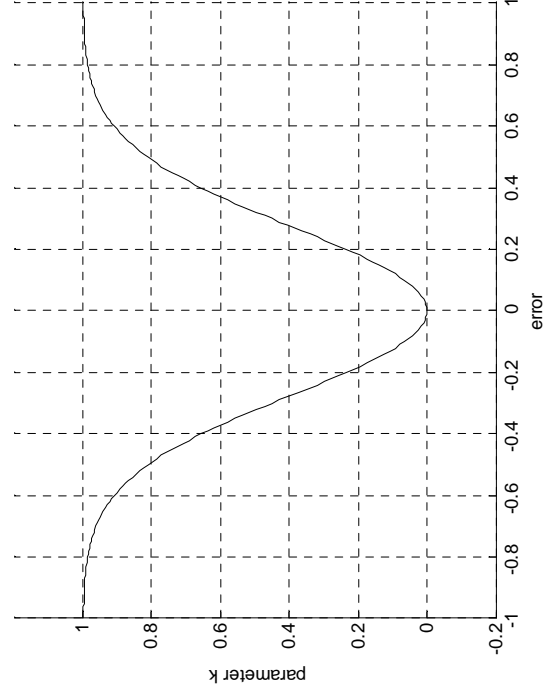

2.82

$$G_1(s) = \frac{15(s+2.3)}{(s+1)} \qquad G_2(s) = \frac{8(s+0.5)}{(s+1)}$$

Design the Switching function.

- Simulations of the system governed by each extreme controller.
- Design the function that relates the error amplitude with the controller parameters.

The switching controller is $\quad G_{swi}(s) = \dfrac{(15-7k)(s+2.3-1.8k)}{(s+1)}$

k is given by a function $\mathbb{R} \rightarrow [0, 1]$ of the error signal.

$$k = 1 - \exp\left(-\frac{e(t)^2}{0.15}\right)$$

smooth function (instead of a relay-type or saturation-type function) to reduce impulse effects

Results

The switching controller ($Gswi$)
- combines the best characteristics of the extreme controllers (G_1 and G_2),
- improving the response of the original fixed controller (G_0)

time response to a step input reference tracking ($t = 1$ sec) and a step disturbance ($t = 15$ sec)

Mario Garcia-Sanz
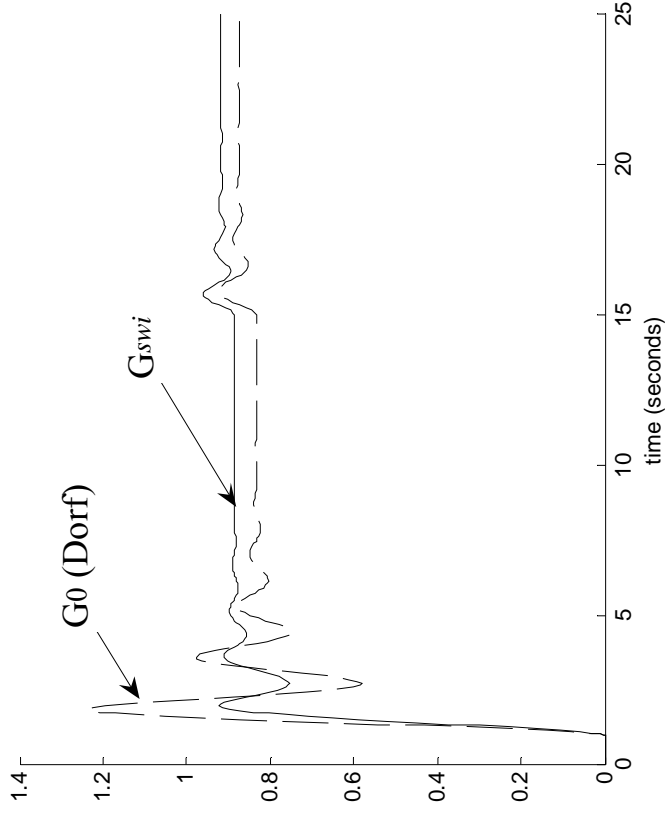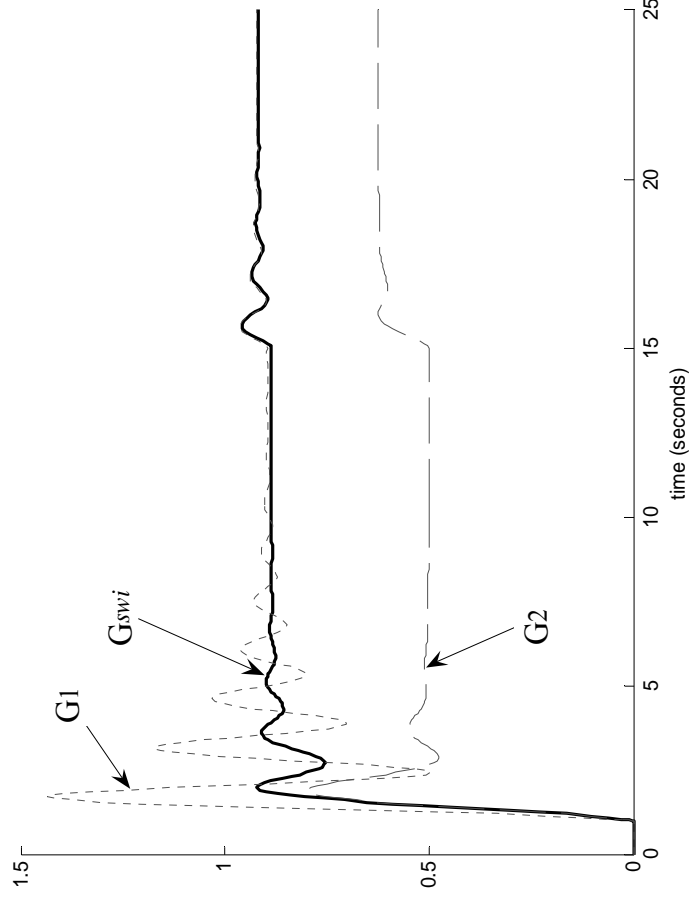
Suitable to be applied to other systems
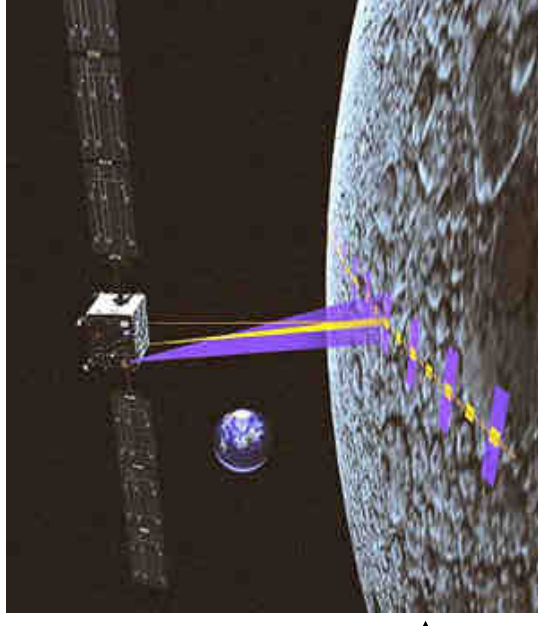
Wind Turbines control

García-Sanz M., Elso J. (2008). **Beyond the linear limitations by combining switching and QFT: Application to wind turbines pitch control systems.** *Int. J. Robust Nonlinear Control*, Vol. 18, N.12.

UAV control

Spacecraft control